

**ADSORPTION STUDY OF POROUS SILICA PREPARED
BY SOL-GEL METHOD: EXPERIMENTS AND
COMPUTER SIMULATION**



**A Thesis Submitted in Partial Fulfillment of the Requirements for
the Degree of Doctor of Philosophy in Chemical Engineering**

Suranaree University of Technology

Academic Year 2020

การศึกษาการดูคั้งของซีลิกาพอรุนที่เตรียมด้วยวิธีโซลเจล: การทดลองและ
การสร้างแบบจำลองทางคอมพิวเตอร์



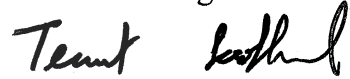
วิทยานิพนธ์นี้เป็นส่วนหนึ่งของการศึกษาหลักสูตรปริญญาวิศวกรรมศาสตรดุษฎีบัณฑิต
สาขาวิชาวิศวกรรมเคมี
มหาวิทยาลัยเทคโนโลยีสุรนารี
ปีการศึกษา 2563

ADSORPTION STUDY OF POROUS SILICA PREPARED BY SOL-GEL

METHOD: EXPERIMENTS AND COMPUTER SIMULATION

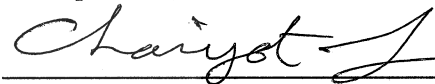
Suranaree University of Technology has approved this thesis submitted in partial fulfillment of the requirements for the Degree of Doctor of Philosophy.

Thesis Examining Committee



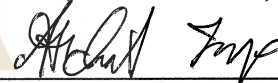
(Dr. Terasut Sookkumnerd)

Chairperson



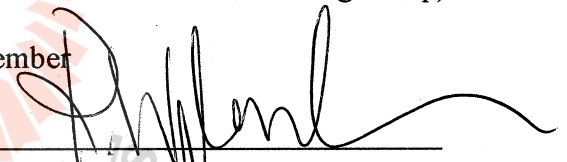
(Prof. Dr. Chaiyot Tangsathitkulchai)

Member (Thesis Advisor)



(Assoc. Prof. Dr. Atichat Wongkoblap)

Member



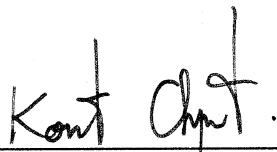
(Asst. Prof. Dr. Ratanawan Kiattikomol)

Member



(Dr. Supunnee Junpirom)

Member



(Assoc. Prof. Ft. Lt. Dr. Kontorn Chamniprasart)

Vice Rector for Academic Affairs and
Internationalization



(Assoc. Prof. Dr. Pornsiri Jongkol)

Dean of Institute of Engineering

ชลธิรา บุญฟู่ง : การศึกษาการดูดซับของซิลิกาพอร์นที่เตรียมด้วยวิธีโซลเจล: การทดลอง และการสร้างแบบจำลองทางคอมพิวเตอร์ (ADSORPTION STUDY OF POROUS SILICA PREPARED BY SOL-GEL METHOD: EXPERIMENTS AND COMPUTER SIMULATION) อาจารย์ที่ปรึกษา : ศาสตราจารย์ ดร.ชัยยศ ตั้งสติย์กุลชัย, 191 หน้า.

งานวิจัยนี้มีวัตถุประสงค์เพื่อศึกษาการเตรียมซิลิกาพอร์นจากโซเดียมซิลิเกตด้วยวิธีโซลเจล และศึกษากระบวนการดูดซับในระบบของเหลวและแก๊ส รวมทั้งศึกษาแบบจำลองทางคอมพิวเตอร์สำหรับการดูดซับแก๊สบนซิลิกาพอร์น โดยวัดสมบัติความพรุนของซิลิกาพอร์นด้วยวิธีการดูดซับไนโตรเจนที่อุณหภูมิ 77 เคลวิน สำหรับชนิดของหมู่ไฮดรอกซิลและปริมาณบนพื้นผิว วิเคราะห์ด้วยเทคนิคฟลูอิดไรซอสเฟอรัม อินฟราเรด สเปกโทรสโกปีและเทอร์โมกราวิเมตริก ตามลำดับ ขนาดรูพรุนเฉลี่ยของซิลิกาพอร์นที่เตรียมได้อยู่ในช่วง 2.2-10.9 นาโนเมตร และปริมาณของหมู่ไฮดรอกซิลอยู่ในช่วง 4.22-7.94 มิลลิโมลต่อกรัมของซิลิกาพอร์น การศึกษาพฤติกรรมดูดซับน้ำโดยซิลิกาพอร์นได้ทำการศึกษาทั้งในการดูดซับในของเหลวแบบกะและการดูดซับในวัฏภาคแก๊สแบบต่อเนื่องในเบคกิ้ง รวมถึงการศึกษาการดูดซับเมทิลินบลูจากสารละลายในระบบดูดซับกะด้วย

การดูดซับแบบกะของสารละลายเอทานอล-น้ำ ทำการทดลองที่ความเข้มข้นของเอทานอลในสารป้อนอยู่ในช่วง 60-95 ไร่ยะ โดยน้ำหนัก พบว่าซิลิกาพอร์นที่เตรียมนั้นสามารถแยกน้ำออกจากเอทานอลโดยสามารถเพิ่มความเข้มข้นของเอทานอลได้สูงถึง 97.34 ไร่ยะโดยน้ำหนัก แบบจำลองไอโซเทิร์มแลงมัวร์สามารถใช้อธิบายดูดซับน้ำจากสารละลายได้ดี สำหรับการศึกษากระบวนการดูดซับทางจลนพลศาสตร์ ได้ทำการศึกษาที่อุณหภูมิการดูดซับต่างๆ โดยแบบจำลองอันดับสองเสมือนมีความเหมาะสมและให้ผลสอดคล้องกับผลการทดลองได้ดีที่สุดในส่วน การศึกษากระบวนการดูดซับทางพลวัตของไอผสมเอทานอล-น้ำบนซิลิกาพอร์นในคอลัมน์เบคกิ้ง ซึ่งว่าซิลิกาพอร์นมีประสิทธิภาพในการแยกน้ำออกจากไอผสมเอทานอล-น้ำ และสามารถเพิ่มความเข้มข้นของเอทานอลข้ามจุดอะซิโโทรอปของเอทานอลได้

สำหรับกระบวนการกำจัดสีสังเคราะห์ในงานวิจัยนี้ได้ทำการศึกษาการดูดซับเมทิลินบลูจากสารละลายโดยใช้ซิลิกาในระบบการดูดซับแบบกะ จากผลการทดลองพบว่าปริมาณของหมู่ไฮดรอกซิลไม่ได้ส่งผลมากนักต่อการดูดซับเมทิลินบลู แต่ปริมาณการดูดซับของเมทิลินบลูจะเพิ่มขึ้นตามขนาดรูพรุนเฉลี่ยของซิลิกาพอร์นที่เพิ่มขึ้น และการศึกษาสมมูลการดูดซับและจลนพลศาสตร์ของการดูดซับเมทิลินบลูสามารถอธิบายด้วยแบบจำลองไอโซเทิร์มของแลงมัวร์และแบบจำลองอันดับสองเสมือนตามลำดับ

ในส่วนของการศึกษาการจำลองแบบทางคอมพิวเตอร์สำหรับการดูดซับ ทำการศึกษาโดยการจำลองโครงสร้างของซิลิกาพอรุนเป็นแบบ โครงสร้างเตตระฮีดรอลของซิลิกอนเตตระออกไซด์ และมีหมู่ไฮดรอกซิลแทนหมู่ซิลานอลที่อยู่บนพื้นผิว โดยใช้แบบจำลองวิธีจีซีเอ็มซีในการศึกษาพฤติกรรมการดูดซับสารประกอบเดี่ยวของแก๊สมีเทนและแก๊สคาร์บอนไดออกไซด์บนซิลิกาพอรุนจำลอง นำผลของไอโซเทิร์มการดูดซับของคาร์บอนไดออกไซด์ที่จากการจำลองทางคอมพิวเตอร์ไปเปรียบเทียบกับผลการทดลอง โดยพบว่าแบบจำลองพอรุนแบบแผ่นขนานที่ผนังประกอบไปด้วยโครงข่ายของซิลิกอนเตตระออกไซด์ สามารถใช้ศึกษาการดูดซับคาร์บอนไดออกไซด์และมีเทนได้เป็นอย่างดี



สาขาวิชา วิศวกรรมเคมี
ปีการศึกษา 2563

ลายมือชื่อนักศึกษา Chantis Benf
ลายมือชื่ออาจารย์ที่ปรึกษา Chaiyot J

CHONTIRA BOONFUNG : ADSORPTION STUDY OF POROUS
SILICA PREPARED BY SOL-GEL METHOD: EXPERIMENTS
AND COMPUTER SIMULATION. THESIS ADVISOR : PROF.
CHAIYOT TANGSATHITKULCHAI, Ph.D. 191 PP.

POROUS SILICA/ ETHANOL/ ADSORPTION/ GCMC SIMULATION

This thesis work was concerned with the preparation of porous silica from sodium silicate by the sol-gel method and studying its adsorption performance in both liquid and gas systems, as well as studying the computer simulation of gas adsorption on porous silica. Porous properties and of porous silica were determined by means of N₂ adsorption at 77 K and the presence of surface silanol groups was identified both qualitatively and quantitatively by FTIR and TGA, respectively. The mean pore size of the porous silica prepared by the sol-gel method was in the mesopore size range varying from 2.2-10.9 nm and silanol contents in the range of 4.22-7.94 mmol/g. The water adsorption behavior by the prepared porous silica was studied both in a liquid batch system and a continuous fixed-bed vapor system, as well as the batch adsorption of methylene blue (MB) from aqueous solution.

For batch adsorption of an ethanol-water mixture and with the initial ethanol feed concentration in the range from 60 to 95 wt%, the prepared porous glass was able to effectively remove water, giving the final concentration as high as 97.34 wt%. The water adsorption isotherms by porous silica were well described by the Langmuir isotherm equation. The kinetics of water adsorption was also studied at various temperatures and the pseudo second-order model was found to excellently describe the experimental kinetic data. The dynamics of water adsorption from an ethanol-water

vapor mixture by the prepared porous silica was conducted in a fixed-bed adsorption column. It was found that the porous silica was able to effectively separate water from ethanol-water vapor mixtures and could break the azeotrope point of ethanol, giving the final ethanol product concentration of higher than 99% by weight.

The removal of MB from aqueous solution by the prepared porous silica was carried out in a batch system. From the results obtained, it was observed that the silanol contents did not greatly affect the methylene blue adsorption. However, the methylene blue adsorption capacity increased with the increase in the mean pore size of porous silica. The equilibrium and kinetics of adsorption were satisfactorily described by the Langmuir isotherm and the pseudo-second-order kinetics model, respectively.

For the simulation study, the structure of porous silica was modeled as a tetrahedral structure of SiO_4 for the pore walls and the surface silanol groups was represented as hydroxyl groups. The GCMC simulation method was then used to investigate the adsorption behavior for the single component of methane (CH_4) and carbon dioxide (CO_2) in the porous silica model. The simulated CO_2 adsorption isotherms were also presented and compared with the experimental data. It was demonstrated that the finite-length slit pore model, whose walls consist of an assemblage of connected SiO_4 , can be employed to represent the structure of porous silica glass for a successful simulation study of CO_2 and CH_4 adsorption.

School of Chemical Engineering

Academic Year 2020

Student's Signature Chanta Benf

Advisor's Signature Chaiyot J

ACKNOWLEDGEMENTS

Firstly, I would like to express my sincere gratitude to my thesis advisor, Prof. Dr. Chaiyot Tangsathitkulchai, for giving me the opportunity to study in this PhD program. He has taught me substantially that will be important for the development of my future career. I am grateful to all the academic member in the School of Chemical Engineering, Suranaree University of Technology (SUT) for their teaching and support and encouragement.

In addition, thanks to all graduate students for making good atmosphere in our research rooms. Financial support from The Royal Golden Jubilee (RGJ) Ph.D. Program under The Thailand Research Fund is greatly appreciated (Grant 1.C.TS/52/A.1 PHD/0343/ 2552).

Finally, I am indebted to all the members of my family for their kind support and understanding through out my study.

Chontira Boonfung

TABLE OF CONTENTS

	Page
ABSTRACT (THAI).....	I
ABSTRACT (ENGLISH).....	III
ACKNOWLEDGEMENTS.....	V
TABLE OF CONTENTS.....	VI
LIST OF TABLES.....	XV
LIST OF FIGURES.....	XVIII
CHAPTER	
I INTRODUCTION.....	1
1.1 Rationale of the study.....	1
1.2 Research objectives.....	4
1.3 Scope of the study.....	5
1.3.1 Preparation of porous silica for adsorption study.....	5
1.3.2 Removal of water from ethanol-water mixture by adsorption.....	5
1.3.3 Removal of methylene blue from aqueous solution by adsorption.....	6
1.3.4 Study CO ₂ adsorption behavior of porous silica by using computer simulation.....	6

TABLE OF CONTENTS (Continued)

	Page
1.4 Outcomes of the research	7
1.5 Organization of thesis	7
1.6 References.....	8
II PREPARATION AND CHARACTERIZATION OF	
POROUS SILICA BY SOL-GEL METHOD.....	10
2.1 Abstract	10
2.2 Introduction	11
2.3 General background of porous silica.....	12
2.3.1 Porous silica	12
2.3.2 Preparation of porous silica by the phase separation method	16
2.3.3 Preparation of porous silica by the sol-gel method.....	17
2.3.4 Determination of surface hydroxyl group of the porous silica products.....	19
2.4 Experimental	21
2.4.1 Apparatus and chemicals	21
2.4.2 Preparation of porous silica.....	22
2.4.3 Characterization of porous silica	25
2.4.3.1 X-ray fluorescence analysis (XRF).....	25
2.4.3.2 X-ray diffraction (XRD)	25

TABLE OF CONTENTS (Continued)

	Page
2.4.3.3 Fourier transform infrared spectroscopy (FTIR)	25
2.4.3.4 Thermogravimetric and differential thermal analysis (TGA-DTA).....	25
2.4.3.5 Surface area and porosity analyzer.....	26
2.5 Results and discussion	27
2.5.1 Porous glass compositions by XRF analysis.....	27
2.5.2 X-ray diffraction (XRD).....	28
2.5.3 Fourier transform infrared spectroscopy (FTIR)	29
2.5.4 Determination of hydroxyl group of the porous silica products	31
2.5.5 Determination of porous properties of the porous silica	34
2.6 Conclusions	37
2.7 References.....	38
III ETHANOL DEHYDRATION BY POROUS SILICA.....	42
3.1 Abstract.....	42
3.2 Introduction	43
3.3 Background information	45

TABLE OF CONTENTS (Continued)

	Page
3.3.1 Ethanol.....	45
3.3.2 Adsorption process	49
3.3.3 Adsorption isotherms.....	51
3.3.4 Adsorption isotherms equations.....	53
3.3.5 Adsorption kinetics models.....	55
3.3.5.1 Pseudo-first-order rate equation.....	55
3.3.5.2 Pseudo-second-order rate equation.....	56
3.3.5.3 Intraparticle diffusion model.....	56
3.3.6 The breakthrough curve.....	58
3.3.7 Adsorption dynamics in a fixed-bed system.....	59
3.3.7.1 Break through equation by the linear-driving force model.....	60
3.3.7.2 Break through equation by Thomas model.....	62
3.3.7.3 Breakthrough equation with axial dispersion.....	64
3.3.7.4 Breakthrough curve characteristics.....	64
3.4 Literature review	66
3.5 Experimental method	68

TABLE OF CONTENTS (Continued)

	Page
3.5.1 Batch adsorption tests in a liquid phase system.....	68
3.5.2 Fixed-bed adsorption tests in a vapor phase system	69
3.6 Results and discussion.....	74
3.6.1 Batch adsorption of water in liquid phase.....	74
3.6.1.1 Water adsorption isotherms.....	74
3.6.1.2 Water adsorption kinetics.....	77
3.6.2 Fixed-bed adsorption in a vapor-phase.....	85
3.6.2.1 Characteristics of water breakthrough curves	85
3.6.2.2 Breakthrough models.....	97
3.6.2.3 Analysis of mass transfer resistance.....	100
3.7 Conclusions.....	103
3.8 References.....	105
IV REMOVAL OF METHYLENE BLUE DYE FROM AQUEOUS SOLUTION WITH POROUS SILICA ADSORBENT	108
4.1 Abstract	108
4.2 Introduction.....	109
4.3 Experimental	110

TABLE OF CONTENTS (Continued)

	Page
4.3.1 Adsorption Kinetics	110
4.3.2 Adsorbent Dosage.....	110
4.3.3 Adsorption Isotherms.....	110
4.3.4 Calibration curve of methylene blue.....	111
4.4 Results and discussion.....	112
4.4.1 Effect of adsorbent dosage.....	112
4.4.2 Effect of adsorption temperature.....	113
4.4.3 Effect of initial concentration.....	114
4.4.4 Adsorption kinetics.....	115
4.4.5 Methylene blue (MB) adsorption isotherms.....	118
4.5 Conclusions.....	126
4.6 References.....	126
V SIMULATION OF CARBON DIOXIDE ADSORPTION ON POROUS SILICA.....	129
5.1 Abstract	129
5.2 Introduction.....	130
5.3 Theory and general background	133
5.3.1 Fluid model	133
5.3.1.1 Carbon dioxide model.....	133
5.3.1.2 Methane model and Nitrogen model.....	133

TABLE OF CONTENTS (Continued)

	Page
5.3.2 Solid model and functional group model	136
5.4 Methodology and experimental.....	138
5.4.1 Experimental Isotherms for N ₂ and CO ₂	
Adsorption	138
5.4.2 Computational methodology.....	129
5.4.2.1 Fluid model of CO ₂	139
5.4.2.2 Fluid model of N ₂ and CH ₄	140
5.4.2.3 Porous silica model.....	140
5.4.2.4 Model of surface functional groups.....	141
5.4.2.5 Defective surfaces.....	143
5.4.2.6 Grand Canonical Monte Carlo ensemble.....	143
5.5 Results and discussion	146
5.5.1 Experimental results	146
5.5.1.1 Porous properties and silanol group contents of porous silica.....	146
5.5.1.2 GCMC Simulation Results for Nitrogen adsorption.....	149
5.5.1.3 Experimental isotherms for CO ₂ adsorption.....	151

TABLE OF CONTENTS (Continued)

	Page
5.5.2 GCMC Simulation results for CO ₂	
adsorption.....	155
5.5.2.1 Adsorption isotherms for various	
pore widths.....	155
5.5.2.2 Effects of functional group	
concentration on CO ₂ adsorption	
isotherms.....	157
5.5.2.3 Effects of the functional group	
allocation on the adsorption of CO ₂	162
5.5.2.4 Adsorption of CO ₂ on a defective	
surface.....	167
5.5.2.5 Comparison between the	
experiment and GCMC	
simulation method.....	169
5.5.3 GCMC Simulation results for methane	
adsorption.....	171
5.5.3.1 Methane adsorption isotherm.....	171
5.5.3.2 Effects of temperature on	
methane adsorption.....	173

TABLE OF CONTENTS (Continued)

	Page
5.5.3.3 Effects of silanol groups concentration on methane adsorption.....	174
5.5.3.4 Effects of silanol group topology on methane adsorption.....	175
5.6 Conclusions.....	178
5.7 References.....	179
VI CONCLUSIONS AND RECOMMENDATIONS.....	184
6.1 Conclusions.....	184
6.2 Recommendations for further works.....	188
APPENDIX LIST OF PUBLICATIONS.....	189
BIOGRAPHY.....	191

LIST OF TABLES

Table	Page
2.1	Typical compositions and properties of commercially available porous silica glass 14
2.2	Brief historical development of porous silica manufacturing.....15
2.3	XRF results for the elemental composition of porous silica samples interpreted as oxides (weight %, normalized to 100%)..... 27
2.4	Summary of functional groups presenting at different wave numbers of FTIR analysis.....30
2.5	The silanol group content determined by TGA techniques..... 33
2.6	Physical properties of porous silica products synthesized at different conditions 36
3.1	Comparison of parameters of type of adsorption process50
3.2	Experimental conditions for batch adsorption of water by porous silica (PS2-200).....69
3.3	Experimental conditions for fixed-bed adsorption of water by porous silica..... 70
3.4	Estimated parameters of various isotherms models for adsorption of water onto porous silica in the liquid phase system..... 77

LIST OF TABLES (Continued)

Table	Page
3.5 (a) List of parameters obtained from pseudo-first-order, pseudo-second-order and intra particle kinetic model fitting for adsorption of water onto porous silica in batch liquid system at 20 °C.....	82
3.5 (b) List of parameters obtained from pseudo-first-order, pseudo-second-order and intra particle kinetic model fitting for adsorption of water onto porous silica in batch liquid system at 30 °C.....	83
3.5 (c) List of parameters obtained from pseudo-first-order, pseudo-second-order and intra particle kinetic model fitting for adsorption of water onto porous silica in batch liquid system at 40 °C.....	84
3.6 Average pore size and silanol group contents of the porous silica.....	86
3.7 The breakthrough time for different operating conditions.....	88
3.8 Adsorption capacity of water by various adsorbents.....	96
3.9 Parameters of Klinkenberg, Thomas and Levenspeil & Bischoff model under column adsorption process	101
3.10 The result of mass transfers resistance for various adsorption conditions	102

LIST OF TABLES (Continued)

Table	Page
4.1 List of parameters obtained from Pseudo-first-order, Pseudo-second-order model fitting for adsorption of methylene blue onto PS2-200 at 30 °C.....	117
4.2 (a) Estimated parameters of various isotherms models for adsorption of methylene blue onto PS2-200 in the liquid phase system.....	120
4.2 (b) Estimated parameters of various isotherms models for adsorption of methylene blue onto PS2-500 in the liquid phase system.....	120
4.2 (c) Estimated parameters of various isotherms models for adsorption of methylene blue onto PS4-200 in the liquid phase system.....	121
4.2 (c) Estimated parameters of various isotherms models for adsorption of methylene blue onto PS4-500 in the liquid phase system.....	121
5.1 Lennard-Jones parameters and partial charge	134
5.2 Porous properties of porous silica synthesized in this study.....	149

LIST OF FIGURES

Figure		Page
2.1	Silanol groups on the surface of porous glass.....	13
2.2	The preparation of porous silica by the phase separation method.....	16
2.3	The sol-gel reaction from sodium silicate	18
2.4	TGA patterns for calculating silanol contents on porous silica.....	20
2.5	Teflon-lined autoclave (250 ml).....	22
2.6	(a) the gel product obtain in the Teflon-lined autoclave after reaction at 100 °C, for 24 hr. and (b) the solid product after washing with distilled water.....	23
2.7	The preparation steps of porous glass by sol-gel process.....	24
2.8	XRD patterns obtained from porous silica samples.....	28
2.9	FITR spectra of porous silica products.....	31
2.10	TGA patterns of porous silica products.....	33
2.11	N ₂ adsorption isotherm at 77 K on the porous silica samples.....	36
3.1	Vapor-liquid equilibrium of a mixture of ethanol and water.....	48
3.2	Types of gas adsorption isotherms according to the IUPAC classification	51
3.3	Typical breakthrough curves of fixed-bed adsorption.....	58

LIST OF FIGURES (Continued)

Figure	Page
3.4	Typical breakthrough curve showing the estimation of breakthrough parameters (t_B = breakthrough time, t_E = equilibrium time, and t_M = mean stoichiometric time)..... 66
3.5	A laboratory-scale fixed-bed adsorption for ethanol dehydration experiments 72
3.6	The calibration curve of the refractive index for determining the ethanol solution..... 73
3.7	Adsorption isotherm of water onto porous silica (PS2-200, 2.4 nm mean pore size and silanol contents 7.94 mmol/g)..... 75
3.8	Water adsorption efficiency of porous silica (PS2-200, 2.4 nm and silanol contents 7.94 mmol/g)..... 76
3.9	Adsorption kinetic curves and predictive capability of different kinetic models for 90 wt.% ethanol (10 wt.% water) (a) at 20 °C and (b) at 30 °C..... 80
3.10	Typical plot of intraparticle diffusion model at 20 °C for (a) 85 wt.% ethanol (15 wt.% water) and (b) 90 wt.% ethanol (10 wt.% water)..... 81

LIST OF FIGURES (Continued)

Figure	Page
3.11 Effects of process variables on the breakthrough curves of water adsorption from ethanol solution by porous silica (a) and (b) amount of silanol group, (c) bed temperature, (d) bed height, (e) pore size, and (f) feed flow rate.....	87
3.12 (a) Comparison of breakthrough time (t_B) for different operating conditions.....	91
3.12 (b) Comparison of equilibrium time (t_E) for different operating conditions	92
3.12 (c) Comparison of adsorption capacity at t_B (q_B) for different operating conditions.....	93
3.12 (d) Comparison of adsorption capacity at t_E (q_E) for different operating conditions.....	94
3.12 (e) Comparison of MTZ for different operating conditions.....	95
3.13 Comparison of breakthrough curves between experimental results and different breakthrough models (bed temperature of 85 °C, bed depth 15 cm (a), and bed depth 25 cm (b), superficial velocity of 3.25 cm/s, water concentration feed of 5 wt.%)	99
4.1 Calibration curve of methylene blue (MB) solution	111

LIST OF FIGURES (Continued)

Figure	Page
4.2	Effect of adsorbent dose on MB adsorption with initial MB concentration of 200 mg/L at the adsorption temperature of 30 °C..... 113
4.3	Effect of temperature on MB adsorption with initial MB concentration of 100 mg/L and 0.1 grams of porous silica.....114
4.4	Effects of initial MB concentration on porous silica PS4-500 with different adsorption temperature.....115
4.5	Adsorption kinetic of Methylene blue (MB) on porous silica PS2-200 at adsorption temperature 30 °C..... 117
4.6 (a)	Adsorption Isotherm of MB on PS2-200 with different temperature..... 122
4.6 (b)	Adsorption Isotherm of MB on PS2-500 with different temperature..... 123
4.6 (c)	Adsorption Isotherm of MB on PS4-200 with different temperature..... 124
4.6 (e)	Adsorption Isotherm of MB on PS4-500 with different temperature..... 125
5.1	Schematic of the CO ₂ molecule..... 131
5.2	(a) schematic of the N ₂ molecule and (b) schematic of the CH ₄ molecule..... 134

LIST OF FIGURES (Continued)

Figure	Page
5.3	Schematic of the SiO ₄ molecule 136
5.4	The solid model of porous silica used in this study..... 141
5.5	Two proposed models for OH groups presenting on the inner walls of porous silica surfaces (a) the random and (b) the fixed topologies 142
5.6	A characteristic of defective surfaces of the porous silica model..... 144
5.7	Flow chart of computer simulation 145
5.8	Isotherms of N ₂ adsorption at 77 K on the prepared porous silica samples 148
5.9	Simulation results of N ₂ in porous silica at 77 K for various pore width from 7-15 Å..... 150
5.10	Simulation results of N ₂ in porous silica at 77 K for various pore width from 20-40 Å..... 150
5.11	CO ₂ adsorption isotherms at 283 K for porous silica prepared at different pH (a) adsorbed amount plotted in mmol/g (b) adsorbed amount plotted in kmol/m ³ 152
5.12	CO ₂ isotherms at 273 K for porous silica prepared at pH 2..... 154
5.13	CO ₂ isotherms at 273 K for porous silica prepared at pH 4..... 154
5.14	Experimental CO ₂ adsorption isotherms at 273, 283 and 293 K for the prepared porous silica..... 155

LIST OF FIGURES (Continued)

Figure	Page
5.15	Adsorption isotherms of CO ₂ on finite-length slit pore model of porous silica at 283 K.....157
5.16	CO ₂ adsorption isotherms at 283 K in a slit pore model of Porous silica with 2 nm. width and different concentrations of OH (a) plotted in semi-log scale and (b) plotted in linear scale..... 159
5.17	Snapshots of CO ₂ molecules in heterogeneous porous silica of 2 nm. in widths at 283 K.....160
5.18	Snapshots of CO ₂ molecules in heterogeneous porous silica of 2 nm. in widths at 283 K and 20% of the functional groups.....161
5.19	Snapshots of CO ₂ molecules in heterogeneous porous silica of 4 nm. in widths at 283 K and 20% of the functional groups..... 164
5.20	Snapshots of CO ₂ molecules in heterogeneous porous silica of 4 nm. in widths at 283 K and 20% of the functional groups at pressure more than 20 kPa.....165
5.21	Effects of functional group allocation on CO ₂ adsorption isotherms at 283 K for the porous silica model of 4 nm widths at (a) plotted in semi-log scale and (b) plotted in linear scale..... 166
5.22	CO ₂ adsorption on perfect and defective surfaces of pore walls of (a) 1 nm and (b) 3 nm pore widths..... 168

LIST OF FIGURES (Continued)

Figure	Page
5.23	Comparison of experimental and simulated isotherms for CO ₂ adsorption by porous silica glass (sample PS2-200) at 283 K..... 170
5.24	Calculated PSD obtained from CO ₂ adsorption isotherms using GCMC simulation.....170
5.25	Methane adsorption isotherms for various pore widths with the random topology contained 5% of functional group at 298 K.....172
5.26	Isotherms obtained for CH ₄ adsorption in the random pore topology having width of 10Å and 5% of functional groups at 283 and 298K..... 173
5.27	Adsorption isotherms of CH ₄ in pore having width of 10Å with different concentration of functional group at 298 K..... 174
5.28	Adsorption isotherms of methane at 298K in pore having width of 10Å with different functional group topologies..... 176
5.29	Snapshots of methane particles in heterogeneous porous silica of 10Å width contained 10% of functional group for the fix topology..... 176

LIST OF FIGURES (Continued)

Figure		Page
5.30	Snapshots of methane particles in heterogeneous porous silica of 10Å width contained 10% of functional group for the random topology (a) and the fix topology (b).....	177



CHAPTER 1

INTRODUCTION

1.1 Rationale of the study

At present, the demand for energy from petroleum-based fuels is increasing which affects the stability of both price and supply. Thailand is highly dependent on fuel import especially for the transportation sector which requires about 72% of oil demand and 28% of gas demand in 2009 (IEA, 2011). Conservative prediction suggests that Thailand will inevitably continue to increase the import of oil and gas to keep up with the economic development of the country. Therefore, to ease the energy burden, the government has a strong policy toward the increasing use of alternative energy sources. Ethanol is an attractive energy source which can be produced by fermentation with concentration varying from a few percent up to about 14% by volume of ethanol. It is further concentrated by fractional distillation under atmospheric pressure to obtain the maximum azeotropic point of 95.6 wt% ethanol. A number of processes have been developed to break the azeotrope of ethanol and water to obtain anhydrous ethanol, such as azeotropic distillation, extractive distillation, molecular sieves adsorption and membrane separation (Banat et al., 2000 and Pinto et al., 2010). Of these separation process, adsorption is an interesting choice due to its simplicity, high separation efficiency and consuming less energy.

New advanced adsorbent development for gas and liquid separation via adsorption processes has received increasing attention by scientists and engineers. However these materials need to be characterized and tested for a wide variety of

adsorbates and adsorption conditions. Porous silica, as one of the potential adsorbents, offers many advantageous properties including, good thermal stability, high mechanical strength, resistance to bacteria and virus, high chemical stability, narrow pore size distribution and excellent shaping ability. With these favorable characteristics, porous glass has also been employed in many other applications such as in the area of biotechnology (Hermann and Gottschalk, 2000), membrane technology (Kuraoka et al., 2001), heterogeneous catalyst and its supports (Takahashi et al., 1997), and as a starting material for the preparation of new inorganic/inorganic composites (zeolite/PG) (Schwieger, 2000) etc.

Porous silica can be conventionally synthesized by two different methods which are the thermal phase separation and the sol-gel method. For the phase separation method, two different interconnected phases of borate and silicate glass are first formed by high temperature melting of a proper composition of a raw mix. By further heat treating the glass product over the temperature range from 180 to 700 °C, the separation of these two glassy phases will occur. By leaching out the alkali-rich borate phase with a hot mineral acid, for example, nitric acid solution, the skeleton of almost pure porous silica can be obtained (D. enke, Janowski and Schwiger, 2003). The second preparation route of porous silica by the sol-gel process can be achieved by the hydrolysis of sodium silicate under acidic conditions to yield SiO₂. The sol-gel process has many advantages such as high purity, homogeneity and modification of material properties by changing the preparation parameters (Brinker and Scherer, 1990). The mean pore size, the interconnectivity and the pore size distributions can be closely controlled by changing the molar ratio of water and precursor, type of precursor, temperature of gelation, drying and stabilization (Brinker and Scherer, 1990 and Hench, 1998). In the

present work, porous silica being used as an adsorbent was prepared by the sol-gel method of sodium silicate (see Chapter 2 for details). The structural and textural properties of porous silica were controlled by varying the conditions of pH levels and the calcination temperature, which are the key factors for controlling the pore size distribution of porous silica and functional group on porous silica respectively.

To illustrate the potential use of porous silica in the area of adsorption, it was decided in this work to apply the prepared porous silica from sodium silicate by the sol-gel method for the dehydration of ethanol both from the gas phase and solution systems, the removal of methylene blue from aqueous solution and carbon dioxide adsorption. The existence of polar silanol group (Si-OH) on the porous silica surface makes it ideal for the capture of water and carbon dioxide (Witoon and Chareonpanich, 2012).

Dyes are present in varying concentrations in wastewater produced by many industries such as textiles, dyestuffs, printing, etc. (Azhar et. Al., 2005). The dyes can be classified as natural and synthetic which are complex organic molecules having functional groups such as carbonyl, methine, nitro, etc. To illustrate the potential use of porous glass in the area of adsorption, it was decided to apply the prepared porous silica for wastewater treatment, that is, for the removal dyes molecules from aqueous solutions. The mesoporous nature of porous silica is advantageous for effective adsorption of large dye molecules. In this study, the prepared porous silica was employed for the adsorption of methylene blue from aqueous solution with the adsorption study being performed in a batch adsorption system.

Global warming has posed serious problems to climate change caused by the rapidly increasing of CO₂ concentration in the atmosphere. One of the most

environmental priorities is to find a way to capture CO₂ which is the major greenhouse gases. The main techniques used for CO₂ capture include solid adsorption, solvent scrubbing and membrane separation process. In this work, the capture of CO₂ by the adsorption process by way of computer simulation was carried out to gain a better understanding the underlying mechanism of interaction between CO₂ molecules and porous silica surface which will benefit the future use of porous silica for CO₂ capture.

1.2 Research objectives

The aims of this research are the development of an improved process for dehydration of ethanol from an aqueous solution and a vapor-phase system as well as the removal of methylene blue from an aqueous solution by using porous silica as an adsorbent. The study of water adsorption behavior by porous silica using a computer simulation was also performed. The specific objectives of the thesis work are as follows.

1.2.1 To prepare porous silica by the sol-gel technique under varying preparation condition as well as the characterization of the prepared porous silica products.

1.2.2 To investigate the use of porous silica as adsorbents for removing water from ethanol solution in batch liquid-phase and vapor-phase fixed bed systems.

1.2.3 To apply the prepared porous silica for studying equilibrium and kinetics of methylene blue adsorption from aqueous solution as a function of various process variables.

1.2.4 To study the behavior of gas adsorbed on porous silica with various pore widths and functional groups by using a computer simulation.

1.3 Scope of the study

The scope of this thesis work is separated into three parts: porous silica preparation, adsorption experiments and adsorption simulation.

1.3.1 Preparation of porous silica for adsorption study

The porous silica is synthesized from sodium silicate by the sol-gel method. The pore size of the porous silica adsorbent is varied by changing the pH of the gel mixture. The amount of silanol contents is controlled by varying the calcination temperature during the preparation steps. The porous silica is characterized by N₂ adsorption at 77 K for determining its porous properties, Fourier transform infrared (FTIR) spectroscopy is used for identifying the type of surface functional groups and thermogravimetric analysis (TGA) technique for determining the silanol contents.

1.3.2 Removal of water from ethanol-water mixture by adsorption

1.3.2.1 Liquid-phase system

The prepared porous silica is employed to remove water by adsorption from a liquid mixture of ethanol and water. The adsorption test is carried out in a batch mode. Batch adsorption test is carried out to study the kinetics and equilibrium of water adsorption process as well as testing various available models pertaining to adsorption equilibrium and kinetics. Attempt is also made to determine the diffusion coefficients of water molecules in the porous structure of the porous silica adsorbents.

1.3.2.2 Gas-phase system

Porous silica is employed to remove water by adsorption in vapor phase of a mixture of ethanol and water. The adsorption test is carried out in a fixed-bed adsorber to collect data for constructing breakthrough curves for water adsorption.

Dynamics of the fixed-bed adsorption is predicted using various available breakthrough models.

1.3.3 Removal of methylene blue from aqueous solution by adsorption

The prepared porous silica is employed to remove methylene blue from aqueous solution in batch adsorption. Batch adsorption tests are carried out to study the kinetics and equilibrium of methylene blue adsorption as well as testing various available models pertaining to adsorption equilibrium and kinetics.

1.3.4 Study CO₂ adsorption behavior of porous silica by using computer simulation

Adsorptions of CO₂ in porous silica with different pore widths are studied in this research using the Monte Carlo simulation method. The molecular model of porous silica is assumed to be composed of an assemblage of SiO₄ crystal. The pore of silica adsorbent is created as a slit pore of two parallel sheets of these SiO₄ crystals. In addition, the hydroxyl (-OH) groups is attached to the silica surface to investigate its role in the adsorption process.

1.4 Outcomes of the research

1.4.1 A precise knowledge on the preparation of porous silica by the sol-gel technique with controlled contents of surface silanol group will be achieved.

1.4.2 The process of producing high concentration of ethanol solution by removing water with porous silica adsorbents for liquid adsorption in a batch system and vapor-phase adsorption in a fixed-bed will be established. Emphasis was placed on breaking the azeotropic concentration to obtain anhydrous ethanol.

1.4.3 The process of removing methylene blue from aqueous solution by using porous silica in batch system is to be established.

1.4.4 Detailed mechanisms of adsorption behavior of carbon dioxide by simulated porous silica will be obtained through the application of GCMC simulation approach.

1.5 Organization of thesis

The contents of the thesis work are divided into 6 chapters. **Chapter 1** is the introduction part; it describes the motivation, objectives of this research, scope and limitation of the research work. **Chapter 2** reports on studying the preparation and characterization of porous silica prepared from sodium silicate. For this part, porous silica was prepared from sodium silicate by the sol-gel method and the effects of pH levels and calcination temperature conditions were investigated, coupled with the results on product characterization. For **Chapter 3**, the application of porous silica in adsorption fields was focused on water adsorption onto porous silica adsorbents in liquid phase and vapor phase. The role of surface silanol groups and porous texture of porous silica on water adsorption were investigated. Various adsorption models were

also tested against the experimental isotherm data. **Chapter 4** describes the application of porous silica for removing methylene blue dye from aqueous solution by adsorption with porous silica adsorbents. Batch adsorption were studied as a function of process variables such as initial concentration of methylene blue, amount of porous silica adsorbent, adsorption temperature, amount of silanol content and mean pore size of porous glass. **Chapter 5** reports the study on adsorption behavior of pure CO₂ and CH₄ by porous silica using GCMC computer simulation. **Chapter 6** summarizes all the findings from this thesis and points out possible future research directions.

1.6 References

- Azhar S.S., Liew A.G., Suhardy D., Hafiz K.F. and Hatim M.D.I. (2005). Dye removal from aqueous solution by using adsorption treated sugarcane bagasse. **American Journal of Applied Sciences**. Vol. 11: 1499-1503.
- Banat F.A., Abu Al-Rub, and Simandl J. (2000). **Separation and purification technology**. Vol. 18, No. 2, 111–118.
- Brinker C.J. and Scherer G.W. (1990). Sol–gel science, the physics and chemistry of sol–gel processing. **Academic Press**. Boston
- D. Enke, F. Janowski and W.Schwiger. (2003). Porous glass in the 21st century a short review. **Micropore and Mesopore Materials**. 60:19-30.
- International Energy Agency, **IEA** (2011)
- K. Kuraoka, Y. Chujo and T. Yazawa. (2001). Hydrocarbon separation via porous glass membranes surface-modified using organosilane compounds. **Journal of Membrane Science**. 182:139-149.

- L. L. Hench (1998). Bioceramics, **Journal of the American Ceramic Society**, Vol. 81, No. 7, 1705-1728.
- M. Hermann and U. Gottschalk. (2000). **Bioforum** 3:172.
- Pinto, R. T. P., Wolf-Maciel, M. R. and Lintomen, L. (2000). Saline extractive distillation process for ethanol purification. **Computers and Chemical Engineering**, 24: 1689-1694.
- T. Takahashi, Ruthven D. M. (1997), **Encyclopedia of Separation Technology**. 95, New York: John Wiley.
- T. Yazawa. (1996). Present status and future potential of preparation of porous glass and its application. **Key Engineering Materials**. 115:123-146.
- Thongthai Witoon and Metta Chareonpanich (2012). Effect of pore size and surface chemistry of porous silica on CO₂ adsorption. **Songklanakarinn Journal of science and Technology**. Vol. 34: 403-407.
- Van T Nguyen, Phuong Thi Mac Nguyen, Liem X. Dang, Donghai Mei, Collin D. Wick and Duong D. Do (2014). A comparative study of the adsorption of water and methanol in zeolite BEA: a molecular simulation study. **Molecular Simulation**. Vol. 40, No. 14, 1113-1124.
- W. Schwieger, M. Rauscher, R. Monnig, F. Scheffler, D. Freude. (2000). in: A. Sayari, M. Jaroniec, T.J. Pinnavaia (Eds.). **Nanoporous Materials II, Studies in Surface Science and Catalysis**. Elsevier. Amsterdam.129:121.

CHAPTER II

PREPARATION AND CHARACTERIZATION OF POROUS SILICA BY SOL-GEL METHOD

2.1 Abstract

This chapter focuses on the preparation of porous silica from sodium silicate by the sol-gel method and the properties of the prepared porous silica were characterized. The preparation conditions including calcination temperature, pH levels of the gel solution, and mass ratio of precursors were investigated for the sol-gel process. Sodium silicate was mixed with deionized water to form an aqueous solution and the solution pH was adjusted by using 2 M of hydrochloric acid and stirred at 40 °C and held for 24 hours to form a gel by the hydrolysis reaction. The gel obtained was washed thoroughly with deionized water to remove any remaining impurities, dried and calcined for 4 hours. The obtained porous silica samples were characterized using X-ray fluorescence analysis (XRF), X-ray diffraction (XRD), Fourier transform infrared spectroscopy (FTIR), a thermogravimetric and differential thermal analyzer (TGA-DTA) and a surface area and porosity analyzer. XRD results indicated that the prepared porous silica from sodium silicate showed a strong peak of SiO₂ with high degree of amorphous phase. The pore size of the porous silica was varied by varying the pH level of the gel mixture, while the amount of silanol content on the surface of porous silica was controlled by varying the calcination temperature. The porous properties of the prepared porous silica were determined based on the analysis of N₂ adsorption isotherms

measured at 77 K (-196°C). The maximum surface area of $798\text{ m}^2/\text{g}$ and the maximum amount of silanol group content of 7.94 mmol/g were obtained under the following preparation condition: chemical weight ratio between sodium silicate and water of 4.5 g:70 ml, pH 2 for the gel mixture and the calcination temperature of 200°C . The result indicates that sodium silicate shows a potential promise for use as an inexpensive material for preparing porous silica, rather than using other more costly precursors.

2.2 Introduction

Porous silica (SiO_2) is one of the inorganic porous materials that can be easily produced from a precursor of sodium silicate. The important features of this material are that it has high thermal and chemical stability, high mechanical strength, good resistance for bacteria, narrow pore size distribution, excellent shaping ability, and can be synthesized with well controlled pore size range and transparency (Shelby, 1997). Porous silica is manufactured mainly by three processes, they are the thermal-phase separation, the sol-gel process and the crystallized process. The present work is concentrated on the preparation of porous silica glass by the sol-gel process. The sol-gel process has a number of advantages over other production methods in terms of purity, homogeneity and flexibility of modifications of material properties by adjusting the preparation parameters (Hench L., 1998). For example, the mean pore size and the functional group contents on the surface of products can be closely controlled by changing the molar ratio of water/precursor, type of precursor (Brinker and Scherer, 1990), calcination temperature and pH of the solution (Witoon and Chareonpanich, 2012).

The commercial production of porous silica by the sol-gel method involves the use of an expensive autoclave for the supercritical drying process and the use of high cost hazardous alkoxides, (for example, tetraethylorthosilicate (TEOS) or tetramethylorthosilicate (TMOS)). Further, the supercritical drying process involves the heating and evacuation of highly inflammable solvents such as alcohols which is risky at a high temperature (260 °C) and a high pressure of about 100 bars. Hence, there is a need to produce porous silica using low-cost inorganic precursors such as sodium silicate (water glass) among others.

This chapter reports on the preparation of porous silica from sodium silicate by the sol-gel method. The effect of pH levels of a mixture solution and the calcination temperature conditions on the physical and porous properties of the prepared porous silica were investigated.

2.3 General background of porous silica

2.3.1 Porous silica

Porous silica is a porous material containing silica (SiO_2) which amounts to about 96% by weight, a specific surface area varying from 10 to 300 m^2/g and an average pore size in the range from 0.4 and 1000 nm with a very narrow pore size distribution. Its porous structure gives rise to several physical properties such as reasonably high surface area, high thermal resistance, low density, low thermal conductivity and high strength (Thomas, 1992). These properties potentially find use in a vast area of applications such as catalysis, separation processes, and in electronics. Typical properties of commercially available porous silica glass prepared by the phase-separation technique obtained by heat treating and leaching out a special alkali-

borosilicate glass are shown in **Table 2.1**. As expected, its major constituent is silicon dioxide with minor composition of B_2O_3 and trace amounts of oxides of Na, Al and Zr. The BET surface area of $200 \text{ m}^2/\text{g}$ is slightly low, and the mean pore size of 5 nm indicates that porous silica is a mesoporous material. The relatively low water uptake of 25 wt% probably shows that the amount of silanol group in the form of hydroxyl group is accordingly low.

Porous silica is mostly composed of SiO_2 , therefore the detection of surface of porous silica is in effect the same as the detection of silica surface. The properties of silica can be explained by different reactivity of the various silanol adsorption sites. The silanol groups (the attachment of hydroxyl groups to silicon atoms) are the key elements to determine the adsorption and diffusion behavior of guest molecules on the external surface (Nawrocki and Buszewski, 1988).

The surface silanol group (Si-OH) on the surface of porous silica, as shown in **Figure 2.1**, can be classified into three types, (i) isolated silanol groups, (ii) vicinal silanol group (paired type), where silanol groups can form hydrogen bonds with each other, and (iii) geminal silanol group where two hydroxyls sit on the same Si atom. Porous silica is one of the inorganic porous materials that has been recognized for nearly 80 years and **Table 2.2** shows its brief historical development.

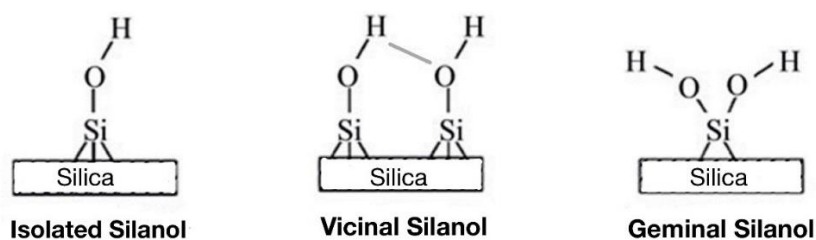


Figure 2.1 Silanol groups on the surface of porous glass (Jal et al., 2004)

Table 2.1 Typical compositions and properties of commercially available porous silica glass (Thomas, 1992)

Properties	Value
Composition on basis weight (%)	
• SiO ₂	96.3
• B ₂ O ₃	2.95
• Na ₂ O	0.04
• Al ₂ O ₃ + ZrO ₂	0.72
Appearance	Opalescent
Refractive index	1.33
Apparent density (g/cm ³)	1.5
Internal pore volume (%)	28
Average pore diameter (nm)	5
Internal surface area (m ² /g)	200
Water adsorption at saturation (%)	25

The advantages and characteristic features of these porous silica are:

- a. High thermal stability
- b. High chemical stability
- c. High mechanical strength
- d. High resistance for bacteria and viruses
- e. Very narrow pore size distribution
- f. Easy control of pore size by controlling the synthesis conditions

Table 2.2 Brief historical development of porous silica manufacturing (Yazawa, 1996)

Porous silica type	Year of production	Research group
SiO ₂	1934	Corning (Nordberg and Hood, 1994)
Developing SiO ₂	1974	Pittsburgh Plate Glass, PPG (J.J. Hammel and T. Allersma, 1974)
Shirasu system	1981	Industrial Research Institute of Miyazaki Prefecture (T. Nakashima and Y. Kuroki, 1981)
TiO ₂ system	1985	Miakonojo College (T. Kokubu and M. Yamane, 1985)
ZrO ₂ system	1986	Nanotechnology Research Institute, Osaka (Y. Mori and K. Eguichi, 1986)
PO ₄ system	1990	Nagoya Institute of Technology (H. Hosono et al., 1993)

2.3.2 Preparation of porous silica by the phase separation method

The preparation of porous silica by the phase separation method is simple and well controlled pore size of porous silica can be achieved by phase separation of the molten base glass and followed by leaching with an inorganic acid and an alkaline solution. The schematic diagram of the preparation method is illustrated in **Figure 2.2**. For the porous silica prepared from borosilicate glass by phase separation, the borosilicate glass product was immersed in an acid solution using the treatment temperature condition in the range of 730 – 760 °C (Yazawa, 1996). As a result of the hot acid treatment, the separated rich phase of $B_2O_3-Na_2O$ was therefore leached out giving the framework of silica rich phase having interconnected pores of small diameter and large pore volume, as illustrated in **Figure 2.2**.

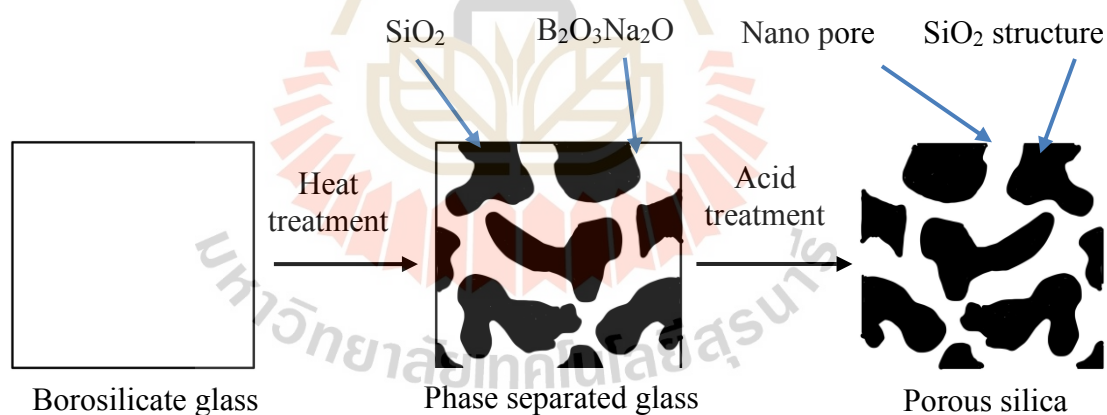


Figure 2.2 The preparation of porous silica by the phase separation method (Yazawa, 1996)

2.3.3 Preparation of porous silica by the sol-gel method

An important application of sol-gel derived porous silica glass is to use it as a matrix for nuclear waste immobilization, where the interconnected porosity is impregnated with a radioactive solution (Santos and Vasconcelos, 2000). Sol-gel process is the formation of an oxide network through polycondensation reactions of a molecular precursor in a liquid.

A sol is a stable dispersion of colloidal particles or polymers in a solvent. The particles may be amorphous or crystalline. A gel consists of a three dimensional continuous network, which encloses a liquid phase. In a colloidal gel, the network is built from agglomeration of colloidal SiO_2 particles. Generally, the sol particles may interact by van der Waals forces or hydrogen bonds. A gel may also be formed from linking polymer chains. In most gel systems used for materials synthesis, the interactions are of a covalent nature and the gel process is irreversible. The gelation process may be reversible if other interactions are involved. The chemical steps involved in the sol-gel process are polymerization, hydrolysis and condensation.

Porous silica glass can also be produced through a less expensive method involving the use of an aqueous solution of sodium silicate as a starting precursor. Sodium silicate is an inexpensive and soluble in water. Sodium silicate molecules do not hydrolyze and condense together when placed in water. However, sodium silicates are slightly basic and when neutralized with an acid such as hydrochloric (HCl) or sulfuric acid (H_2SO_4), hydrolysis will occur and silanol (Si-OH) groups will form as shown schematically in **Figure 2.3**. Once silanol groups are formed, the silicate molecules will form siloxane bonds with other silicate molecules and bridge together

to form nanoparticles, resulting in a sol. The two primary reactions involving silica glass formation from sodium silicate are shown as in **Figure 2.3**:

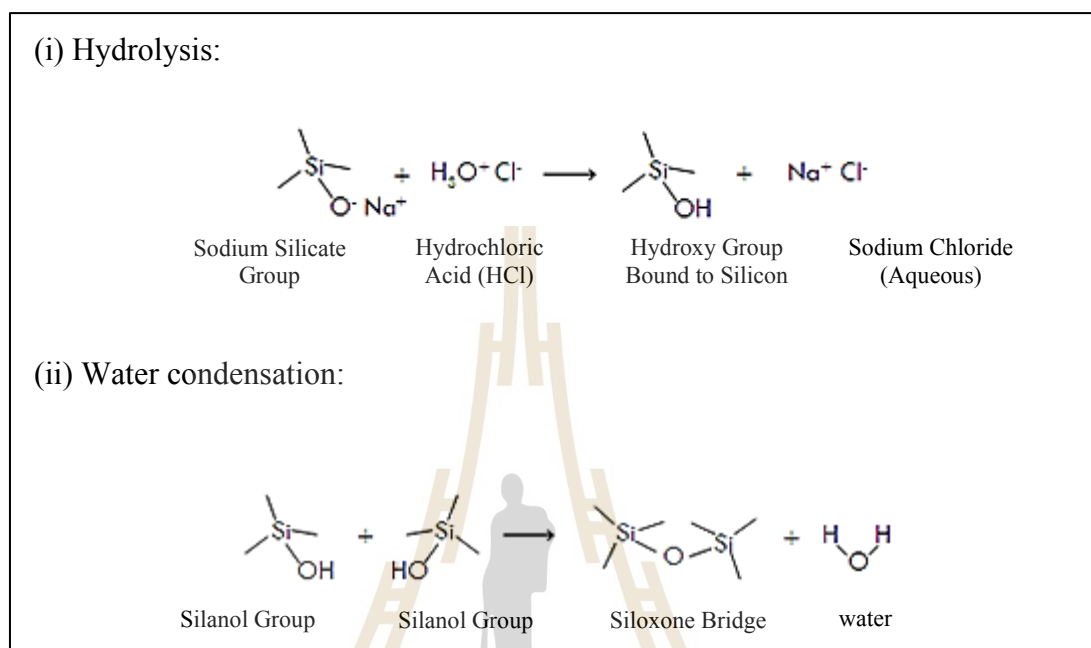


Figure 2.3 The sol-gel reaction from sodium silicate (Brodhacker, 2011)

The hydroxyl group content of silica can be determined by several different chemical and physical methods (Vansant et al., 1995). Thermogravimetric analysis (TGA) is an example of a simple and inexpensive physical method (Farias and Airoidi, 1998). The most important parameters to be considered in the thermogravimetry of silica are the heating rate and the end point of the measurement. It has been suggested that the temperature range of 200 – 600 °C are required to remove geminal silanol and vicinal silanol, and the temperature to remove isolated silanol is higher than 600 °C (Kim et al., 2009).

2.3.4 Determination of silanol contents of the porous silica products

The condensation of all types of silanol group occurs by the reaction of two silanol groups on the silica surface resulting in the release of one molecule of water and the formation of one siloxane group. It is assumed that no other groups than water is released from the sample. Based on this hypothesis, the hydroxyl (-OH) content of the silanol group (Si-OH) on porous silica surface can be estimated using the equation previously suggested by Lauri Niinisto and coworkers, (2015). The total silanol group content was calculated from the measured TGA data by using the entire second weight loss ranging from 200 °C to the end point of the measurement at 1000 °C.

$$n_{OH}(SiO_2) = 2n_{H_2O} = \frac{2[WL(T_0) - WL(T_{final})]}{100M_{H_2O}} \quad (2.1)$$

where $n_{OH}(SiO_2)$ is the hydroxyl group constant on the silica particles

$WL(T_0)$ is the weight of the silica particles (wt.%) at 200 °C

$WL(T_{final})$ is the weight of the silica particles (wt%) at 1000 °C

M_{H_2O} is the molecular weight of the water

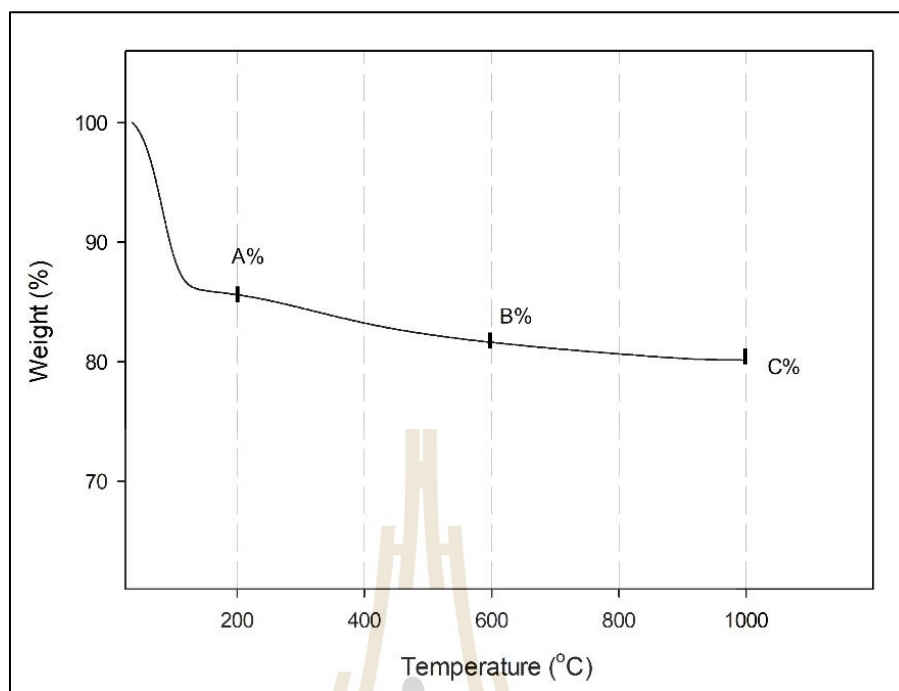


Figure 2.4 TGA patterns for calculating silanol contents on porous silica

Silanol group contents on porous silica can be estimated from weight-loss data in **Figure 2.4** and **Equation 2.1**. The measured TGA data at 200 °C has A%, 600 °C has B% and 1000 °C has C% of weight remaining. The hydroxyl group on the porous silica range of 200-600 °C = $\frac{2(A-B)}{100 \times 18}$. The amount of hydroxyl group over this range of temperatures is the hydroxyl group contents of geminal silanol and vicinal silanol, whereas the hydroxyl group on the porous silica over the range of 600-1000 °C = $\frac{2(B-C)}{100 \times 18}$ is isolated silanol contents.

2.4 Experimental

This section describes the apparatus, chemical, and methodology used for conducting the experiments on porous silica preparation.

2.4.1 Apparatus and chemicals

1. Teflon-lined autoclave, 250 mL capacity (see Figure 2.5)
2. Sieves (ASTM11, Retsch) and sieve shaker (analysette, FRITSCH)
3. Electric oven (600, Memmert)
5. Analytical balance (BP221S, Sartorius)
6. pH meter (CG840, SCHOTT)
7. Automated adsorption apparatus (ASAP 2010, Micromeritics)
8. X-ray diffractometer (XRD, Bruker D2 PHASER)
9. Thermogravimetric analyzer (SDT 2960 Simultaneous DTA–TGA, TA Instruments)
10. Fourier transform infrared spectrophotometer (FT-IR Perkin Elmer Spectrum GX, Perkin Elmer)
11. X-ray fluorescence (XRF) analyzer (Horiba XGT-5200 X-ray Analytical Microscope)
12. Sodium silicate (Na_2SiO_3) (commercial grade)
13. Hydrochloric HCl (37 % w/w)

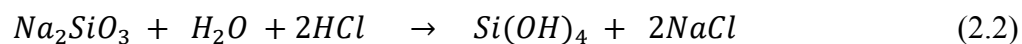


Figure 2.5 Teflon-lined autoclave (250 ml)

2.4.2 Preparation of porous silica

The porous silica was obtained through a sol-gel process consisting of hydrolysis and condensation of sodium silicate. Sodium silicate (4.5 g) was mixed with 70.0 ml of deionized water in a 250 ml Erlenmeyer flask and stirred to give a clear solution. Three solution samples were prepared and the pH of each separate solution was adjusted to 2.0, 3.0 and 4.0 by using 2 M of hydrochloric acid. The respective solution was stirred continuously at 40 °C for 24 hours and then the solution was transferred into a Teflon-lined autoclave (**Figure 2.5**) and heated at 100 °C for 24 hours in an electric oven to obtain the gel product as shown in **Figure 2.6 (a)**. This preparation procedure was followed from the work of T. Witoon and M. Chareonpanich, 2012. The obtained gel was filtered, and washed several times with distilled water to obtain the solid product as shown in **Figure 2.6 (b)**. After that, the gel was dried at 105 °C for 12 hours and calcined in air at either 200 °C or 500 °C (Witoon and Chareonpanich, 2012).

The reaction mechanisms for the formation of porous silica preparation by the sol-gel process are shown in **Figure 2.3** and the overall reaction is shown in Equation 2.2.



The obtained porous glass was kept for further analysis and characterization and for the adsorption studies. **Figure 2.7** shows the flow diagram for the preparation of porous silica from sodium silicate by the sol-gel process used in the present study.



Figure 2.6 (a) the gel product obtain in the Teflon-lined autoclave after reaction at 100 °C, for 24 hr. and (b) the solid product after washing with distilled water

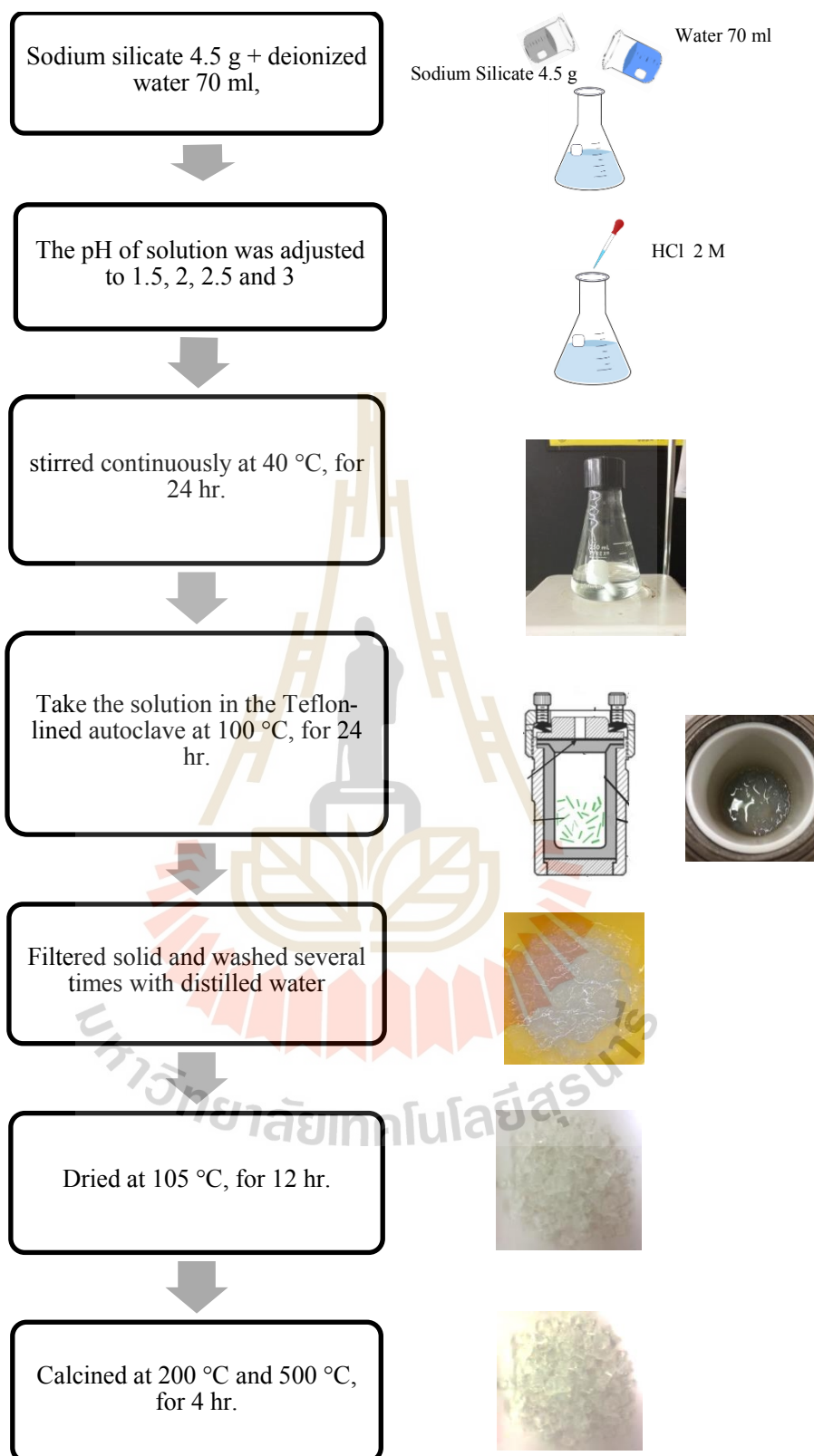


Figure 2.7 The preparation steps of porous glass by sol-gel process

2.4.3 Characterization of porous silica

2.4.3.1 X-ray fluorescence analysis (XRF)

The oxide analysis of the porous silica sample was determined using XRF Analysis Instruments (Horiba XGT-5200 X-ray Analytical Microscope) with calibration software prepared from standard reference materials.

2.4.3.2 X-ray diffraction (XRD)

The porous silica was subjected to X-ray diffraction analysis to detect the silica content and degree of crystallinity using an XRD instrument (XRD-D2 from BRUKER) equipped with Cu-K α radiation with tube voltage and current of 30 kV and 10 mA, respectively. The 2Theta of measurement is in the range of 10 to 60° by the powder method, with an increment step of 0.02° and a scanning speed of 0.04° per second.

2.4.3.3 Fourier transform infrared spectroscopy (FTIR)

The functional groups on the surface of porous silica were ascertained by using FT-IR Perkin Elmer Spectrum GX, Fourier transform infrared for the wavenumber ranging from of 400-4000 cm⁻¹.

2.4.3.4 Thermogravimetric and differential thermal analysis (TGA-DTA)

The amount of silanol groups on the surface of porous silica was determined in a simultaneous DTA-TGA analyzer (SDT 2960 Simultaneous DTA-TGA, TA Instruments) by heating the sample under the flow of N₂ from room temperature to 1000 °C using a low heating of rate of 10 °C/min and the weight remaining as a function of increasing temperature was recorded. The weight losses of the sample at 200 and 1000 °C were used in Equation 2.1 for the determination of the individual and total silanol group contents.

2.4.3.5 Surface area and porosity analyzer

The Brunauer-Emmett-Teller (BET) surface area, total pore volume and pore size distribution were determined from N₂ adsorption isotherms at 77 K using a surface area analyzer (Micromeritics ASAP2010). Before the measurement, a known weight of porous silica sample was degassed at 200°C for 12 hours under vacuum in a degassing port. Then, adsorption isotherms were collected by dosing the sample with nitrogen gas at 77 K over an increasing pressure increments. The relative pressures (P/P⁰) used for adsorption and desorption were in the range from 0.003 to 0.989 and 0.946 to 0.009, respectively. From the N₂ adsorption isotherm data, the BET surface area (m²/g) was calculated using BET theory ((Brunauer et al., 1938). The mesopore volume was estimated from the BJH theory (Barrett et al. 1951). The total pore volume was determined from the volume of N₂ adsorbed at the relative pressure (P/P⁰) of 0.98 and then converted it to the volume of liquid N₂ at 77 K. The mean pore size (\bar{D}) was computed from the formula, $\bar{D} = \frac{4V_T}{A_{BET}}$, assuming a cylindrical pore, where V_T and A_{BET} are total pore volume and BET surface area, respectively.

2.5 Results and discussion

2.5.1 Porous glass compositions by XRF analysis

Typical chemical composition results (weight %) from XRF analysis of the porous silica prepared at various conditions are shown in **Table 2.3**. It is seen that silicon dioxide is the dominant component of the prepared porous silica which constitutes more than 99% of total composition, with minor oxide compositions of chlorine, calcium, titanium and iron. As a result, the purity of porous silica prepared by the sol-gel method is extremely high. Varying the pH of the precursor solution from 2 to 4 has no significant effect on the porous silica composition.

Table 2.3 XRF results for the elemental composition of porous silica samples interpreted as oxides (weight %, normalized to 100%)

Sample	Oxides				
	SiO ₂	Cl	CaO	TiO ₂	Fe ₂ O ₃
PS2-200	99.421	0.149	0.014	0.391	0.025
PS2-500	99.213	0.380	0.017	0.338	0.052
PS3-200	99.430	0.252	0.016	0.294	0.009
PS4-200	99.366	0.342	0.018	0.254	0.020
PS4-500	99.267	0.386	0.016	0.375	0.055

2.5.2 X-ray diffraction (XRD)

The XRD results from porous silica samples are displayed in **Figure 2.8**, showing the signal varying between $2\theta = 10^\circ$ to $2\theta = 60^\circ$. The diffraction patterns are similar for all samples prepared under differing conditions which appear as a broad distribution with reflection (peak appearance) at about $2\theta = 21^\circ$ - 25° indicating that the materials are highly amorphous and consist of SiO_2 (Bhavorntanayod and Rungrojchaipon, 2009; Paramita et al. 2017). There are no additional peaks being observed for all samples. This result indicated the absence of impurities in the gel network after the deionized water washing that removed most of the NaCl formed during the gelation reaction.

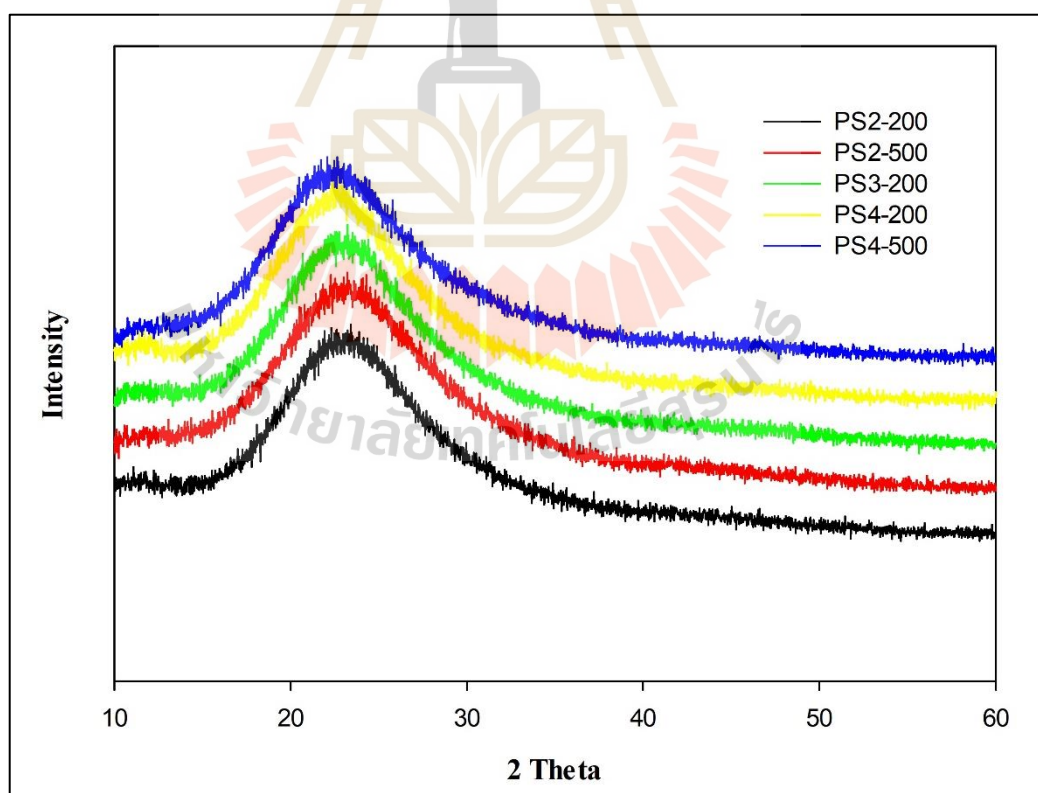


Figure 2.8 XRD patterns obtained from porous silica samples

2.5.3 Fourier transform infrared spectroscopy (FTIR)

Characterization of porous silica product with FTIR was performed to identify the major chemical groups present in the porous silica samples and the results are shown in **Figure 2.9**. The porous silica samples contain silanol and siloxane groups with varying intensity. The adsorption band of the siloxane groups are shown in the three regions of wave numbers. The FTIR spectra of most porous silica samples gave the strong band around $1000 - 1300 \text{ cm}^{-1}$ which is attributed to siloxane bonds (Si-O-Si) asymmetric stretching vibration. The peaks near and small bands around $760-850 \text{ cm}^{-1}$ and $450-490 \text{ cm}^{-1}$ represent the characteristics of Si-O-Si groups (Coates, 2000; M. Dawy, 2002). The absorption band of the silanol group comprises a vibration adsorption band OH bonding of Si-OH at wave numbers between $1620-1640 \text{ cm}^{-1}$ and a broadband at wavenumbers around $3200-3800 \text{ cm}^{-1}$ is assigned to the silanol groups on the surface of the porous silica samples (Coates, 2000; Karbowski et al., 2010; Wahyuni et al., 2018). The shoulder at about $900 - 980 \text{ cm}^{-1}$ is also related to the residual silanol groups, resulting from a stretching motion of oxygen atoms not bridging two Si atoms, with contributions from Si-O- and Si-OH vibrations (Coates, 2000; Aguiar et al., 2009). The band of OH stretching vibration correlates to silanol active sites (Widjonarko et al., 2014). The water adsorbed onto material surface correlates with the presence of silanol active sites, oxygen atom of water molecules interacts with hydrogen atom of porous silica to form hydrogen bonding. **Table 2.4** summarizes the assignment for the infrared spectrum of the various function groups present at several wavenumbers.

Table 2.4 Summary of functional groups presenting at different wave numbers of FTIR analysis

Functional group	Group frequency, wavenumber (cm ⁻¹)	Assignment	References
Si-O	1000-1300	Si-O-Si asymmetric stretching vibration	J. Coates, 2000
Si-O	900-980	Si-OH stretching vibration	J. Coates, 2000; Aguiar H. et al., 2009
Si-O	760 – 850	Si-O-Si asymmetric wagging vibration	M. Dawy, 2002
Si-O	450 – 490	Si-O-Si bending vibration	M. Dawy, 2002
O-H	1620-1640	O-H bend at silanol group	V. H. Le, 2013
O-H	3731	Isolated silanols (OH stretch)	J. Coates, 2000; T. Karbowski et al., 2010
O-H	3200-3650	Vicinal hydrogen bonded silanols and Germinal silanol (OH stretch)	J. Coates, 2000; T. Karbowski et al., 2010

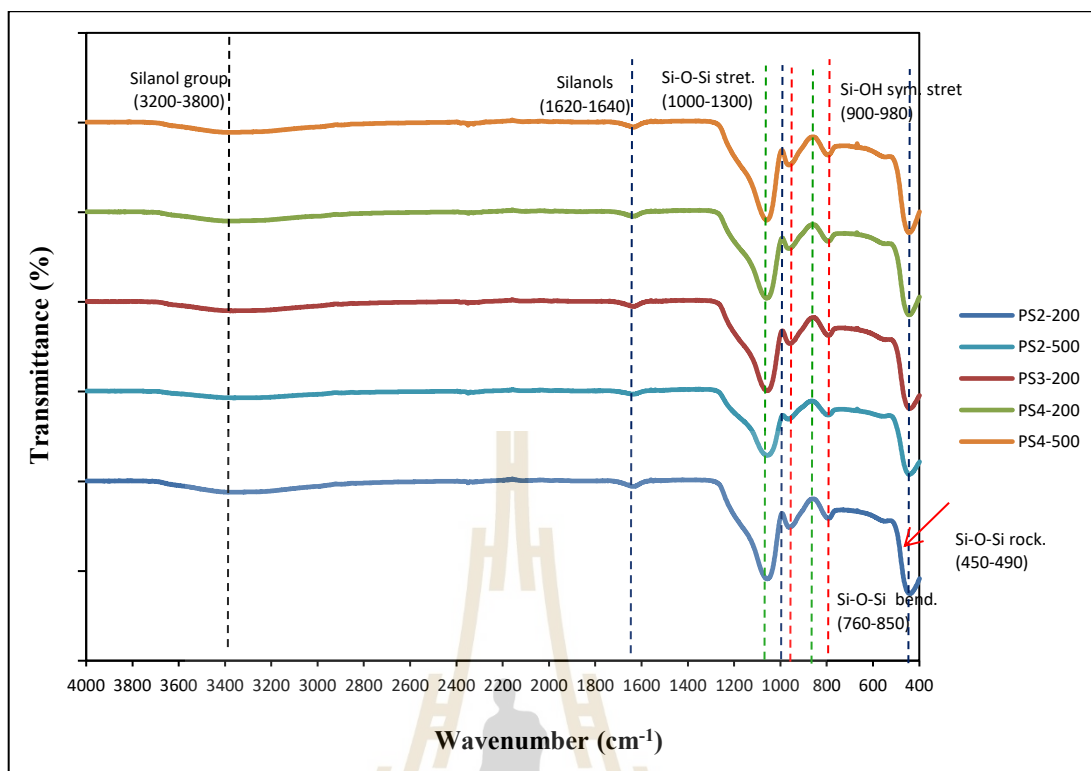


Figure 2.9 FTIR spectra of porous silica products

2.5.4 Determination of hydroxyl group of the porous silica products

Thermogravimetric analysis (TGA) was adopted in this study for the determination of the concentration of silanol group (-OH) on the surface of porous silica samples. The non-isothermal heating by TGA on the porous glass samples was programmed from room temperature to the final temperature of 1000 °C. **Figure 2.10** shows the drop of sample weight from 200 °C to almost a constant value at 800 °C, for porous silica samples prepared with different pH and calcination temperatures. The temperature-dependent behavior of the weight loss was similar in all cases. It appeared that there were two weight loss regions of the TGA curves. The first region showed the abrupt decrease of the sample weight for temperatures lower than 120 °C, and this was attributed to the removal of physically adsorbed water from the silica surface (Witton

and Chareonpanich, 2012). The second consecutive region from 120 to 200 °C displayed a gradual decrease of the sample weight which was the result of slow condensation of the existing silanol groups (Witoon and Chareonpanich, 2012). The weight loss over the temperature from 200 to 600 °C (zone II) represents the decomposition of the geminal and vicinal silanol groups, whereas the weight loss from 600 to 1000 °C (zone III) results from the decomposition of the isolated silanol. **Table 2.5** shows the computed silanol group contents in terms of hydroxyl group (OH) contents. It is noted that the amounts of each type of silanol and the total silanol contents decreased when the porous silica was synthesized at higher values of pH and a higher calcination temperature. It was observed that the increase in the calcination temperature at a constant pH during the preparation steps tended to decrease the amount of silanol content (PS2-200 vs PS2-500). Increasing the pH values from 2 to 4 at a constant calcination temperature of 200 °C also decreased the silanol contents. The total silanol content decreased from 7.94 mmol/g at pH 2 to 2.77 mmol/g at pH 4. This can be attributed to the increasing rate of silanol condensation in the synthesis reaction at a higher pH value (Witoon and Chareonpanich, 2012).

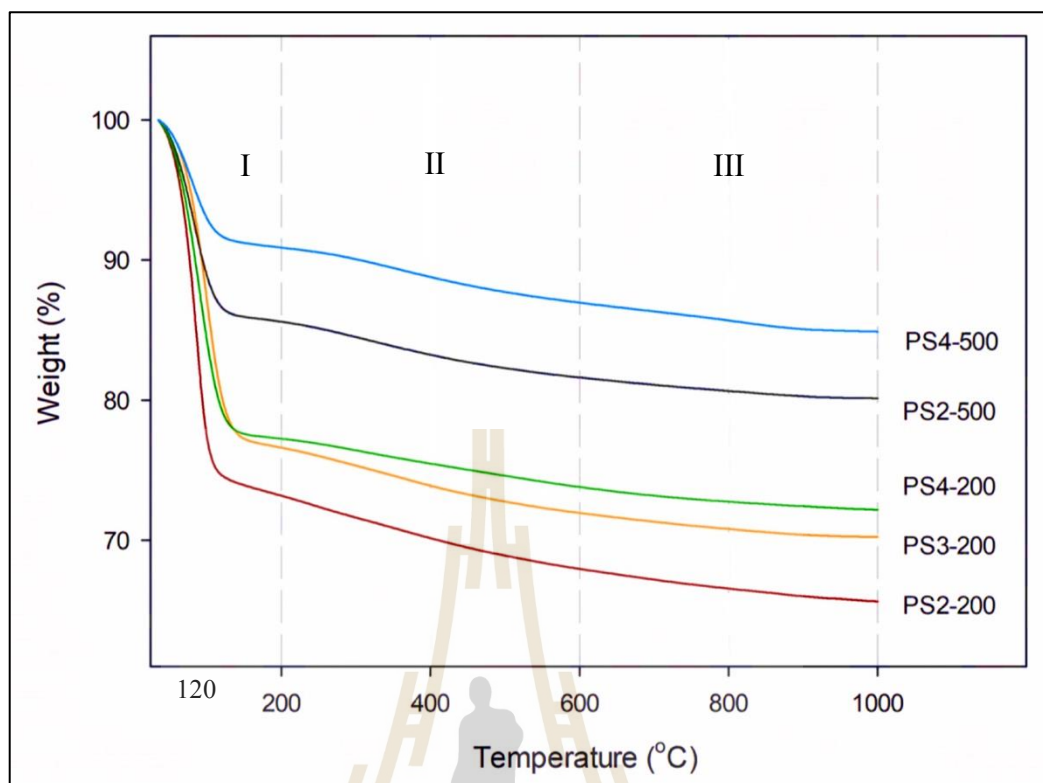


Figure 2.10 TGA patterns of porous silica products

Table 2.5 The silanol group content determined by TGA techniques

Samples	Geminal and Vicinal Silanols Content (mmol OH/g)	Isolated Silanols Content (mmol OH/g)	Total Si-OH Group Content (mmol/g)
PS2-200	4.48	3.46	7.94
PS2-500	3.92	0.26	4.18
PS3-200	4.32	1.73	6.05
PS4-200	3.86	0.36	4.22
PS4-500	2.63	0.14	2.77

*porous silicas were designated as PSX-Y where X is the pH of solution mixture, Y is the calcination temperature and PS is the Porous Silica.

2.5.5 Determination of porous properties of the porous silica

Figure 2.11 shows isotherms of N₂ adsorption at 77 K of the tested porous silica. The adsorption isotherms for PS2-200 and PS2-500, having small pore sizes, showed a continuous increase in the amount of N₂ adsorbed with an increase of relative pressure up to the value of 0.17, before it approached a constant value at higher relative pressures. These isotherms did not show hysteresis loops and their shapes resembled the initial part of the Type II isotherm, according to the IUPAC classification (Sing et al., 1985). The porous glass synthesized at pH 3 (PS3-200), having an intermediate pore size, showed an adsorption isotherm with a hysteresis loop. According to the IUPAC classification of isotherms with hysteresis loops (Sing et al., 1985), this porous glass exhibited Type H2 isotherm. It showed a broad, almost flat plateau, and the steep characteristic of a desorption branch. This type of isotherm indicates that the pore structure of an adsorbent consists of interconnected networks of pores having different shapes and sizes (Rouquerol et al., 1999). The isotherms of porous glass having large pore sizes (PS4-200 and PS4-500) also showed isotherms with hysteresis loops, which can be classified as Type H1 isotherm (Sing et al., 1985). The isotherms showed a relatively narrow loop, with very steep and almost parallel adsorption and desorption branches, indicating that the adsorbent has a narrow distribution of uniform pores (Rouquerol et al., 1999).

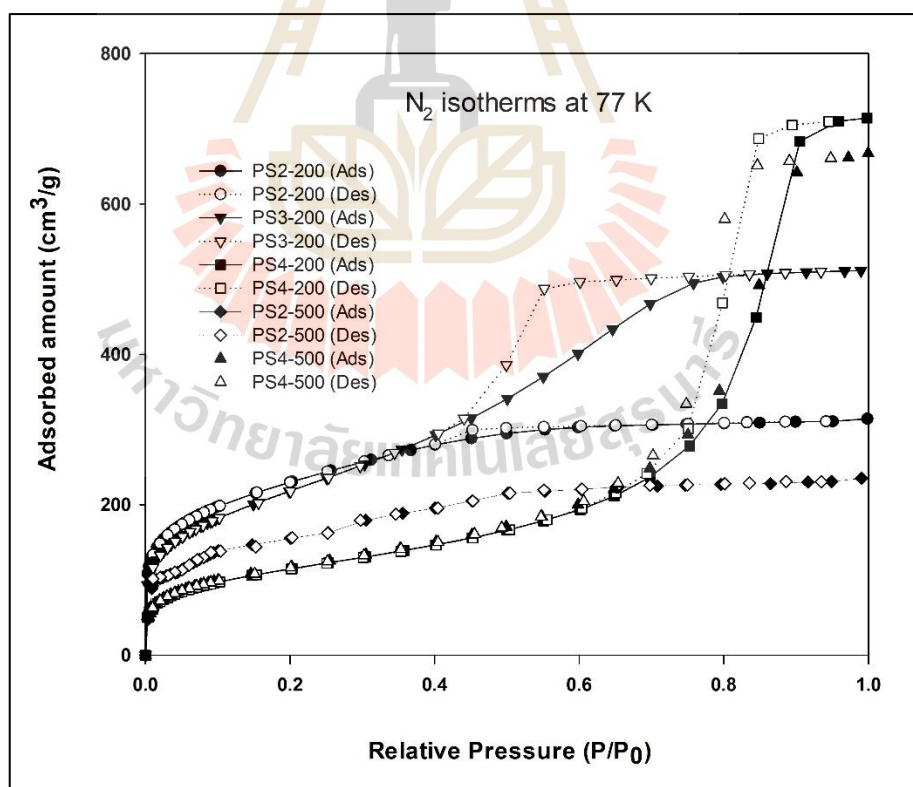
The derived N₂ adsorption isotherms of the prepared porous glass were used to determine the porous properties of the adsorbents and the results are presented in **Table 2.6**. Based on the percentage of mesopore volume, it can be seen that all the porous glass samples exhibited a mesoporous type of adsorbent materials, with the mesopore volume varying from 62.4% to 98.5%. The average pore size increased from

the value of 2.4 to 10.3 nm as the pH changed from the value of 2 to 4 (compare samples PS2-200, PS3-200, and PS4-200). The increase in pore size of the porous glass with increased pH was also observed in the previous studies (Munoz-Aguado et al., 1996; Witoon and Chareonpanich, 2012). This was hypothesized to result from the increasing formation of highly branched silica oligomers due to the increasing condensation rate of silanol species that can prevent gel shrinkage as the pH of solution was increased. Increasing the pH also enhanced the development of mesopores of the prepared porous glass. The mesopore volume and the total pore volume increased almost threefold as the pH increased from the value of 2 to 4. On the other hand, the total BET surface area was found to decrease with the increase of pH, with the value decreasing almost twofold from 798 to 413 m²/g. The porous properties of the porous glass were also affected to a certain extent by the change in the calcination temperature. However, the average pore size remained almost unchanged by the increase in the calcination temperature from 200 to 500 °C. However, an increase in the calcination temperature from 200 to 500 °C decreased the BET surface area by 21% and 2.2% for the PS2 and PS4 samples, respectively.

Table 2.6 Physical properties of porous silica products synthesized at different conditions

Samples *	Average Pore Size (nm)	BET Surface Area (m ² /g)	Micropore Volume (cm ³ /g)	Mesopore Surface Area (m ² /g)	Total Pore Volume (cm ³ /g)	Mesopore Volume (cm ³ /g)
PS2-200	2.4	798	0.183 (37.6%)	719	0.487	0.304 (62.4%)
PS2-500	2.2	630	0.062 (15.9%)	596	0.391	0.329 (84.1%)
PS3-200	5.0	778	0.062 (7.8%)	739	0.791	0.729 (92.2%)
PS4-200	10.3	413	0.017 (1.5%)	399	1.105	1.088 (98.5%)
PS4-500	10.9	404	0.016 (1.6%)	390	1.032	1.016 (98.4%)

*porous silicas were designated as PSX-Y where X is the pH of solution mixture, Y is the calcination temperature and PS is the Porous Silica.

**Figure 2.11** N₂ adsorption isotherm at 77 K on the porous silica samples.

2.6 Conclusions

In this work, porous silica was prepared by the sol-gel technique using sodium silicate as a precursor. The preparation conditions including calcination temperature, and pH levels were investigated for the sol-gel process. The results indicated that pH level in solution of 2 gave porous silica with the highest amount of silanol group of 7.94 mmol/g and 4.18 mmol/g for calcination temperature at 200 °C and 500 °C, respectively. Sol-gel process is an effective method to control the pore structure and the amounts of silanol group of porous silica. The porous silica obtained was amorphous, having the average pore size of 2.2 to 10.9 nm, and the BET result showed that the specific surface area of the porous silica was 404 to 798 m²/g. The use of low pH value and a low calcination temperature during the preparation step gave the largest specific surface area. It is also clear that other porous properties such as mesoporous area and total pore volume showed the same trend as to the effect of pH and calcination temperature.

2.7 References

- Brinker C.J. and Scherer G.W. (1990). Sol–gel science, the physics and chemistry of sol–gel processing. **Academic Press**. Boston.
- Chayakorn Bhavornthanayod and Pesak Rungrojchaipon (2009). Synthesis of zeolite a membrane from rice husk ash. **Journal of Materials and Minerals**, Vol. 19, No. 2: 79-83
- Chaturaporn Nimjaroen, Shigeki Morimoto and Chaiyot Tangsathitkulchai (2009). Preparation and properties of porous glass using fly ash as raw material. **Journal of Non-Crystalline Solids**, Vol. 355:1737-1741
- Dian Maruto Widjonarko, Jumina, Indriana Kartini and Nuryono (2014). Phosphonate modified silica for adsorption of Co (II), Ni (II), Cu (II) and Zn (II). **Indonesian Journal of Chemistry**, Vol. 14, No. 2: 143-151
- Duong D.Do (1998). Adsorption analysis equilibria and kinetics. **Imperial College Press**. Singapore.
- Ezzat Rafiee, Shabnam Shahebrahimi, Mostafa Feyzi and Mahdi Shaterzadeh (2012). Optimization of synthesis and characterization of nanosilica produced from rice husk (a common waste material). **International Nano Letters**, 2:29
- Farias R.F. and Airoidi C. (1998). Thermogravimetry as a reliable tool to estimate the density of silanols on a silica gel surface. **Journal of Thermal Analysis and Calorimetry**. 53: 751-756.
- Gladys Ayu Paramita Kusumah Wardhani, Nurlela Nurlela, Mia Azizah (2017). Silica content and structure from corncob ash with various acid treatment (HCl, HBr, and Citric Acid). **Molekul**, Vol.12, No. 2:174-181

- Hench L. L. (1998). Bioceramics, **Journal of the American Ceramic Society**, Vol. 81, No. 7, 1705-1728.
- John Coates (2000). Interpretation of infrared spectra, a practical approach. Encyclopedia of Analytical Chemistry, Meyers ed., **John Wiley & Sons Ltd**, Chichester, 10815-10837.
- Jong Min Kim, Sang Mok Chang, Sung Min Kong, Kyo-Seon Kim, Jinsoo Kim and Woo-Sik Kim. (2009). Control of hydroxyl group in silica particle synthesized by the sol-precipitation process. **Ceramics International**. 35: 1015-1019.
- K. Lisa Brodhacker (2011). Sol-Gel Processing. Alt-Az Initiative for Lightweight Optics. Kona, Hawaii.
- Lijuan Chen, Xiaoping Wang, Zhixin Jia, Yuanfang Juo and Demin Jia (2015). Use of precipitated silica with silanol groups as inorganic chain extender in polyurethane. **Material and Design**. 87: 324-330
- M. Dawy (2002). Electrical properties and infrared studies of heated Mica sheets. **Egyptian Journal of Soil Science**. Vol. 25, No. 1:137-152
- Munoz-Aguado M.J and Gregorkiewitz, M. (1996). Preparation of silica-based microporous inorganic gas separation membranes. **J. Membr Sci**. Vol. 111, 7–18.
- Nawrocki J. and Buszewski B. (1988). Influence of silica surface chemistry and structure on the properties, structure and coverage of alkyl-bonded phases for high-performance liquid chromatography. **Journal of Chromatography**. 449: 1–24.

- Rouquerol, F, Rouquerol, J and Sing, K. (1999). Adsorption by Powders and Porous Solids: Principles, Methodology and Applications; **Academic Press**: Cambridge, MA, USA.
- S. Ek, A. Root, M. Peussa and L. Niinisto (2001). Determination of the hydroxyl group content in silica by thermogravimetry and a comparison with HMAS NMR results. **Thermochimica Acta**. 379: 201-212.
- Shelby, J.E., 1997. Introduction to glass science and technology. **The Royal Society of Chemistry**.
- Sing, K.S.W.; Everett, D.H.; Haul, R.A.W.; Moscou, L.; Pierotto, R.A.; Rouquerol, J.; Siemieniewska, T. (1985). Reporting Physisorption Data for Gas/Solid systems, with special reference to the determination of surface area and porosity, International Union of Pure and Applied Chemistry. **Pure Appl. Chem**. Vol. 57, 603–619.
- Thongthai Witoon and Metta Chareonpanich (2012). Effect of pore size and surface chemistry of porous silica on CO₂ adsorption. **Songklanakarinn Journal of science and Technology**. Vol. 34: 403-407.
- Thomas H. E. (1992). Porous and reconstructed glasses. **Engineered Material Handbook**: Ceramic and Glasses.
- T. Yazawa (1996). Present Status and Future Potential of Preparation of Porous Glass and Its Application. Porous Ceramic Materials. Ed. D-M. Liu, **Trans Tech Publications**, Switzerland, pp.125-146.
- Vansant E.F., Van Der Voort P., Vrancken K.C. (1995). Characterization and chemical modification of the silica surface. **Elsevier**.

Van Hai Le, Chi Nhan Ha Thuc and Huy Ha Thuc (2013). Synthesis of silica nanoparticles from Vietnamese rice husk by sol-gel method. **Nanoscale Research Letters**. 8:58



CHAPTER III

ETHANOL DEHYDRATION BY POROUS SILICA

3.1 Abstract

This chapter focuses on the equilibrium adsorption of water from an ethanol mixture solution in liquid phase and vapor phase by porous silica prepared by the sol-gel method. In addition, the effects of temperature, mean pore size, and amount of surface silanol group of porous silica on water vapor adsorption were investigated. The experimental results illustrated that the water adsorption in the liquid phase and the vapor phase depended on both the porous structure and the amount of silanol group.

The experiments were divided into two parts with the first part involving water adsorption in a batch liquid phase system, covering the temperature of adsorption between 20-40 °C and the ethanol concentration in the range of 60-95% by weight. The batch adsorption system was able to increase the concentration of ethanol up to 97.3% by weight. It was found that the Langmuir equation could best describe the equilibrium adsorption of water and the pseudo second-order model could well predict the adsorption kinetics of water by porous silica. In the second part, the separation of ethanol-water mixtures in gas phase using porous silica was conducted in a laboratory-scale fixed-bed adsorption system by collecting the breakthrough data for water adsorption. Effects of process parameters including adsorbent quantity, temperature, mean pore size, amount of silanol group on the surface of porous silica, and vapor feed flow rate on the dynamics of water adsorption by porous silica were investigated. The adsorption system was able to break the azeotropic composition of 95.6% by weight of

ethanol, giving the final ethanol product concentration of higher than 99% by weight. Water breakthrough data were presented and compared reasonably well with those predicted by the Klinkenberg's equation based on a linear-driving force model for water uptake rate.

3.2 Introduction

At present, the demand for energy from petroleum-based fuels is increasing which affects the stability of both price and supply. Thailand is highly dependent on fuel import especially for the transportation sector which accounts for about 72% of oil demand and 28% of gas demand in 2009 (IEA, 2011). Conservative prediction suggests that Thailand will inevitably continue to increase the import of oil and gas to keep up with the economic development of the country. Therefore, to ease the energy burden, the government has a strong policy toward the increasing use of alternative energy sources.

On this aspect, the exploitation of energy from biomass is quite promising due to the abundant availability of biomass in various forms. The generation of energy from biomass is effectively achievable through thermal conversion processes, for example, direct combustion, gasification and pyrolysis as well as by fermentation to produce ethanol fuel. Fermentation is the process by which microorganisms such as yeast and bacteria convert organic molecules into many various products. More importantly and interestingly, for biofuels the typical useful fermentation product such as ethanol can be directly used as a liquid fuel in transport vehicles.

Ethanol produced by fermentation ranges in concentration from a few percent up to about 14% by volume and is further concentrated by fractional distillation under

atmospheric pressure to the maximum azeotropic point of 95.6% by weight of ethanol. A number of processes have been developed to break the azeotrope of an ethanol-water mixture to obtain anhydrous ethanol, such as azeotropic distillation, extractive distillation, molecular sieves adsorption and membrane separation (Banat et al., 2000 and Pinto et al., 2000). Extractive distillation can bring ethanol concentration up to an anhydrous level but the energy consumption is also high and it requires the use of toxic organic entrainers such as benzene, hexane, isooctane and acetone (Pinto et al., 2000). Alternatively, the dehydration of ethanol by adsorption and membrane separation are more attractive because of its non-toxicity and lower energy consumption, which amounts to 50–80% of the overall energy required by the fermentative process (Ladisich, 1997 and Banat et al., 2000).

The separation of water from ethanol by adsorption with a porous adsorbent offers many desirable advantages including ease of operation, low operating cost, capability of pore size and surface chemistry modification, availability of many types of adsorbents and capability of adsorbent regeneration. Among the various possible adsorbents for ethanol dehydration, porous silica is a viable and potential adsorbent for effective removal of water from an ethanol-water mixture. It has a number of promising characteristics such as high thermal stability, resistance to chemical attack and narrow pore size distribution (Thomas, 1992). Furthermore, the presence of associated hydroxyl groups or known as silanol groups can give a favorable effect for the adsorption of water through the formation of hydrogen bonds (Nuyen et al., 2014).

In this study, porous silica was prepared from sodium silicate by the sol-gel method and was used to investigate the removal of water from the mixture of water and ethanol for an ethanol concentration range near the azeotropic concentration. The

experiments were divided into two parts. The first part is focused on the batch adsorption of water in the liquid phase of ethanol solution to obtain water adsorption isotherms at various temperatures. The second part involved the study of water removal from the mixture of water and ethanol in vapor phase using a continuous fixed-bed adsorber packed with porous silica (or known as adsorption distillation method) by collecting water breakthrough data as a function of time. The effect of process variables on the dynamics of water adsorption were investigated, including the amount of porous silica adsorbent, feed flow rate, adsorption temperature, the amount of silanol group and pore structure of the adsorbent.

3.3 Background information

3.3.1 Ethanol

Ethanol (ethyl alcohol) is a clear colorless liquid. It is a straight chain alcohol and its molecular formula is C_2H_5OH . It is an alcohol whose molecules contain a hydroxyl group (OH) which is bonded to a carbon atom. Ethanol boils at $78.5^\circ C$ and has a density of 0.789 g/mL at $20^\circ C$ (Raymond et al., 1991). Ethanol has become more attractive in fuel industry either as a fuel itself or as an additive that helps enhancing the octane number and combustibility of gasoline.

There are two general methods for ethanol production, namely by chemical synthesis from ethylene and by biochemical process through the fermentation of sugars. Zymase, an enzyme from yeast, is used to change the simple sugars into ethanol and carbon dioxide in the fermentation process. The fermentation reaction is represented by the following simple equation (Wasey, 2002):



The ethanol produced by fermentation ranges in concentration from a few percent up to about 14% by volume of ethanol. Ethanol is normally concentrated by atmospheric distillation of aqueous solutions but the maximum composition of the vapor from aqueous ethanol is 96% by volume of ethanol and 4% by volume of water, known as an azeotropic mixture. Therefore, pure ethanol cannot be directly obtained by a simple distillation process.

The mixture of ethanol and water forms an azeotrope at about 89% mole of ethanol and 11% mole of water (96% volume of ethanol and 4% volume of water) at normal atmospheric pressure and temperature at 351 K. This azeotropic composition is strongly temperature and pressure dependent and vanishes at temperatures below 303 K. **Figure 3.1** shows vapor-liquid equilibrium of a mixture of ethanol and water at atmospheric pressure. Hydrogen bonding causes pure ethanol to be hygroscopic to the extent that it readily absorbs water from the air. The polar nature of the hydroxyl group causes ethanol to dissolve many ionic compounds. Processes have been developed to break the azeotropic point of ethanol and water for the preparation of anhydrous ethanol, such as azeotropic distillation, adsorption separation and membrane separation. Among these processes, adsorption is particularly attractive because of its lower energy consumption, which takes up 50–80% of the overall energy required by the fermentative plan (Banat et al., 2000). The various facts about ethanol are highlighted as follows.

- 1) Using ethanol as a fuel

At present, ethanol is used in combustion engines in three different forms.

- (i) Pure ethanol (100%) can be utilized only in specially modified engines.

- (ii) The concentration of ethanol over 99.5% by weight of ethanol.

This ethanol can be blended with gasoline in various ratios and with different names as follows: E10 is a blend consisting of ethanol: gasoline 10: 90 by volume, E20 is a blend consisting of ethanol: gasoline 20:80 by volume. This combination is usable in any combustion engines. E85 is a blend consisting of ethanol: gasoline 85: 15 by volume. A standard engine can be modified to run on E85.

- (iii) The ability to increase considerably the octane number of gasolines by conversion of ethanol into ETBE (Ethyl Tertiary Butyl Ether) which is a substitute to replace MTBE (Methyl Tertiary Butyl Ether).

2) The benefits of using ethanol

- (i) Ethanol is friendly to the environment

Overall, ethanol is considered to be better for the environment than gasoline. Fueled vehicles run on ethanol produce lower carbon monoxide and carbon dioxide emissions, and the same or lower levels of hydrocarbon and oxides of nitrogen emissions (IEA, 2011 and Thomas et al., 2012).

- (ii) Ethanol is widely available and easy to use

Flexible fuel vehicles that can use E85 are widely available and come in many different styles from most major auto manufacturers. Flexible fuel vehicles have the advantage of being able to use E85, gasoline, or a combination of the two, giving drivers the flexibility to choose the fuel that is most readily available and best suited to their needs (Thomas et al., 2015).

(iii) Ethanol is good for the economy

Ethanol production supports farmers and creates domestic jobs.

Because ethanol is produced domestically, from domestically grown crops, it could reduce dependence on foreign oil and increases the nation's energy independence.

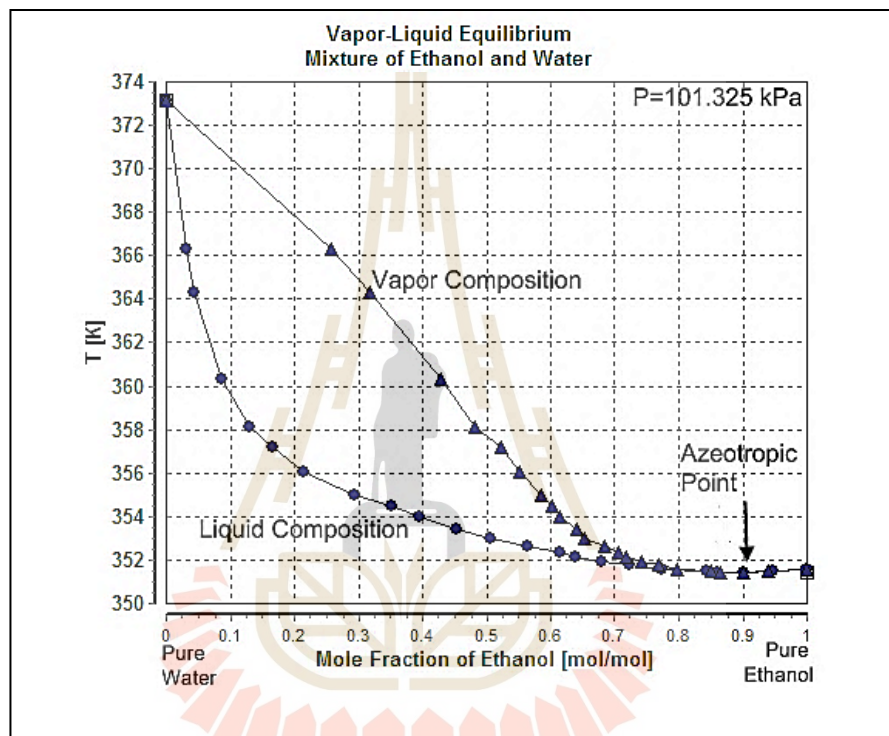


Figure 3.1 Vapor-liquid equilibrium of a mixture of ethanol and water

(Wilfried Cordes, 2008)

3.3.2 Adsorption process

Adsorption process occurs when a gas or a liquid substance accumulates on the surface of a porous solid by interaction forces, forming a molecular or atomic layer. The porous solid is called adsorbent and the substance which is adsorbed is called adsorbate. Generally, adsorption is divided into two types, namely physical adsorption and chemical adsorption.

In the physical adsorption process, the attraction between adsorbate molecules and the adsorbent occurs by the intermolecular forces i.e. van der Waals forces. These forces are relatively weak. During the process of physical adsorption, there is no breakage of the covalent structure of the adsorbate taking place, so this adsorption process is very rapid with the equilibrium established quickly. Physical adsorption is an exothermic and reversible process.

Chemical adsorption involves the transfer of electrons between adsorbent and adsorbate molecules with the formation of chemical bonds by chemical reaction, so these interactions are stronger than the force of physical adsorption. Chemical adsorption is more specific between the adsorbate and the surface site of adsorbent. Chemical adsorption is a slow reaction process for which the equilibrium may take a long time to achieve. The differences in the physical adsorption and chemical adsorption process are summarized in **Table 3.1**.

Table 3.1 Comparison of parameters of type of adsorption process (Ruthven, 1997).

Parameter	Physical adsorption	Chemical adsorption
Heat of adsorption	low	high
Nature of adsorbed phase	monolayer or multilayer	monolayer only
Temperature range	only significant at relatively low temperatures	possible over a wide range of temperature
Temperature dependence of uptake (with increasing temperature)	decrease	increase
Forces of adsorption	no electron transfer although polarization of adsorbate may occur	electron transfer leading to bond formation between adsorbate and adsorbent molecules
Rate of adsorption (at 273 K)	fast	slow
Desorption	easy by reducing pressure or increasing temperature	difficult (high temperature required to break bonds)
Desorbed species	adsorbate unchanged	may be different from the original adsorptive
Specificity	non-specific	very specific

3.3.3 Adsorption isotherms

The equilibrium relationship between an adsorbate and an adsorbent is usually defined in terms of an adsorption isotherm which expresses the amount of adsorbate being adsorbed as a function of the fluid-phase concentration or partial pressure for gas and vapor at a constant temperature. IUPAC has extended the original adsorption isotherm classification proposed by Brunauer, Deming, Deming, and Teller (Type I – Type V) to give six classes of gas adsorption isotherms, as shown in Figure 3.2 (Rouquerol, et al., 1999).

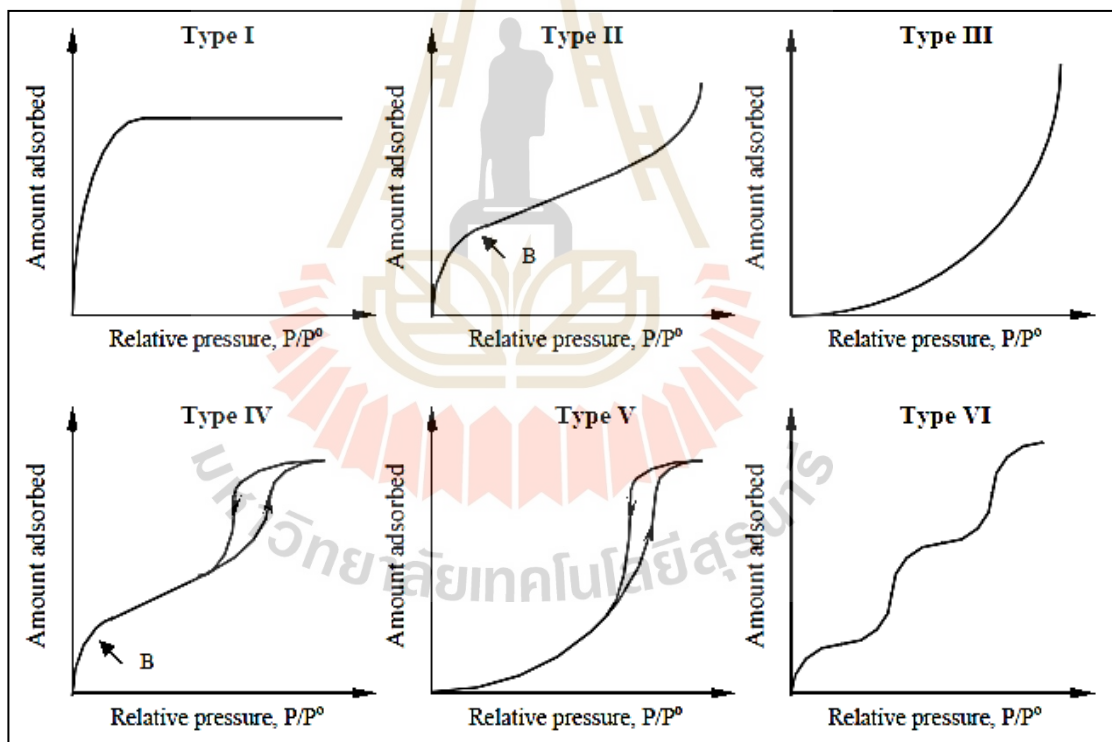


Figure 3.2 Types of gas adsorption isotherms according to the IUPAC classification (Rouquerol, et al., 1999).

Type I isotherm is concave to the relative pressure (P/P^0) axis. This isotherm rises sharply at low relative pressures and reaches a plateau as the relative pressure approaches unity. Type I isotherm represents a system where only monolayer adsorption occurs.

Type II isotherm is concave to the relative pressure axis, then almost linear and finally convex to the relative pressure axis. At the knee of the isotherm (point B), the uptake is usually considered to represent the completion of the monolayer and the beginning of the formation of the multimolecular layer (multilayer adsorption). This isotherm is obtained with non-porous or macroporous adsorbents which allow unrestricted monolayer-multilayer adsorption to occur at high relative pressures.

Type III isotherm is convex to the relative pressure axis and therefore without the knee of the isotherm. This isotherm indicates the weak adsorbent-adsorbate interactions. Type III isotherm is not common.

Type IV isotherm is closely related to the Type II isotherm at low relative pressures but tends to level off at high relative pressures. This isotherm exhibits a hysteresis loop which is associated with the filling and emptying of the mesopores by capillary condensation phenomenon.

Type V isotherm is initially convex to the relative pressure axis and also tends to level off at high relative pressure. This isotherm is similar to Type III isotherm except there is an existence of a hysteresis loop. Type V isotherm is relatively rare.

Type VI isotherm is a stepped isotherm. This isotherm is associated with layer-by-layer adsorption on a highly uniform surface. The sharpness of the steps is dependent on the adsorption system and the temperature. Type VI isotherm is also relatively rare.

3.3.4 Adsorption isotherms equations

The quantity of adsorption that can be taken up by an adsorbent is a function of both the characteristics and concentration of adsorbate and the temperature.

(1) Linear adsorption isotherm

The linear isotherm is realized at low adsorbate concentrations, for example, the adsorption of water from a high ethanol concentration solution by zeolite adsorbent since water concentration in the vapor feed to the adsorption column is relatively low (~5 – 10% by weight). The isotherm equation reads,

$$q = Kc \quad (3.1)$$

where K is the Henry's constant, q is the mass of water adsorbed in g/mL of adsorbent and c is the concentration of adsorbate in g/mL. In this case then, K is dimensionless.

(2) The Langmuir adsorption isotherm

In this model, adsorption is considered to be in a dynamic equilibrium, whereby the rate of adsorption of gas molecules onto a flat surface is equal to the rate of desorption of molecules from the surface.

The Langmuir adsorption isotherm was developed based on the following assumptions (Do., 1998):

- 1) Ideal gas behavior is assumed for the bulk gas phase
- 2) The molecules are adsorbed at definite, localized sites
- 3) Each site can accommodate only one molecule. Therefore, maximum adsorption corresponds to a monolayer capacity.
- 4) Surface is homogeneous, that is the energy of adsorption is constant over all sites and there is no interaction between adjacent adsorbed molecules.

When applied to liquid adsorption, the final derived Langmuir isotherm is obtained as follows,

$$q = \frac{k_L q_m C_e}{1 + k_L C_e} \quad (3.2)$$

where q is mass of adsorbate adsorbed in g/mL or g/g of adsorbent

q_m is the maximum loading corresponding to complete coverage of the surface by the adsorbate in g/mL or g/g of adsorbent.

C_e is the equilibrium concentration of adsorbate in the liquid phase, g/mL

k_L is Langmuir or affinity constant of the Langmuir adsorption isotherm

The constants in the Langmuir isotherm equation can be determined by plotting C_e/q versus C_e from the following linear equation of Langmuir isotherm,

$$\frac{C_e}{q} = \frac{1}{q_m k_L} + \frac{C_e}{q_m} \quad (3.3)$$

from which q_m is equal to $(slope)^{-1}$ and k_L is obtained from the ratio of slope/intercept.

(3) The Freundlich adsorption isotherm

The empirically derived Freundlich isotherm is in the following form:

$$q = K C_e^{1/n} \quad (3.4)$$

where q is mass of adsorbate adsorbed in g/mL of adsorbent or g/g adsorbent

C_e is the equilibrium concentration of adsorbate in the bulk phase g/mL

K and n are constants of Freundlich adsorption isotherm equation

The Freundlich adsorption isotherm was developed based on the monolayer adsorption on a heterogeneous surface i.e., adsorption energy is not constant but dependent on adsorption loading. It has no Henry's law limit and no saturation limit at a high concentration.

The constants in the Freundlich isotherm can be determined by plotting q versus C_e on log-log scale based on the following linear equation,

$$\log q = \log K + \frac{1}{n} \log C_e \quad (3.5)$$

where n is slope⁻¹ and K is 10^{intercept}.

3.3.5 Adsorption kinetic models

3.3.5.1 Pseudo-first-order rate equation

The Lagergren pseudo-first-order model is based on the assumption that the rate of change of solute uptake with time is directly proportional to difference in saturation concentration and the amount of solid uptake with time, which is generally applicable over the initial stage of an adsorption process. The pseudo first-order rate equation is represented by the following equation (Lagergren, 1898),

$$\frac{dq_t}{dt} = K_1(q_e - q_t) \quad (3.6)$$

where q_e is the adsorption capacity at equilibrium (g/g)

q_t is the adsorption capacity at time t (g/g)

K_1 is the pseudo-first-order rate constant for the kinetic model (min^{-1})

Integrating **Equation 3.6** with boundary conditions, $t = 0, q = 0$ and $t = t, q = q_t$, gives the linear form as shown in **Equation 3.7**.

$$\ln(q_e - q_t) = \ln q_e - K_1 t \quad (3.7)$$

By plotting $\ln(q_e - q_t)$ versus time (t), the value of K_1 can be determined from the slope of the straight line.

3.3.5.2 Pseudo-second-order rate equation

The pseudo-second-order kinetic model is based on the assumption that the rate limiting step is chemical sorption and predicts the behavior over the whole range of adsorption. For this condition, the adsorption rate is dependent on adsorption capacity not on concentration of adsorbate. The pseudo second-order model is represented by **Equation 3.8** (Ho and Mckay, 1998).

$$\frac{dq_t}{dt} = K_2 (q_e - q_t)^2 \quad (3.8)$$

where q_e is the adsorption capacity at equilibrium (g/g)

q_t is the adsorption capacity at time t (g/g)

K_2 is the pseudo-second-order rate constant for the kinetic model ($\text{g} \cdot \text{g}^{-1} \text{min}^{-1}$). By integrating Equation 3.8 with the integration limits, $t = 0, q = 0$ and $t = t, q = q_t$, we obtain

$$\frac{1}{q_e - q_t} = \frac{1}{q_e} + K_2 t \quad (3.9)$$

which can be rearranged to give

$$\frac{1}{q_t} = \frac{1}{V_0} + \frac{1}{q_e} t \quad (3.10)$$

with $V_0 = K_2 q_e^2$ being the initial adsorption rate, and K_2 can be determined from the intercept of the plot of $\frac{1}{q_t}$ versus t .

3.3.5.3 Intraparticle diffusion model

The intraparticle diffusion model assumes that the adsorption can occur through three consecutive steps including film diffusion, intra-particle diffusion and sorption. Since sorption is a fast and non-limiting step in the adsorption process, the adsorption rate can be limited by film diffusion and/or intra-particle diffusion (Kumar et al., 2011). The intraparticle diffusion model is expressed as in **Equation 3.11** (Weber and Morris, 1963).

$$q_t = K_I t^{0.5} + C \quad (3.11)$$

where K_I is the intraparticle diffusion rate constant and the value of K_I can be determined from the slope of the linear plot between q_t and \sqrt{t} .

3.3.6 The breakthrough curve

There are two widely used approaches to obtain the breakthrough curve for a given adsorption system: (i) direct experimentation or (ii) mathematical modeling. The experimental method could provide a direct and concise breakthrough curve for a given system (Seader and Henley, 2006). The breakthrough curve is obtained by plotting column effluent concentration versus volume treated or the time of treatment (see Figure 3.3). **Figure 3.3** shows a typical plot of the ratio of outlet solute concentration (C) to inlet solute concentration (C_0) in the fluid as a function of time from the start of the flow. The derived S-shaped curve is called the breakthrough curve.

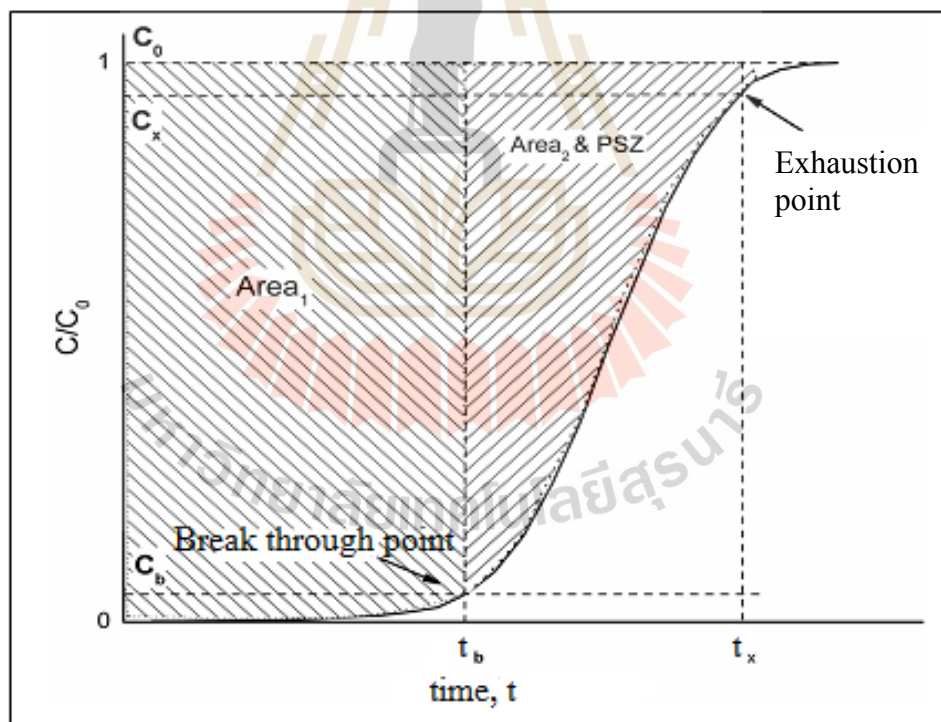


Figure 3.3 Typical breakthrough curves of fixed-bed adsorption (Seader and Henley, 2006)

The breakthrough time (t_B) is the time at which the outlet solute concentration is less than the maximum allowable concentration, for example, $\frac{c}{c_0} = 0.05$. When the breakthrough time is reached, the adsorption step should be discontinued to allow for adsorbent regeneration. If the adsorption step were to continue for $t > t_b$, the outlet solute concentration will rise sharply, eventually approaching the inlet concentration as the entire bed becomes saturated. The time required to reach $\frac{c}{c_0} = 0.95$ is designated as t_E , the equilibrium time or the time at exhaustion point.

The steepness of the breakthrough curve determines the extent to which the capacity of an adsorbent bed can be utilized. Thus, the shape of the breakthrough curve is very important in determining the length of the adsorption bed. In actual practice, the steepness of the concentration profiles shown previously can increase or decrease, depending on the type of adsorption isotherm involved as well as the degree of mass transfer resistances (external and internal), which in turn depends on the porous texture of an adsorbent.

3.3.7 Adsorption dynamics in a fixed-bed system

The general mass balance for a differential section of an absorber filled with a fixed-bed of adsorbent particles can be described by the following equation:

$$-D_L \frac{\partial^2 c}{\partial z^2} + \frac{\partial(uc)}{\partial z} + \frac{\partial c}{\partial t} + \left(\frac{1-\varepsilon_b}{\varepsilon_b} \right) \frac{\partial \bar{q}}{\partial t} = 0 \quad (3.12)$$

The first term takes into account the axial dispersion effect, where D_L is the axial dispersion coefficient, and the second term takes into account the contribution by convective mass transfer. The third term is the accumulation term of adsorbate. The

fourth term is the average uptake rate of adsorbate by the adsorbent particles from which

$$\bar{q} = \left(\frac{3}{R_p^3} \right) \int_0^{R_p} r^2 q dr \quad (3.13)$$

where q is the adsorbed-phase concentration, being a function of time (t) and radial distance (r) and R_p is the radius of a spherical adsorbent particle.

3.3.7.1 Break through equation by the linear-driving force model

If the linear-driving force model can be assumed for the uptake rate, we can write

$$\frac{d\bar{q}}{dt} = k_p(q^* - \bar{q}), \quad q^* = q^*(c) \quad (3.14)$$

where k_p is called “the particle mass transfer coefficient” and q^* is the adsorbed-phase concentration that is in equilibrium with adsorbate concentration in the bulk phase (c). When there is no axial dispersion effect ($D_L = 0$) and with a linear isotherm ($q = Kc$), the final solution for the breakthrough curve under these conditions is due to Klinkenberg (Seader and Henley, 2006) which yields,

$$\frac{c}{c_F} \approx \frac{1}{2} \left[1 + \operatorname{erf} \left(\sqrt{\tau} - \sqrt{\xi} + \frac{1}{8\sqrt{\tau}} + \frac{1}{8\sqrt{\xi}} \right) \right] \quad (3.15)$$

where $\xi = \frac{k_p K z}{u} \left(\frac{1 - \varepsilon_b}{\varepsilon_b} \right)$ is the dimensionless distance coordinate, $\tau = k_p \left(t - \frac{z}{u} \right)$

is the dimensionless time coordinate corrected for displacement, $\operatorname{erf}(x)$ is the error

function, t is the time length of the bed, u is the interstitial velocity, ε_b is the bed void fraction, K is Henry's constant for a linear adsorption isotherm and k_p is the particle overall mass transfer coefficient. Equation 3.15 is accurate to within 0.6% error for $\xi > 2.0$ (Seader and Henley, 2006).

The particle mass transfer coefficient (k_p) is related to the external and internal mass transfer resistances as follows,

$$\frac{1}{k_p K} = \frac{R_p}{3k_c} + \frac{R_p^2}{15D_e} \quad (3.16)$$

where k_c is the external mass-transfer coefficient in m/s , D_e is the effective diffusivity in m^2/s and R_p is adsorbent particle radius in m . The first term in Equation 3.16 is the overall mass-transfer resistances, the second and third term is external and internal ones, respectively. The external mass-transfer coefficient of particles in a fixed-bed of solid can be represented by Equation (3.17) as follows

$$Sh = 2 + 1.1Re^{0.6}Sc^{1/3} \quad (3.17)$$

where Sh = Sherwood number = $\frac{k_c D_p}{D_i}$, Re = Reynolds number = $\frac{D_p G}{\mu}$ and Sc = Schmidt number = $\frac{\mu}{\rho D_i}$, G is the fluid mass velocity and D_i is the molecular diffusivity.

3.3.7.2 Break through equation by Thomas model

Thomas model (Thomas, 1944) was developed for a curved isotherm of an equilibrium Langmuir equation and 2nd-order reversible reaction kinetics based on an ion exchange theory. The basic assumptions of Thomas or reaction model are negligible axial and radial dispersion in the fixed bed column and the adsorption is described by a pseudo second-order reaction rate principle which reduces to a Langmuir isotherm at equilibrium with no intra-particle diffusion and external resistance during the mass transfer processes. The expression for adsorption kinetics is described by,

$$\frac{\partial q}{\partial t} = k_1(q_0 - q)C - k_2q(C_0 - C) \quad (3.18)$$

where k_1 and k_2 are velocity constants, C_0 is the inlet concentration of adsorbate in the fluid stream, and q_0 is the adsorbed-phase concentration which is in equilibrium with the feed concentration (C_0). The above expression describes the second-order reversible reaction kinetics which can be applicable to both favorable and unfavorable adsorption conditions.

By assuming plug flow, negligible axial dispersion, the mass balance equation of an adsorbate (Equation 3.12) and Equation 3.18 were solved by Thomas to obtain the solution as shown below

$$\frac{c}{c_0} = \frac{J(\beta\xi, \tau)}{J(\beta\xi, \tau) + [1 - J(\xi, \beta\tau)] \exp\{[(\beta - 1)(\tau - \xi)]\}} \quad (3.19)$$

where $\beta = \frac{1}{1+bC_0}$ = equilibrium factor (a measure of isotherm curvature), $\tau = k_t C_0 \left(t - \frac{z}{u} \right)$ and $\xi = \frac{k_t q_0 z}{u} \left(\frac{1-\epsilon_b}{\epsilon_b} \right)$. For the long bed condition, the solution can be approximated by

$$\frac{c}{C_0} = \frac{1}{1 + \exp[k_t(q_0 m_c - C_0 V_{eff})/Q]} \quad (3.20)$$

where k_t is the Thomas rate constant, q_0 is the adsorptive capacity of adsorbent that is in equilibrium with the feed concentration, that is, $q_0 = q_m b C_0 / (1 + b C_0)$, m_c is the mass of adsorbent in the column, V_{eff} is the throughput volume, and Q is the volumetric flow rate.

For the evaluation of breakthrough results Thomas model is applied to the experimental data of the column studies. The linearized form of the Thomas model is

$$\ln \left(\frac{C_0}{c} - 1 \right) = \frac{k_t q_0 m_c}{Q} - k_t C_0 t \quad (3.21)$$

The value of k_t and q_0 are obtained from the slope and intercept of the linear plot in

Equation 3.21.

3.3.7.3 Breakthrough equation with axial dispersion

Levenspiel and Bischoff presented a breakthrough equation that accounts for the axial dispersion effect of fluid flow. The axial dispersion coefficient is assumed to be independent of both the axial position and the concentration of tracer. The Levenspiel and Bischoff model is given by the following expression:

$$\frac{C}{C_0} = \frac{1}{2} \operatorname{erfc} \left\{ \frac{1 - \frac{t}{\bar{t}}}{2 \left[\frac{D_z}{U Z} \left(\frac{t}{\bar{t}} \right) \right]^{1/2}} \right\} \quad (3.22)$$

where $\bar{t} = \frac{Z}{U} \left[1 + K \left(\frac{1 - \epsilon_b}{\epsilon_b} \right) \right]$, Z is the bed height of the fixed-bed column (m), D_z is the axial dispersion coefficient (m^2/s) and U is the superficial velocity (m/s).

3.3.7.4 Breakthrough curve characteristics

Figure 3.4 depicts a typical breakthrough curve showing the various definitions of breakthrough parameters. The breakthrough time (t_B) is the time at which the detected exit solute concentration (C) is at 5% of the feed concentration (C_0), that is $C/C_0 = 0.05$, and the equilibrium time (t_E) is defined as the time at which C/C_0 is 0.95. The amount of solute adsorbed at time t (q_s) can be estimated from the product of solute feed rate (Q_s) multiplied by the mean stoichiometric time (t_M). Therefore, we have

$$q_s = Q_s t_M = C_0 Q t_M \quad (3.23)$$

where Q_s is the solution feed flow rate, C_0 is the water concentration in the feed, and t_M can be calculated from the area above the breakthrough curve at time t corresponding to the exit solute concentration C .

t_M = area above breakthrough curve

$$t_M = \int_0^t \left[1 - \frac{C}{C_0} \right] dt \quad (3.24)$$

When applying Equation (3.22) to the conditions at breakthrough time (t_B) and equilibrium time (t_E), Equation 3.24 becomes

$$t_{MB} = \int_0^{t_B} \left[1 - \frac{C}{C_0} \right] dt \quad (3.25)$$

and

$$t_{ME} = \int_0^{t_E} \left[1 - \frac{C}{C_0} \right] dt \quad (3.26)$$

The amounts of water adsorbed at time t_B and t_E can then be then computed, respectively, from **Equations 3.26** and **Equation 3.27** as

$$q_B = C_0 Q t_{MB} \quad (3.27)$$

and

$$q_E = C_0 Q t_{ME} \quad (3.28)$$

Figure 3.4 depicts the determination of t_B , t_E and t_M from a general breakthrough curve.

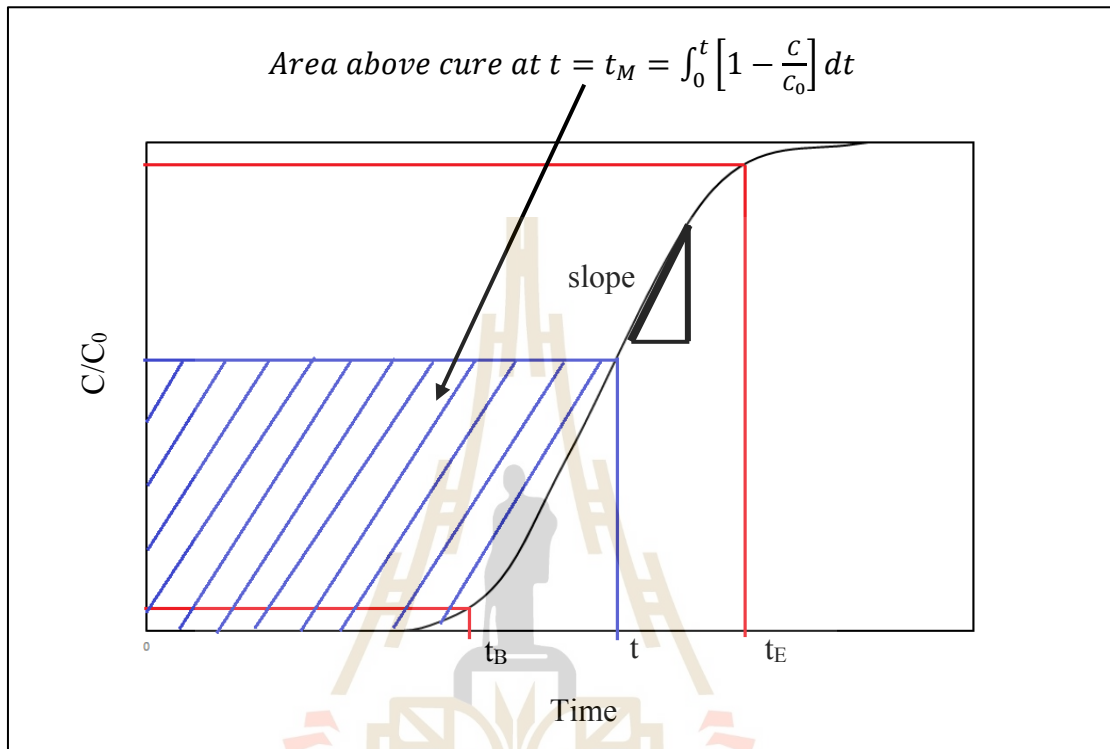


Figure 3.4 Typical breakthrough curve showing the estimation of breakthrough parameters (t_B = breakthrough time, t_E = equilibrium time, and t_M = mean stoichiometric time).

3.4 Literature review

There is growing interests in the dehydration of ethanol-water by adsorption using porous silica and other adsorbents for gas and liquid separation and only the adsorption performance of some adsorbents are briefly presented here.

The combination of distillation followed by adsorption is a viable separation method for removing water from ethanol. Distillation requires a disproportionate increase in energy at product concentrations above 92% weight of ethanol due to the

shape of the equilibrium curve which, in effect, controls the minimum reflux for a thermally saturated, 12% weight of ethanol feed. Consequently, stopping the distillation at 92% or less combined with an appropriate adsorption technique to obtain anhydrous product may reduce the overall energy requirements as compared to the traditional distillation approaches (Ladisich and Dyck, 1979). There are several studies that use this process to separate water from ethanol by using various adsorbents, for example, silica gel, barium oxide, zeolites and biosorbents. The adsorption distillation method employs about 4 MJ/kg for ethanol production which is less than the azeotropic distillation of 6-9 MJ/kg for ethanol production.

Carmo and Gubulin (2002) carried out ethanol-water separation employing a PSA adsorption cycle with zeolite 3A as the adsorbent. The cycle was operated under the following operating variables: feed flow rate of 2, 4, 6 and 8 L/hr, adsorption temperature at 200°C and adsorption pressures of 2, 4 and 6 bars. All experimental runs were performed under a vacuum pressure of 0.2 bar in the desorption step. The effects of these variables on the enrichment and recovery percentage of the product, on the productivity and on the total cycle time were studied, using the adsorption pressure as a parameter. They also studied the influence of such variables as adsorption pressures, desorption pressures, flow rates and adsorption temperatures, on the enrichment, recovery, productivity and on the total cycle time. The data were obtained from operational cycles in a Kahle's system. The experiments were organized by a 3 levels factorial design. The obtained results indicated that the optimum conditions occurred at adsorption pressure of 3.40 bar, the feed flow rate of 5.52 L/hr and the temperature of column of 250 °C. This condition can produce up to 99.68% by weight of ethanol,

recovery percentage of 89.69% ethanol production 7.46 grams ethanol per gram of adsorbent and cycle time of 28.98 s.

Kuan-Shyang W. et al., (2010) studied the equilibrium isotherms of water and ethanol vapor on biosorbents (potato starch, corn starch, cassava starch and cellulose) and zeolite 3A. In this study the microbalance gravimetric method was used to obtain the water adsorption isotherms at 273 K and at a low relative pressure ($P/P^0 = 0.6$). The results showed that the water-ethanol uptake ratio in potato starch was the highest at 64.2. The obtained water-ethanol uptake ratio from high to low are potato starch, cellulose, corn starch, cassava starch and zeolite 3A. The mechanism of water adsorption by cellulose and starch was similar. There are also OH groups in the glucose unit of starch-based adsorbents that can form hydrogen bonds with water and ethanol. The isotherm models that were used to fit the experimental data are Langmuir, modified-BET, Smith Henderson, Oswin, Ferro-Fintan, GAB and Peleg. The Langmuir model was better for the zeolite 3A adsorption system, the starch biosorbent isotherms were best fitted by the Peleg model and the Smith model was best for describing water adsorption for the cellulose system.

3.5 Experimental method

3.5.1 Batch adsorption tests in a liquid phase system

Porous silica (sample PS2-200 prepared as in Chapter 2) weighing 0.2 g was mixed with a constant volume of 4 ml ethanol solution in an Erlenmeyer flask and shaken at a constant temperature in the range from 20 – 40 °C, using a temperature-controlled shaking bath for the period of 180 min. For each solution the sample was collected at 10 min time intervals for the analysis of ethanol concentration using a

refractometer (NAR-2T, Atago). The sample was collected until the final equilibrium concentration was attained. The initial concentrations of ethanol solution were varied from 60-95 wt.% and the tests were performed at different adsorption temperatures. Both the equilibrium and kinetics of water adsorption by the porous silica were studied. Table 3.2 shows the experimental conditions used for the batch adsorption tests.

Table 3.2 Experimental conditions for batch adsorption of water by porous silica (PS2-200)

Run	Ethanol concentration (% wt.)	Temperature (°C)
1		20
3	60	30
4		40
5		20
7	85	30
8		40
9		20
11	90	30
12		40
13		20
15	95	30
16		40

3.5.2 Fixed-bed adsorption tests in a vapor phase system

The number of experiments used for the fixed-bed adsorption study were determined using a 2^4 factorial experiment assigned by Minitab software, with four process variables affecting the adsorption performance, including the amount of silanol group, feed flow rate, bed height and adsorption temperature. The experimental conditions used for the parametric study of fixed-bed adsorption of water by porous silica are summarized in **Table 3.3**. A total of 20 experimental runs were performed in this study.

Table 3.3 Experimental conditions for fixed-bed adsorption of water by porous silica

Run	Samples	Mean pore size (nm)	Silanol content (mmol/g)	Feed flow rate (ml/min)	Bed height (cm)	T _{bed} (°C)
1	PS2-200	2.4	7.94	1.5	15	85
2					25	
3				15		
4				25		
5	PS2-500	2.2	4.18	1.5	15	85
6					25	
7				15		
8				25		
9	PS2-200	2.4	7.94	1.5	15	95
10					25	
11				15		
12				25		
13	PS2-500	2.2	4.18	1.5	15	95
14					25	
15				15		
16				25		
17	PS4-200	10.3	4.22	1.5	15	85
18				3	25	
19	PS4-500	10.9	2.77	3	15	
20				1.5	15	

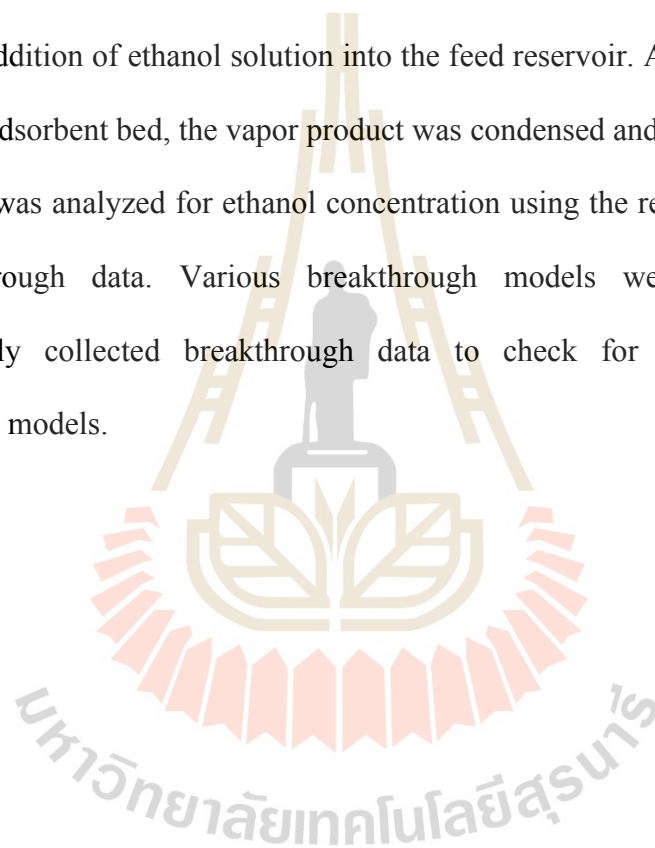
*porous silicas were designated as PSX-Y where X is the pH of mixture and Y is the calcination temperature.

The adsorption of water by porous silica was performed in a fixed bed column. Before starting the tests, the adsorption column was run with non-porous glass beads being packed in the column to check for the ethanol concentration in the vapor feed by condensing out the vapor leaving the column.

A schematic of the bench-scale packed bed adsorber for ethanol-vapor dehydration is shown in **Figure 3.5**. The porous silica adsorbent was first packed in a jacketed column made of glass with an inside diameter of 1.0 cm and a height of 30 cm.

The column wall temperature was maintained at 85-95 °C to prevent vapor condensation by circulating a controlled temperature hot water through the column jacket. Next, a starting aqueous solution with known ethanol concentration was poured into a 1000 ml flask (feed reservoir) and heated to generate a mixture of ethanol-water vapor.

The concentration and volume of the feed solution is kept constant by continuous addition of ethanol solution into the feed reservoir. After the vapor passed through the adsorbent bed, the vapor product was condensed and collected over a time interval and was analyzed for ethanol concentration using the refractometer to obtain the breakthrough data. Various breakthrough models were tested with the experimentally collected breakthrough data to check for the validity of the breakthrough models.



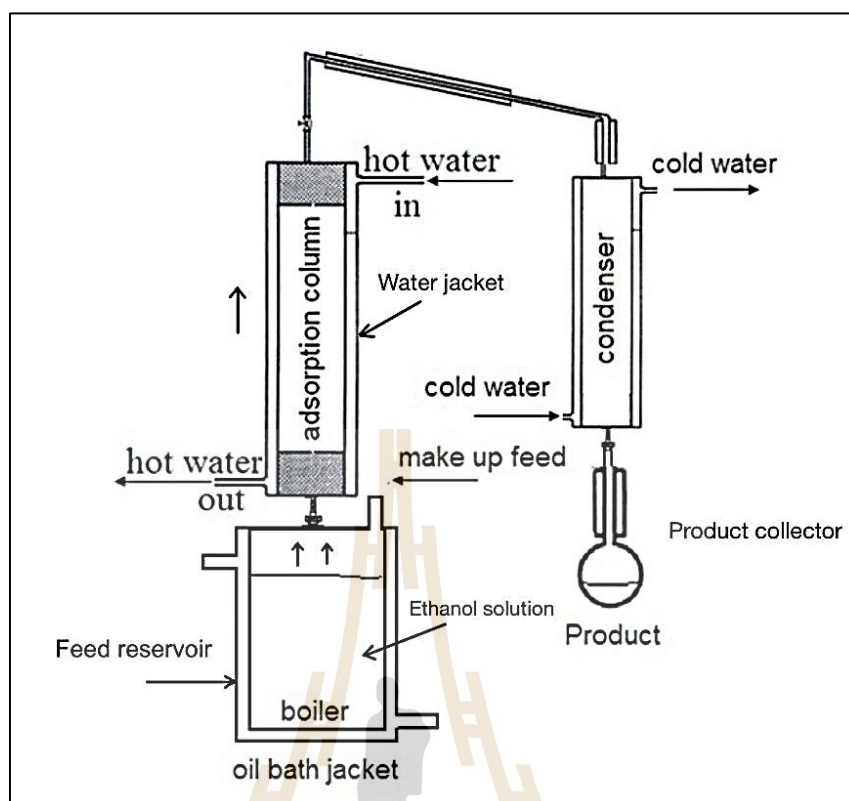


Figure 3.5 A laboratory-scale fixed-bed adsorption for ethanol dehydration experiments

In this study, the ethanol concentration was determined by measuring the refractive index of the ethanol-water mixtures with the assistance of a calibration curve. To produce the calibration curve, the refractive indices of solutions with known concentrations of ethanol and water (88 - 100 %wt. ethanol) were determined. In using the calibration curve, the refractive index of a sample with an unknown concentration was measured and its concentration determined directly by reading out from the calibration curve (a plot of ethanol concentration vs solution refractive index).

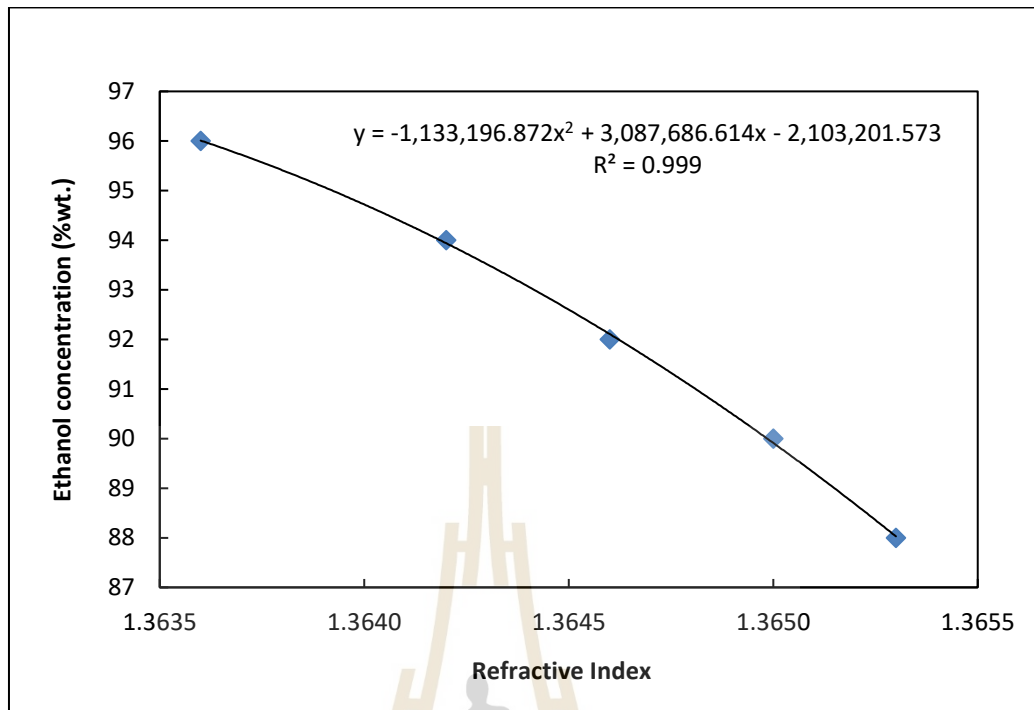


Figure 3.6 The calibration curve of the refractive index for determining the ethanol solution

Figure 3.6 shows the obtained calibration curve and the calibration data was conveniently fitted with the second-order polynomial function which gave the following equation, to determine the concentration of ethanol solution from the refractive index.

$$Y = -1133196.872X^2 + 3087686.614X - 2103201.573$$

where Y is the ethanol concentration (% by weight.) and X is the refractive index.

3.6 Results and discussion

3.6.1 Batch adsorption of water in liquid phase

This part reports on the equilibrium and kinetics of water adsorption on porous silica from the ethanol-water liquid mixture. Equilibrium water adsorption data were analyzed by the Langmuir isotherm and Freundlich isotherm in order to check for the most appropriate isotherm model. Moreover, kinetic results of the adsorption process were also presented to describe the rate of water sorption by porous silica adsorbents.

3.6.1.1 Water adsorption isotherms

The adsorption isotherm of water on porous silica (PS2-200) are shown in **Figure 3.7**, illustrating the relationship between the amount of water adsorbed per unit mass of porous silica (q_e) and the concentration of water at equilibrium (C_e) at varying temperatures. It was observed that the water uptake decreased with the increase in the temperature, indicating that the adsorption of water in liquid phase onto porous silica surface is due to physical adsorption. It was hypothesized that water molecules could interact with the silanol groups on the silica surface, possibly by hydrogen bonding. The experimental isotherm data obtained were tested with Langmuir and Freundlich isotherms employing Equation 3.2 and 3.4, respectively.

Table 3.4 shows the fitted parameters derived from the Langmuir and Freundlich adsorption models. Comparison of the R^2 values as appeared in **Table 3.4** for different adsorption temperatures revealed that the Langmuir model was the best fitting model to explain the equilibrium adsorption of water on porous silica in ethanol solution over the equilibrium concentration of water from 0.05-0.37 g/L. The results indicated that the water sorption on porous silica studied is monolayer adsorption on a

surface containing a finite number of adsorption sites (Khalighi et al., 2012). This indicates that the surface reaches an equilibrium point where the maximum adsorption of the surface is achieved. The maximum monolayer adsorption capacity for the water uptake was found to be 0.283 g water/g porous silica at 20 °C. As to the effect of adsorption temperature, the monolayer capacity (q_m) decreased with the increase of temperature but the Langmuir or affinity constant (k_L) also decreased with the increase of temperature from 20 to 40 °C indicating a favorable adsorbent-adsorbate interaction at a low adsorption temperature. The affinity parameter K of the Freundlich equation also decreased with the increase of adsorption temperature, in agreement with the effect of temperature on the Langmuir constant. Similarly, the heterogeneity parameter (n) appeared to decrease with the increase of adsorption temperature over the range of 20-40 °C, but the effect is not so pronounced with the value of n varying from 3.39 to 3.12.

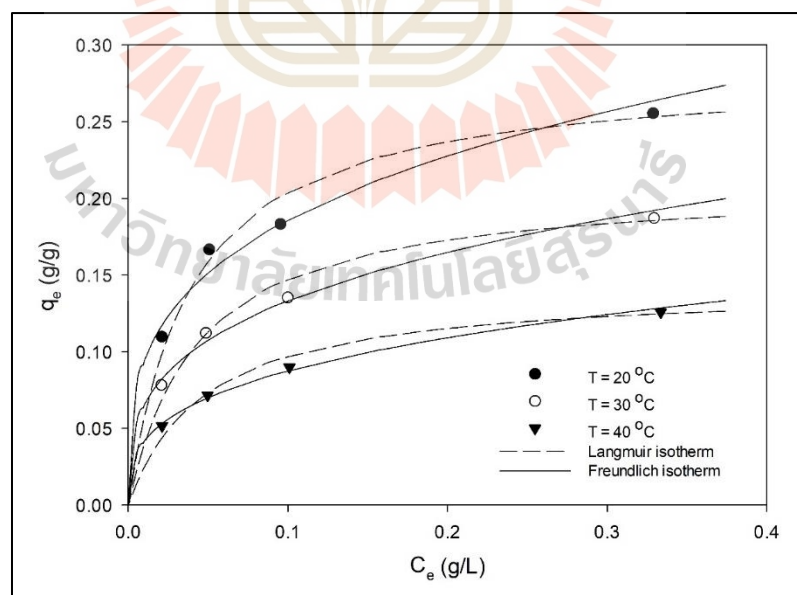


Figure 3.7 Adsorption isotherm of water onto porous silica (PS2-200, 2.4 nm mean pore size and silanol contents 7.94 mmol/g)

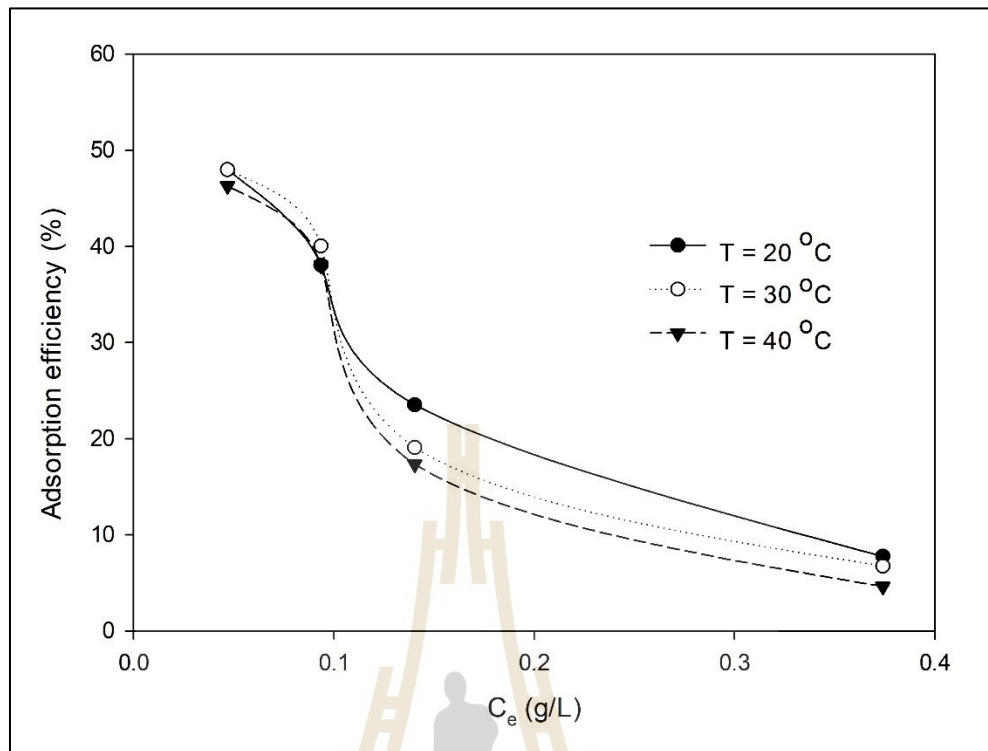


Figure 3.8 Water adsorption efficiency of porous silica (PS2-200, 2.4 nm and silanol contents 7.94 mmol/g)

From the equilibrium water adsorption isotherm, the percentage of water adsorption efficiency (η) was calculated using the following equation:

$$\eta = \frac{C_0 - C_e}{C_0} \times 100$$

where C_0 is the initial concentration of water and C_e is the equilibrium concentration of water. **Figure 3.8** depicts the water adsorption efficiency as a function of water concentration at equilibrium. The obtained data show that the adsorption efficiency decreased with increasing of water concentration at equilibrium. It is probable that for the given porous silica adsorbent, there is a certain number of adsorption sites available

for water adsorption. Therefore, the number of adsorption sites are not sufficient to accommodate the increasing number of water molecules as the water concentration increases, leading to the drop in the adsorption efficiency for water adsorption.

Table 3.4 Estimated parameters of various isotherms models for adsorption of water onto porous silica in the liquid phase system

Adsorption temperature	Langmuir			Freundlich		
	q_m (g/g)	k_L (L/g)	R^2	K	1/n	R^2
20 °C	0.283	25.501	0.9947	0.366	0.295	0.9626
30 °C	0.210	23.330	0.9963	0.271	0.308	0.9855
40 °C	0.142	21.148	0.9959	0.183	0.320	0.9941

3.6.1.2 Water adsorption kinetics

Typical example of the water adsorption kinetic curve for the porous silica is shown in **Figure 3.9**. The adsorption rate reflects the amounts of water adsorbed as a function of time. The slope at each point represents the instantaneous adsorption rate. The initial adsorption stage increased rapidly, which is probably due to the adsorption of water molecules on the external surface of the adsorbent particles. The following rate is a slow adsorption process. The reason for this phenomenon is attributed to the large number of internal pores in the porous silica structure. Water molecules must first transport through pores by diffusion and then adsorbed by interacting with silanol groups through hydrogen bonds. The tortuosity of interconnected pores and the increasing amount of water adsorbed inside the pores

increase the diffusional resistance, hence causing the drop in the diffusion rate to the adsorption sites.

The kinetic data were fitted with the pseudo first-order and pseudo second-order adsorption kinetic models and the intraparticle diffusion model as shown in **Figure 3.9** and **Figure 3.10**, respectively. Overall, the pseudo-second-order model appeared to give the best prediction of adsorption kinetics as compared to other models (see Table 3.5 (a)-(c) for R^2). **Table 3.5** lists the kinetic parameters derived from the data fitted by various kinetic models for various adsorption temperatures. The rate constant decreased with the increase in water concentration (%wt.) of the pseudo first-order and pseudo second-order models. This is mainly attributed to the increased amount of adsorbed water inside the pores that could impede the transport of water molecules deep into the internal pores. The equilibrium adsorption of water onto the porous silica (q_e) decreased with an increase in temperature. This indicates that the adsorption process is exothermic, in line with the results on adsorption isotherms presented previously.

Multilinear profiles were obtained for the intraparticle diffusion model, as shown plotted in **Figure 3.10**, based on Equation (3.11), giving K_{I1} , C_1 and R_1^2 being the slope, intercept and correlation of the first steeper portion, respectively, while K_{I2} , C_2 and R_2^2 indicate the slope, intercept and correlation of the second linear portion, respectively (**Table 3.5**). There are theoretical interpretations of the intraparticle diffusion equation. C is an arbitrary constant representing the boundary layer thickness, and a larger value of C represents a thicker boundary layer (Magdy and Altaher, 2018). If the value of C is zero, which corresponds to no boundary layer, the linear line will pass through the origin. Thus, film diffusion could be ignored due to

less thickness, thus intraparticle diffusion would remain as the rate controlling step through the entire adsorption kinetic process. **Figure 3.10** shows that multilinear plots, showing that the first line passing through near the origin point, while the second line did not pass through the origin ($C_2 \neq 0$). This indicates that more than one process could affect the adsorption process. Therefore, these implied that the intraparticle diffusion was not the only rate-controlling step and the presence of boundary layer might affect the adsorption (Yakout and Elsherif, 2010). The values of K_{I1} are much greater than the values of K_{I2} , this implies that the intraparticle diffusion (internal mass transfer) step mainly controls the adsorption process (Inyinbor et al., 2016). As to the effect of water concentration, Table 3.5 indicated that increasing water concentration tended to increase the value of parameter K_{I1} but exerted lesser effect on the K_{I2} parameters. This indicates the increasing of water transport through the external film and hence smaller mass transfer resistance as compared to the intraparticle resistance.

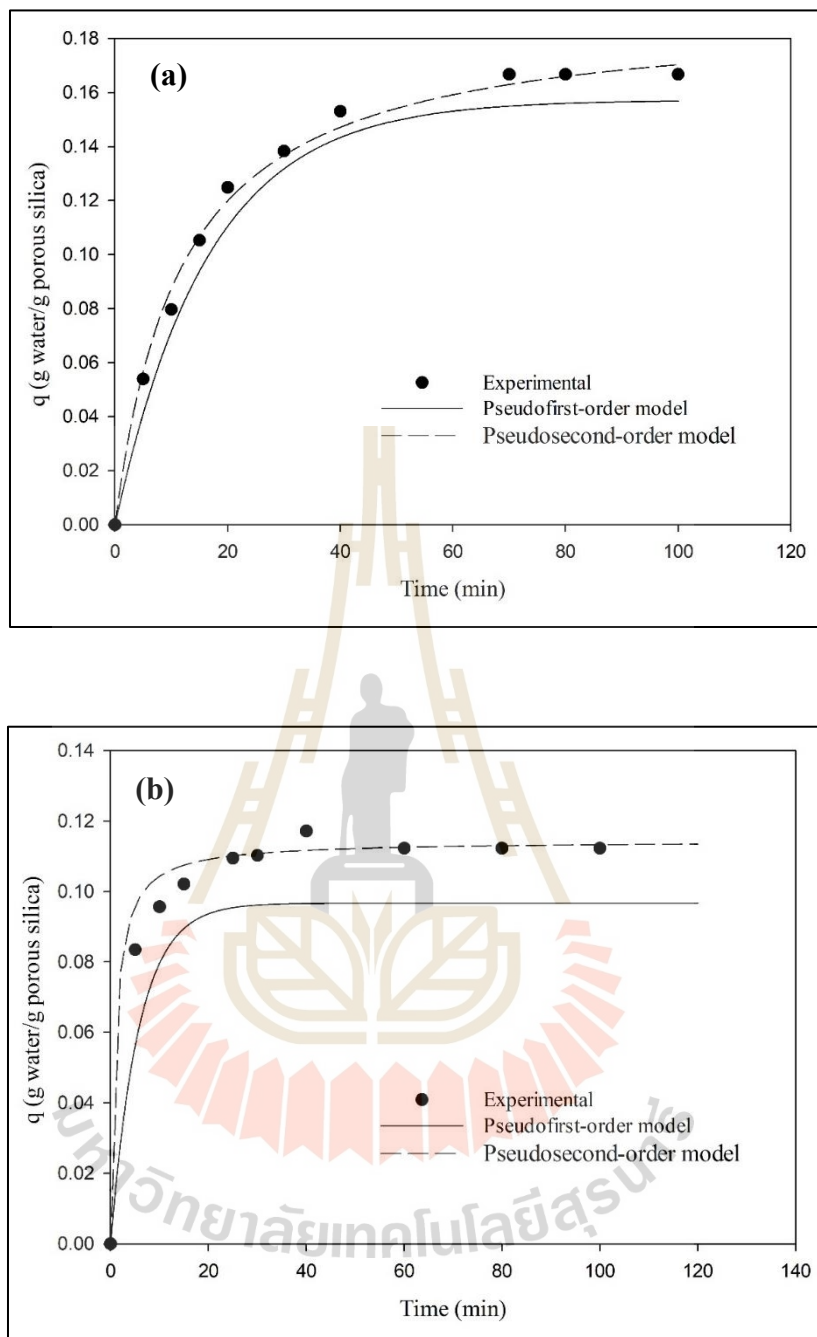


Figure 3.9 Adsorption kinetic curves and predictive capability of different kinetic models for 90 wt.% ethanol (10 wt.% water) (a) at 20 °C and (b) at 30 °C

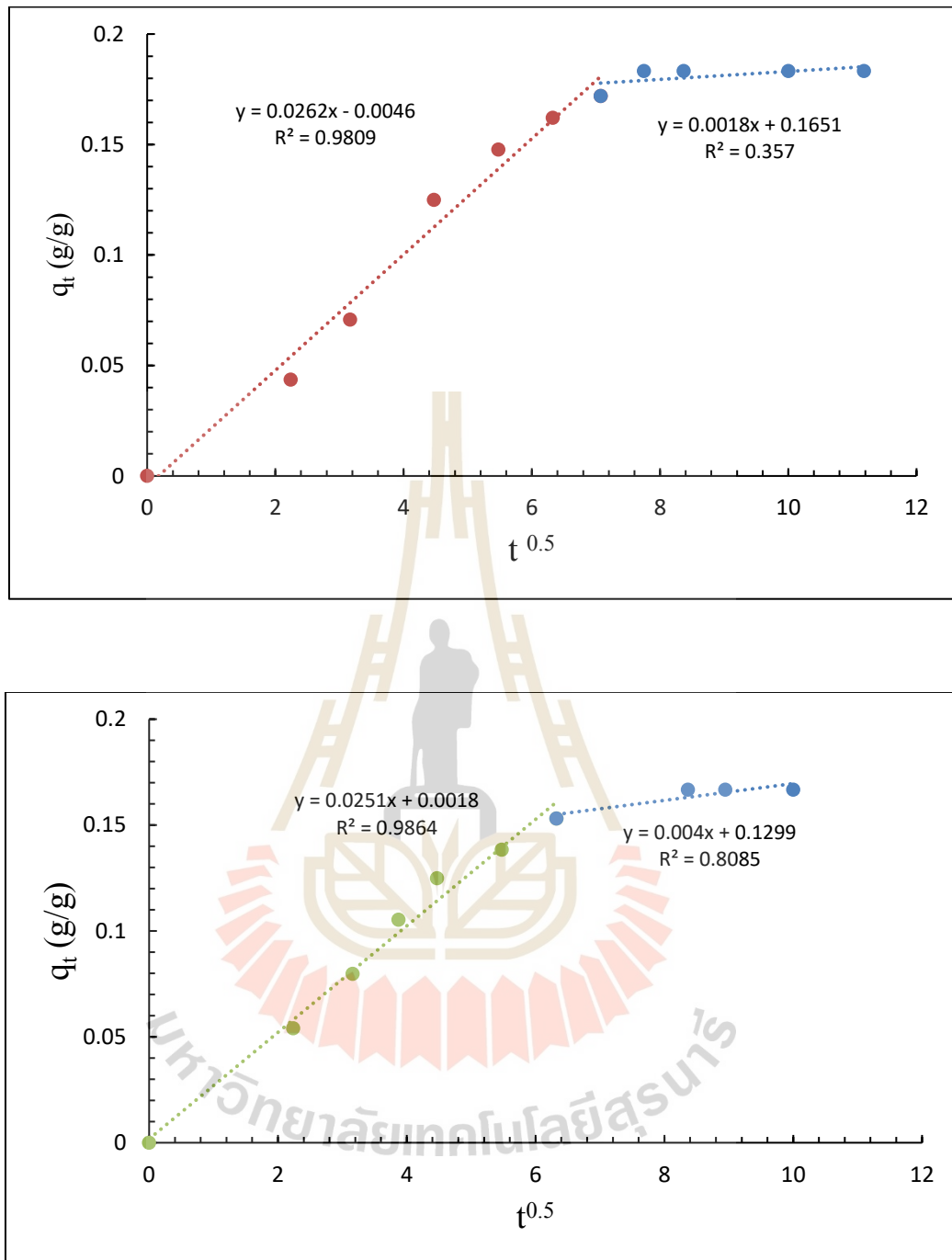


Figure 3.10 Typical plot of intraparticle diffusion model at 20 °C for

(a) 85 wt.% ethanol (15 wt.% water) and

(b) 90 wt.% ethanol (10 wt.% water)

Table 3.5 (a) List of parameters obtained from pseudo-first-order, pseudo-second-order and intra particle kinetic model fitting for adsorption of water onto porous silica in batch liquid system at 20 °C.

Constants (20 °C)	Initial concentration of water (%wt.)			
	5	10	15	40
q_e experimental (g/g)	0.1098	0.1667	0.1833	0.2556
Pseudo first order model				
q_e calculated (g/g)	0.1087	0.1572	0.1858	0.2865
K_1 (g/g min)	0.0663	0.0607	0.0553	0.0489
R^2	0.9903	0.9933	0.9987	0.9816
Δq_e (% error)	1.0018	5.6989	1.3639	12.089
Pseudo second order model				
q_e calculated (g/g)	0.1143	0.1703	0.1878	0.2708
K_2	0.6273	0.4477	0.2499	0.0534
R^2	0.9935	0.9978	0.9945	0.9679
Δq_e (% error)	4.0984	2.1596	2.4550	5.9468
Intra particle diffusion model				
C_1 (g/g)	-0.0002	0.0018	-0.0046	-0.0276
K_{I1} (g/g.min ^{1/2})	0.0172	0.0251	0.0262	0.0371
R_1^2	0.9743	0.9864	0.9809	0.9266
C_2 (g/g)	0.0841	0.1299	0.1651	0.1711
K_{I2} (g/g.min ^{1/2})	0.0029	0.0040	0.0018	0.0096
R_2^2	0.7801	0.8085	0.3570	0.5024

Table 3.5 (b) List of parameters obtained from pseudo-first-order, pseudo-second-order and intra particle kinetic model fitting for adsorption of water onto porous silica in batch liquid system at 30 °C.

Constants (30 °C)	Initial concentration of water (%wt.)			
	5	10	15	40
q_e experimental (g/g)	0.0784	0.1123	0.1354	0.1871
Pseudo first order model				
q_e calculated (g/g)	0.0649	0.0966	0.1060	0.1499
K_1 (g/g min)	0.1672	0.1736	0.1049	0.0899
R^2	0.9913	0.9752	0.9739	0.9616
Δq_e (% error)	17.22	13.98	21.71	19.88
Pseudo second order model				
q_e calculated (g/g)	0.0800	0.1144	0.1392	0.2001
K_2	11.360	9.1143	3.2697	1.2450
R^2	0.9998	0.9984	0.9994	0.9985
Δq_e (% error)	2.04	1.87	2.81	6.95
Intra particle diffusion model				
C_1 (g/g)	0.0003	0.0069	0.0064	0.0072
K_{I1} (g/g.min ^{1/2})	0.0218	0.0273	0.0282	0.0372
R_1^2	0.9992	0.9400	0.9768	0.9792
C_2 (g/g)	0.0701	0.1109	0.1293	0.1500
K_{I2} (g/g.min ^{1/2})	0.0012	0.0002	0.0006	0.0051
R_2^2	0.6945	0.0258	0.3224	0.6464

Table 3.5 (c) List of parameters obtained from pseudo-first-order, pseudo-second-order and intra particle kinetic model fitting for adsorption of water onto porous silica in batch liquid system at 40 °C.

Constants (40 °C)	Initial concentration of water (%wt.)			
	5	10	15	40
q_e experimental (g/g)	0.0517	0.0716	0.0899	0.1258
Pseudo first order model				
q_e calculated (g/g)	0.0498	0.0738	0.0839	0.1181
K_1 (g/g min)	0.1083	0.0840	0.0551	0.0486
R^2	0.9913	0.9894	0.9851	0.9930
Δq_e (% error)	3.5676	3.0848	6.5948	6.0925
Pseudo second order model				
q_e calculated (g/g)	0.0531	0.0740	0.0920	0.1306
K_2	9.1249	2.9658	0.9389	0.5023
R^2	0.9997	0.9994	0.9955	0.9678
Δq_e (% error)	2.7117	3.3325	2.3587	3.8057
Intra particle diffusion model				
C_1 (g/g)	-0.0016	-0.0008	-0.0007	-0.0102
K_{I1} (g/g.min ^{1/2})	0.0109	0.0125	0.0135	0.0190
R_1^2	0.9647	0.9857	0.9723	0.9652
C_2 (g/g)	0.0480	0.0647	0.0682	0.1006
K_{I2} (g/g.min ^{1/2})	0.0004	0.0008	0.0024	0.0029
R_2^2	0.7670	0.7174	0.6104	0.5024

3.6.2 Fixed-bed adsorption of water in vapor-phase

3.6.2.1 Characteristics of water breakthrough curves

Figure 3.11 shows the effect of process variables, including silanol content, temperature, bed height, average pore size and vapor feed rate on the characteristics of breakthrough curves. It is observed that these variables can affect the location of the breakthrough curve on the x-axis, that is, the breakthrough time (t_B) and the slope of the linear portion of the curve. It is important to note that the breakthrough time is indication of adsorption efficiency of the adsorbent bed, whereas the slope reflects the mass transfer resistance of an adsorbate inside the pores; the steeper the slope, the lower the mass transfer resistance. **Table 3.6** lists the average pore size and silanol group concentration of the tested porous silica.

Table 3.7 summarizes the relevant breakthrough characteristic parameters as functions of pertinent process variables, including the breakthrough time (t_B), the equilibrium time (t_E), water adsorption capacity at t_B (q_B), water adsorption capacity at t_E (q_E), percent of bed saturation at , the slope of breakthrough curve (m) and the length of mass transfer zone (MTZ).

From the breakthrough results in **Figure 3.11 (a)** and **3.11 (b)**, it was found that the increase in the silanol group content for PS2-200 compared to PS2-500 caused the slope of the breakthrough curve to decrease. This is probably attributed to the consequent increase of mass transfer resistance for water diffusion caused by the presence of increasing number of the silanol groups that could impede the transport of water molecular inside the pores. **Figure 3.11 (c)** and **Table 3.7** show that as the temperature of water adsorption increased, there was a tendency for the slope m to slightly increase. It was hypothesized that the increase in temperature could increase

the diffusion rate of water molecules to the adsorption sites, hence giving a decrease in the mass diffusion resistance.

The increase in bed height from 15 to 25 cm had virtually no effect on the slope of the breakthrough curve from the viewpoint of mass transfer resistance for pore diffusion (see Figure 3.11 (d) and Table 3.7). The increase of average pore size caused a slight increase in the slope of the breakthrough curve as shown in **Figure 3.11 (e)**, as would be expected from the lowering of mass transfer resistance for larger pore size. Increasing the gas flow rate through the bed had a tendency to increase the slope of the breakthrough curve, as shown in **Figure 3.11 (f)** and from **Table 3.7**. This is explained by the lowering of the external gas-film mass transfer resistance as the vapor flow rate is increased.

Table 3.6 Average pore size and silanol group contents of the porous silica

Samples	Average pore size (nm)	Silanol contents (mmol/g)
PS2-200	2.4	7.94
PS2-500	2.2	4.18
PS4-200	10.3	4.22
PS4-500	10.9	2.77

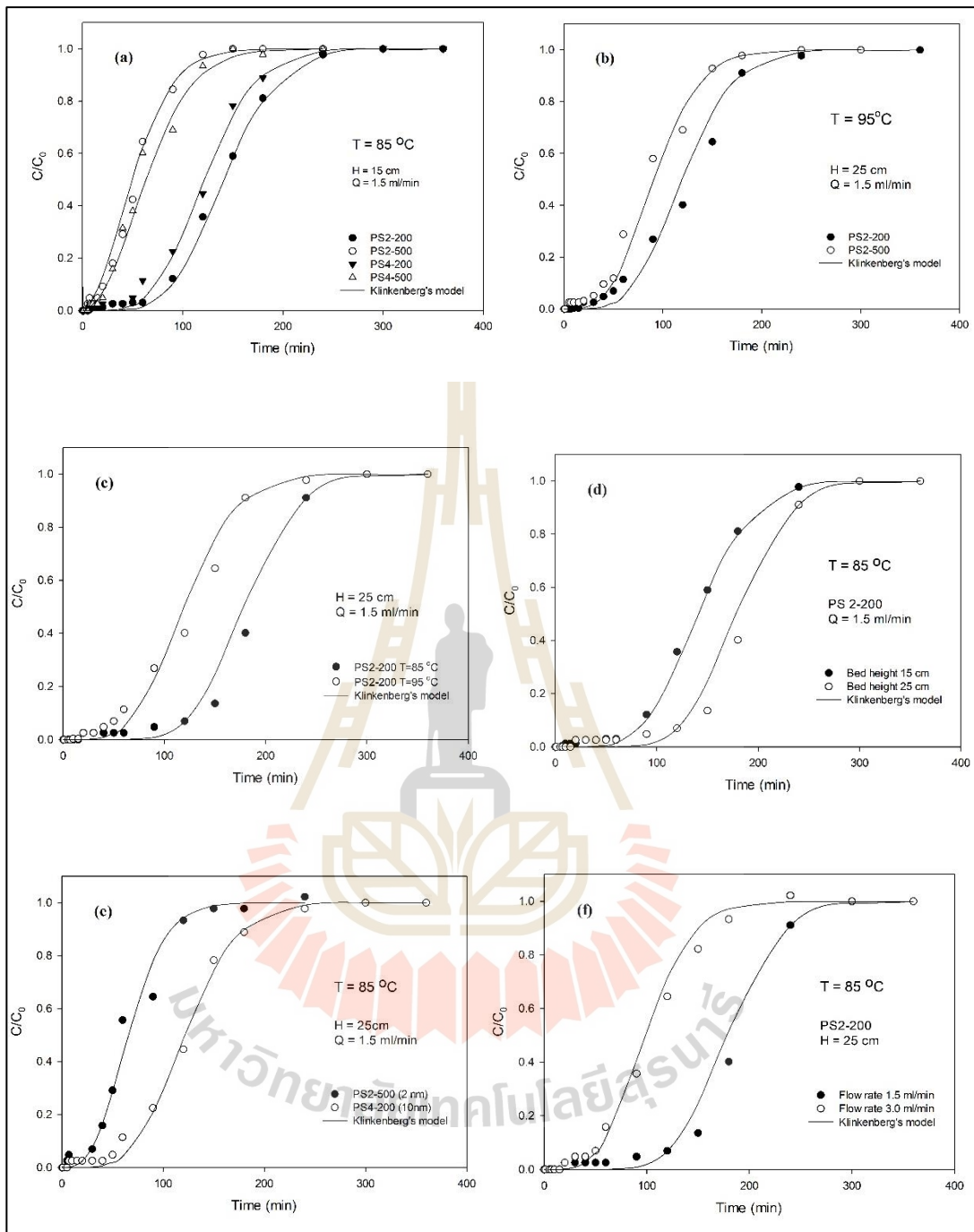


Figure 3.11 Effects of process variables on the breakthrough curves of water adsorption from ethanol solution by porous silica (a) and (b) amount of silanol group, (c) bed temperature, (d) bed height, (e) pore size, and (f) feed flow rate.

Table 3.7 The breakthrough time for different operating conditions

Run	Temperature (°C)	Sample*	Feed flow rate (ml/min)	Bed height (cm)	Breakthrough time, t_B (min)	Equilibrium time, t_E (min)	Capacity at t_B , q_B (q water/q PS)	Capacity at t_E , q_E (q water/q PS)	% Bed at t_B	Slope* *	MTZ (cm)
1	85	PS2-200	1.5	15	47.94	284.25	0.1230	0.2955	41.64	0.0068	12.47
2				25	84.03	326.05	0.1694	0.3268	51.84	0.0061	18.56
3			3.0	15	33.81	223.29	0.1184	0.2803	42.24	0.0083	12.73
4				25	40.47	255.57	0.1199	0.3072	39.02	0.0080	21.04
5		PS2-500	1.5	15	26.53	224.84	0.0841	0.2641	31.85	0.0094	13.23
6				25	36.01	231.84	0.0911	0.2920	31.18	0.0095	21.12
7			3.0	15	13.88	168.69	0.0880	0.2355	37.37	0.0114	13.77
8				25	28.17	164.68	0.0812	0.2510	32.34	0.0109	20.72
9	95	PS2-200	1.5	15	42.30	268.85	0.1375	0.2796	49.19	0.0072	12.64
10				25	68.63	311.73	0.1468	0.2876	51.02	0.0084	19.50
11			3.0	15	28.75	220.93	0.1099	0.2616	42.01	0.0098	13.05
12				25	32.02	272.14	0.1273	0.2687	47.39	0.0092	22.06
13		PS2-500	1.5	15	28.27	192.37	0.0666	0.2234	29.82	0.0106	12.80
14				25	24.23	251.03	0.0912	0.2537	35.96	0.0112	22.59
15			3.0	15	16.60	159.40	0.0481	0.2003	24.02	0.0145	13.44
16				25	24.08	188.67	0.0848	0.2315	36.62	0.0128	21.81
17	85	PS4-200	1.5	15	33.43	288.65	0.0824	0.2566	32.10	0.0072	13.26
18				25	43.49	306.46	0.0802	0.1888	42.50	0.0068	21.45
19		3.0	15	18.29	236.50	0.0905	0.2243	40.34	0.0088	13.84	
20		PS4-500	1.5	15	22.44	209.51	0.0549	0.1829	30.02	0.0093	13.39

*porous silicas were designated as PSX-Y where X is the pH of mixture and Y is the calcination temperature.

** slope of breakthrough curve

Figure 3.12 (a) and (b) show the breakthrough time (t_B) and the equilibrium time (t_E) for different operating conditions. The decrease in the breakthrough time and the equilibrium time with an increase in the vapor flow rate should be attributed to a shorter contact time between water and porous silica at higher flow rates. As the bed height (mass of adsorbent) and the amount of silanol group increased, the breakthrough time increased. This is due to the increase of the available surface area and binding sites for the water sorption as adsorbent mass increases. The increasing in the average pore size gave higher t_B and t_E which resulted from the lowering of mass transfer resistance inside the pore, allowing more time for adsorption to take place. Increasing temperature caused t_B and t_E to decrease, simply by the effect of increasing gas velocity in the void space of adsorbent bed, leading to less contact time for adsorption.

Figure 3.12 (c) shows that the water uptake capacity per unit mass at breakthrough time (q_B) slightly increased with the increasing of bed height in the fixed-bed column at adsorption temperature of 85 °C. The water capacity per unit mass at equilibrium times (q_E) on porous silica (**Figure 3.12 (d)**) also showed an increase with the increasing bed height. The bed height of 25 cm, the feed flow rate 1.5 mL/min and the adsorption temperature 85 °C for PS2-200 showed the highest q_E , which occurred for porous silica containing the largest amount of silanol content.

Comparing, the effect of pore size between 2.2 nm (PS2-500) and 10.3 nm (PS4-200) with a constant amount of silanol group, the water adsorption capacity at t_B (q_B) and the water adsorption capacity at t_E (q_E) for the pore size of 2.2 nm was greater than those of 10.3 nm pore size. In the case of different silanol group content, the amount of water adsorbed for porous silica with a higher the silanol group content of 7.94 mmol/g (PS2-200) was greater than that for the porous silica with a

lower the silanol content of 4.18 mmol/g (PS2-500), as shown in **Figure 3.12 (c)** and **(d)**. The adsorption capacity at t_B (q_B) and the adsorption capacity t_E (q_E) increased as the silanol group content increased. This clearly indicates that the water adsorption capacity could be significantly enhanced by the increasing amount of silanol group content.

The effect of flow rate on the water adsorption in fixed-bed was investigated for the inlet vapor concentration of 95% by weight. The water adsorption capacity obtained at different flow rates of 1.5 mL/min and 3.0 mL/min are shown in **Figure 3.12 (c)** and **(d)**. It was observed that an increase in flow rate significantly reduced the water adsorption capacity. This could be explained by the fact that at a higher flow rate, the water molecules had less time to diffuse into the adsorbent pores. Accordingly, the low feed flow rate was beneficial to the water adsorption capacity. Besides, the effect of temperature on the water adsorption capacity by using porous silica was studied at adsorption temperatures of 85 °C and 95 °C shown in **Figure 3.12 (c)** and **(d)**. The water adsorption capacity at t_B (q_B) and the water adsorption capacity at t_E (q_E) decreased with an increase in temperature. This indicates that the adsorption process is exothermic.

Figure 3.12 (e) shows the effect of process variables on the width of MTZ. There was a general tendency for the width of MTZ to increase with the increase of vapor feed rate, bed height, and amount of silanol group. However, the width of MTZ was found to be insensitive to the change in the average pore size and temperature. Overall, the width of MTZ was shorter than the bed height under all conditions.

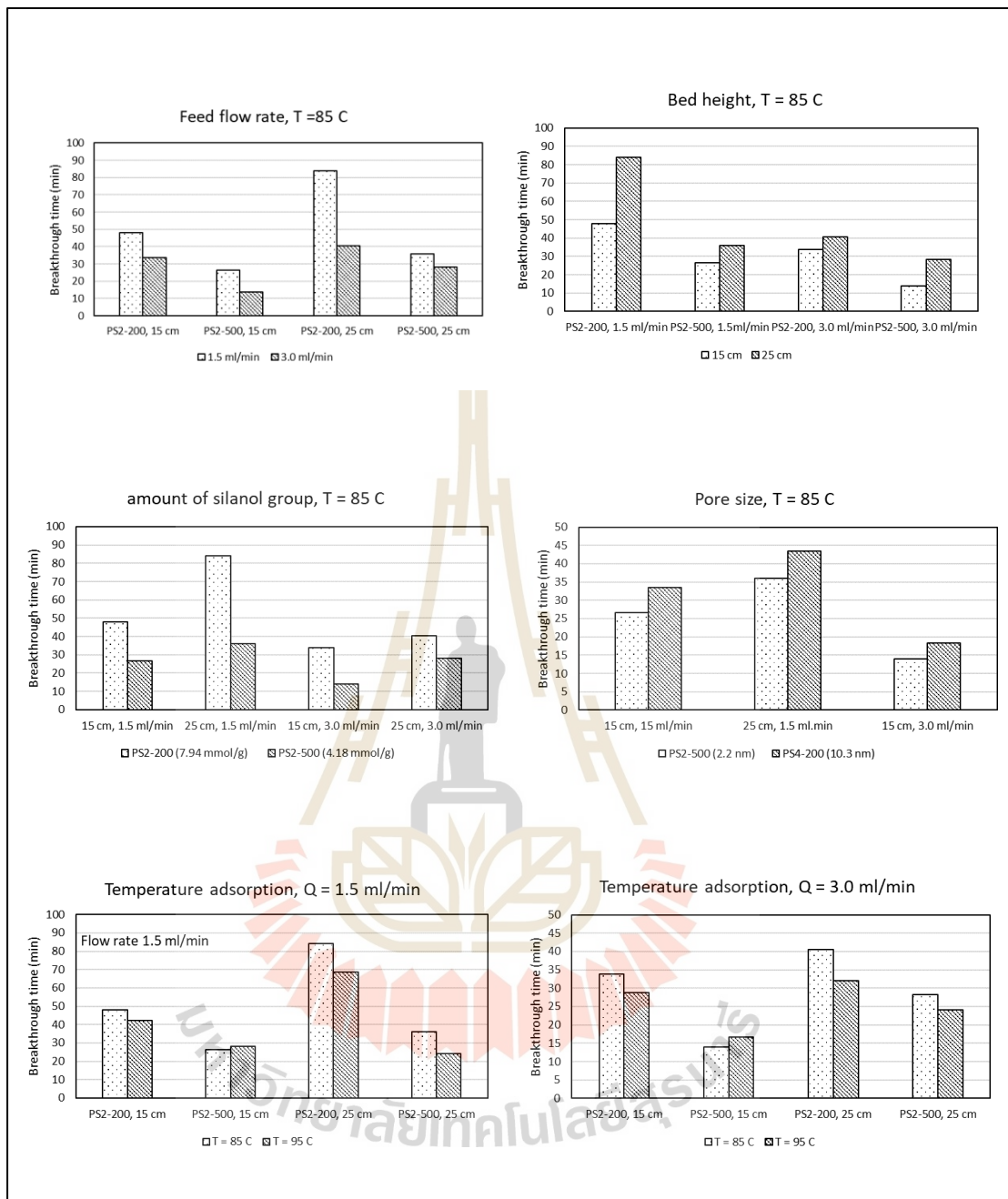


Figure 3.12 (a) Comparison of breakthrough time (t_B) for different operating conditions

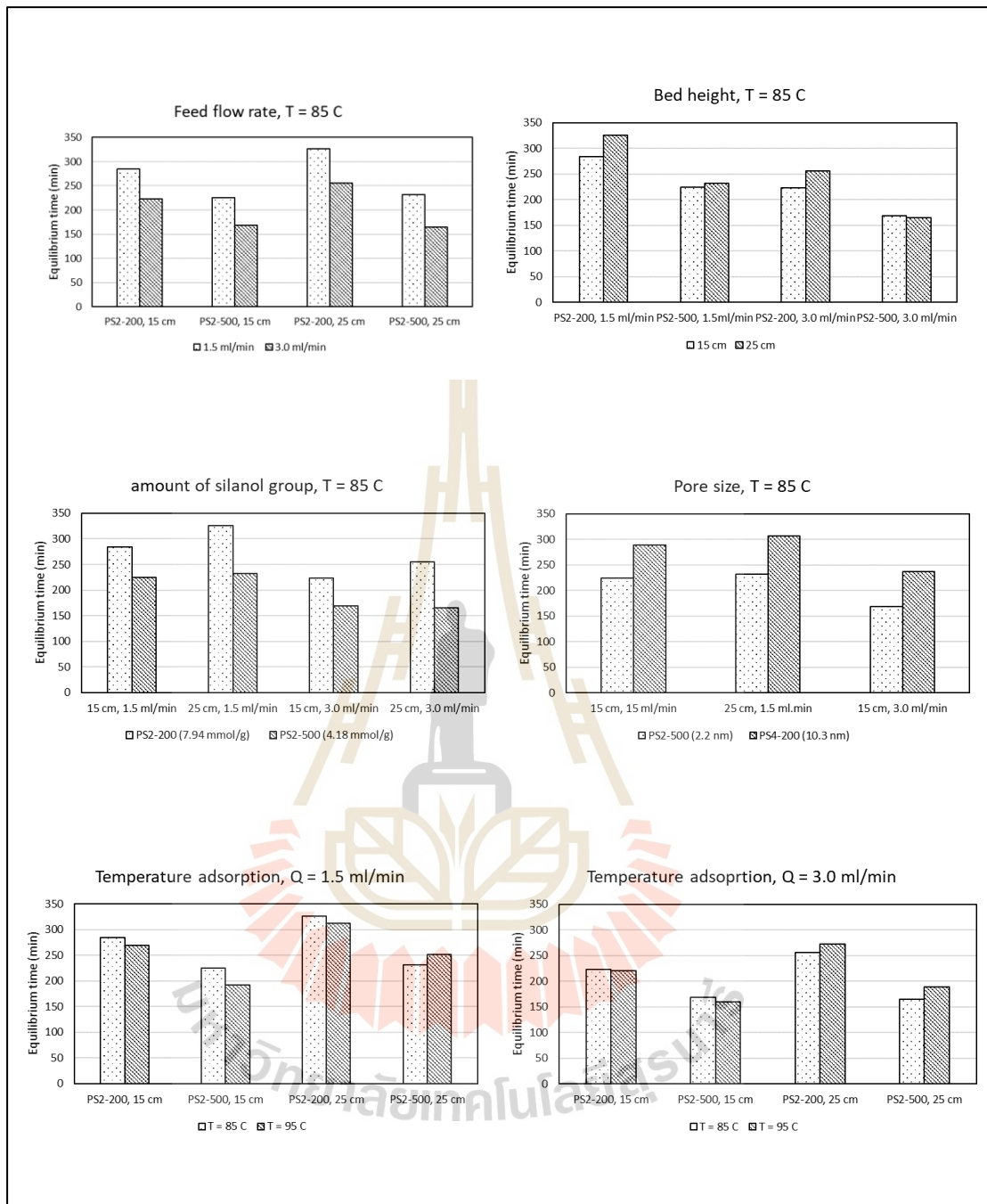


Figure 3.12 (b) Comparison of equilibrium time (t_E) for different operating conditions

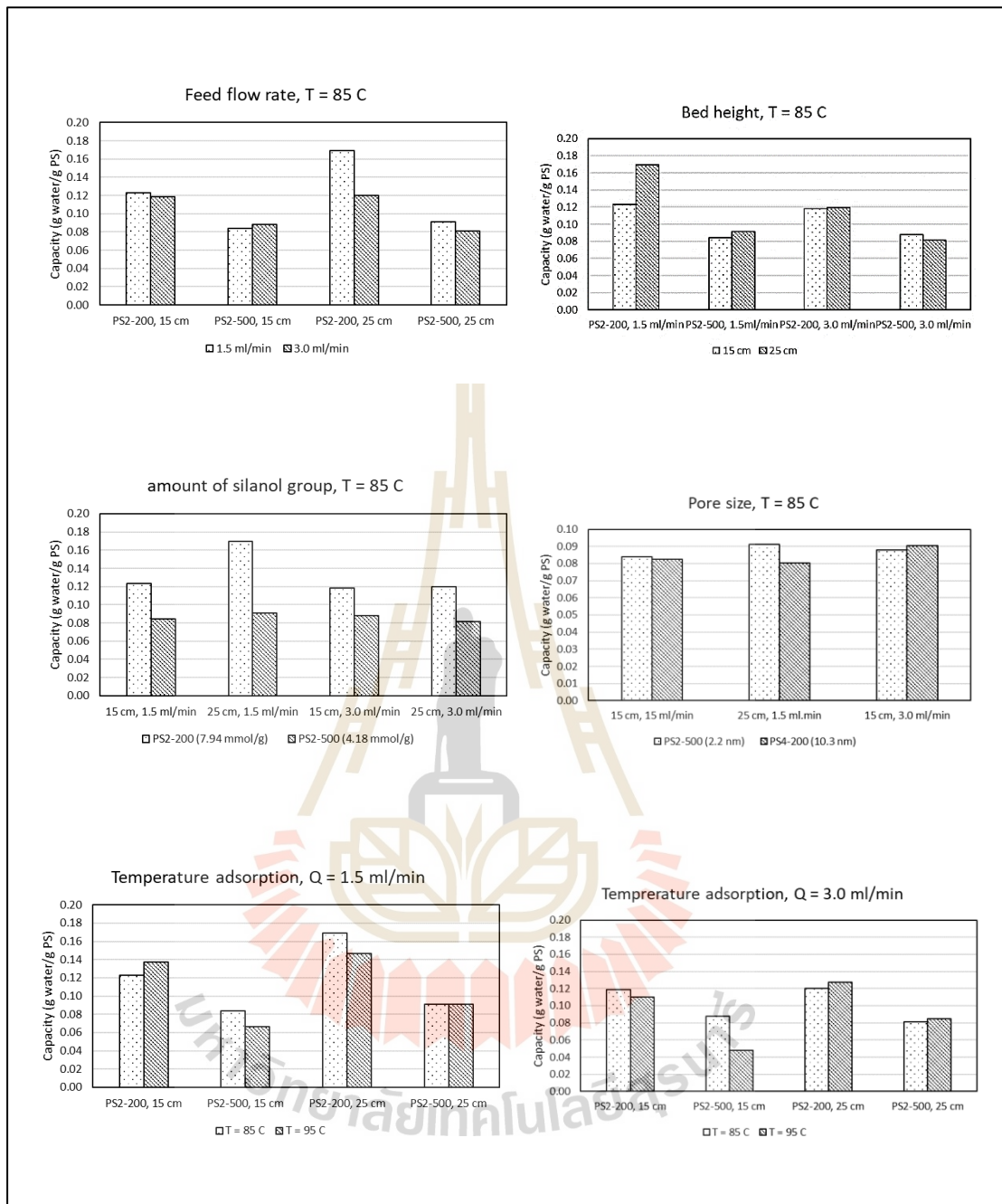


Figure 3.12 (c) Comparison of adsorption capacity at t_B (q_B)

for different operating conditions.

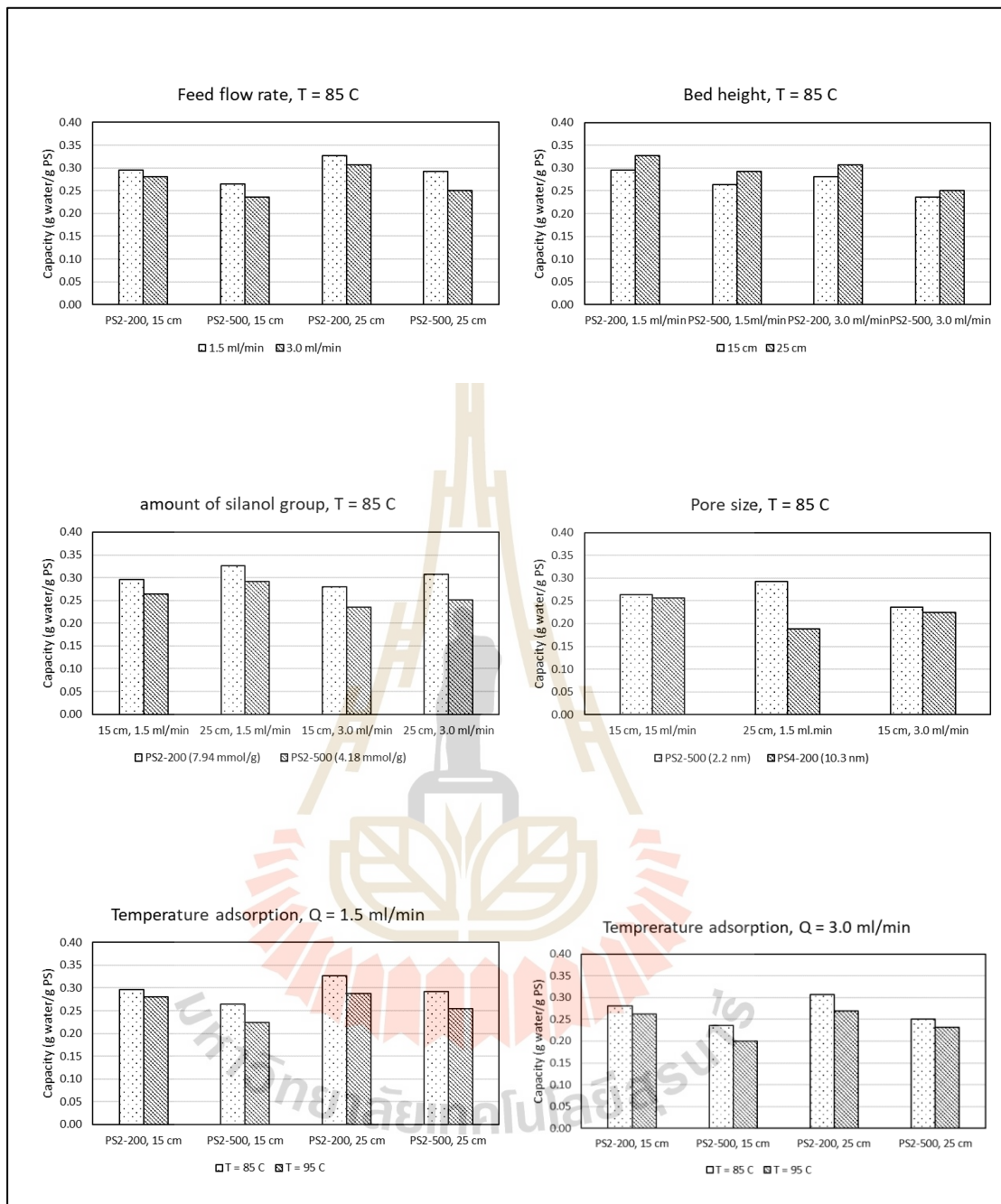


Figure 3.12 (d) Comparison of adsorption capacity at t_E (q_E)

for different operating conditions.

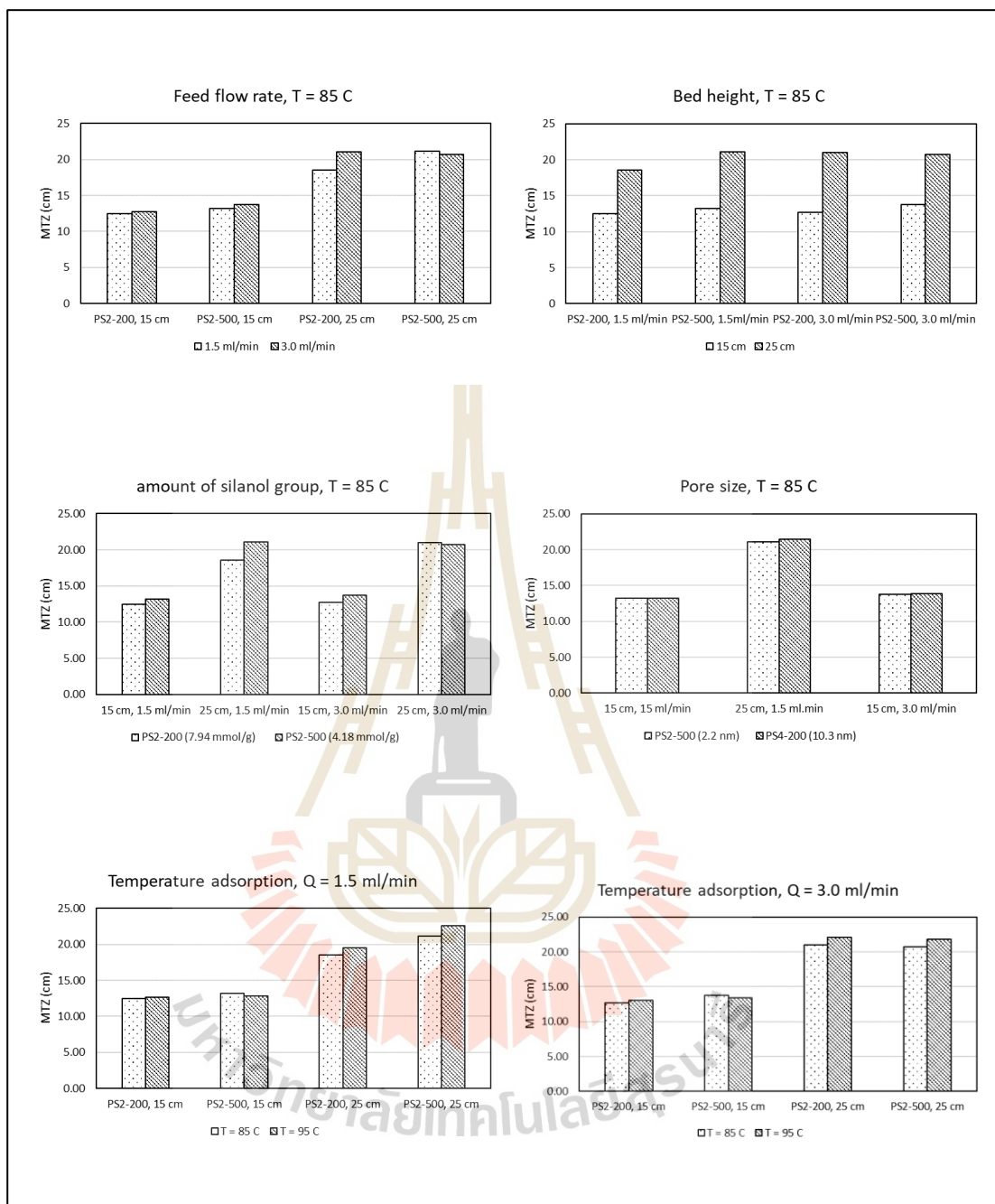


Figure 3.12 (e) Comparison of MTZ for different operating conditions.

Table 3.8 Adsorption capacity of water by various adsorbents

Adsorbent	Water capacity (g water/g)	Refferance
Cornmeal adsorbent	0.160	Ladlish et al., 1984
Molecular sieve 3A	0.186	Krysztof K. et al., 2008
Cassava-based adsorbent	0.051	Chontira B. and Panarat R., 2010
Silica gel		
• Blue silica gel	0.053	Megawati et al., 2016
• White silica gel	0.056	
Porous aluminium oxide material	0.290	S Reshetnikov and I Kurzina, 2019
Porous silica	0.327	This work

The comparison of adsorbed amount of water by various adsorbents in a fixed-bed system is typically shown in **Table 3.8**. The differences in water adsorption capacity should be predominantly attributed to the differences in their chemical and porous properties of the adsorbents employed. It is interesting to note that the amount of water adsorbed by porous glass from this study is highest as compared to the other types of adsorbents, possibly due to the dominant role of the silanol surface groups. Therefore, porous silica is considered as a promising candidate for the efficient removal of water from ethanol.

3.6.2.2 Breakthrough models

For the evaluation of breakthrough results, Klinkenberg's model and Thomas model were applied to the experimental data of the column studies. Levenspiel and Bischoff model was also applied to check for the effect of axial dispersion on the dynamic behavior of the fixed-bed adsorption of water. The regression coefficient (R^2) derived from model fitting between the experimental and predicted results was used as a criterion for the best data fitting by the regression analysis. The estimated values of model parameters with the obtained regression coefficient (R^2) are shown in **Table 3.9**. In testing the Klinkenberg and Levenspiel models, the Henry's constant of the linear isotherm was assumed constant.

Further notice on the optimum rate parameter (k , k_{th} and D_z) of the three models indicate that the values of all parameters increased with the increase in the bed height and feed flow rate.

(a) Thomas model

The behavior of the column was modelled using the Thomas model and the experimental data were fitted to the Thomas model to determine the Thomas rate constant (k_{th}) and maximum adsorptive capacity (q_0) and the results are shown in **Table 3.9**. It can be seen that with the increase of bed height and the amount of silanol groups, the k_{th} values decreased. As the feed flow rate and adsorption temperature increased, the values of k_{th} increased while the values of q_0 decreased.

(b) Levenspiel and Bischoff model

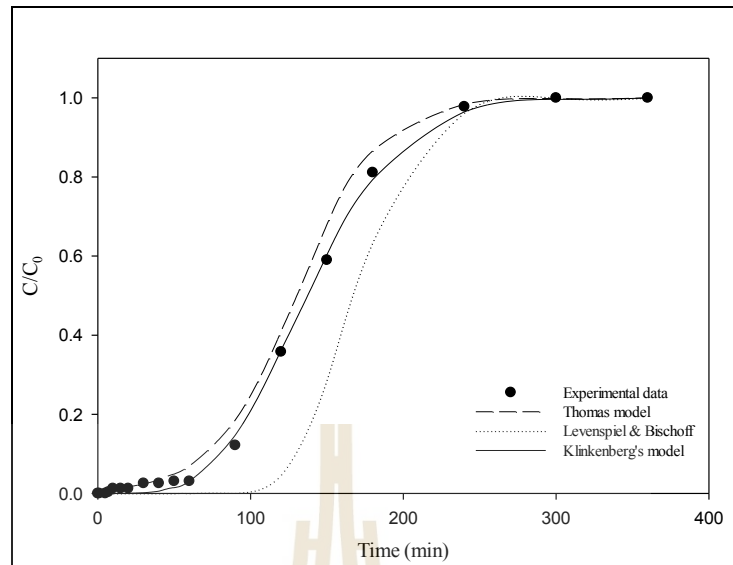
The Levenspiel and Bischoff model was applied to experimental data for describing the breakthrough curve. This approach focused on the estimation of parameters D_z . For all breakthrough curves, the respective values of D_z

was calculated and presented in **Table 3.9**. The values of D_z increased as bed height was increased, but it decreased with the increase of the feed flow rate, the amount of silanol group and the adsorption temperature.

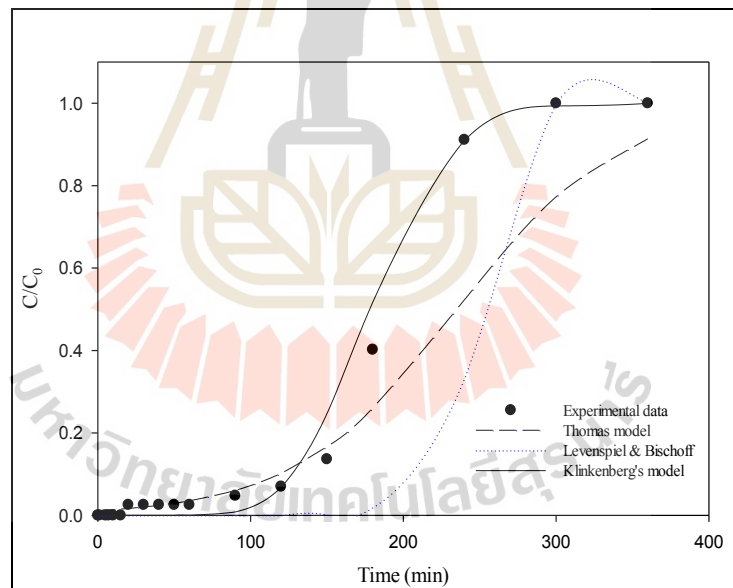
(c) Klinkenberg's model

The Klinkenberg's model assumes that it has a constant fluid velocity, negligible axial dispersion and linear driving force mass-transfer model. This model is represented by **Equation 3.9**. The fitting method of this model between experimental and calculated data was carried out using numerical method for error minimization by R^2 . The obtained value of k and K for Klinkenberg's model are presented in **Table 3.9**. The value of k decreased with an increase of the amount of silanol group, the feed flow rate, the adsorption temperature, and the average pore size. Comparison of the predicted breakthrough models curve and the experimental curves is shown in **Figure 3.13**, the Klinkenberg model predicts the values closer to the experimental values.

Based on the testing of breakthrough models with breakthrough data, the Klinkenberg model was able to describe the breakthrough data the best, followed by the Thomas model and the Levenspiel and Bischoff model (see **Figure 3.13**). The Levenspiel and Bischoff model which takes into account the effect of axial dispersion slightly improved the prediction capability only at the beginning preliminary of the breakthrough data for water adsorption in a fixed bed of porous silica adsorbent.



(a)



(b)

Figure 3.13 Comparison of breakthrough curves between experimental results and different breakthrough models (bed temperature of 85 °C, bed depth 15 cm (a), and bed depth 25 cm (b), superficial velocity of 3.25 cm/s, water concentration feed of 5 wt.%)

3.6.2.3 Analysis of mass transfer resistance

Based on the analysis of breakthrough data by the Klinkenberg's model, the overall mass-transfer resistances ($\frac{1}{kK}$), the external mass transfer resistance ($\frac{R_p}{3k_c}$) and internal mass transfer resistance ($\frac{R_p^2}{15D_e}$), for different operation conditions were estimated and the result are displayed in **Table 3.10**. From Table 3.10 the overall mass transfer resistance ($\frac{1}{kK}$) and the internal mass transfer resistance ($\frac{R_p^2}{15D_e}$) increased with the increasing of temperature, feed flow rate and the average mean pore size. The external mass transfer ($\frac{R_p}{3k_c}$) decreased with the increase of feed flow rate and the adsorption temperature. The increase of bed height (mass of adsorbent) and the amount of silanol group did not affect the external mass transfer, and $\frac{1}{kK} \approx \frac{R_p^2}{15D_e} \gg \frac{R_p}{3k_c}$. This is consistent with the fact that the water adsorption rate on the porous silica was mainly controlled by internal mass transfer resistance. From the comparison of the mass transfer at difference temperatures, the mass transfer rate increased as the temperature was increased.

Table 3.9 Parameters of Klinkenberg, Thomas and Levenspiel & Bischoff model under column adsorption process

Run	Temp (°C)	Sample*	Feed flow rate (ml/min)	Bed height (cm)	Klinkenberg's model			Thomas model			Levenspiel & Bischoff		
					K	k, (x10 ⁻³)	R ²	k _{th} , (x10 ⁻³)	q ₀ , (g/g PS)	R ²	K	D _z , (x10 ⁻³ m ² /s)	R ²
1	85	PS2-200	1.5	15	1274	1.910	0.999	0.738	0.324	0.946	1274	1.564	0.943
2				25	1274	2.520	0.992	0.378	0.353	0.895	1274	2.194	0.982
3			3.0	15	1274	1.399	0.964	0.812	0.294	0.987	1274	1.291	0.946
4				25	1274	2.257	0.996	0.790	0.329	0.992	1274	1.923	0.949
5		PS2-500	1.5	15	870.3	1.997	0.988	0.770	0.275	0.970	870.3	1.637	0.916
6				25	870.3	2.316	0.982	0.559	0.185	0.984	870.3	2.203	0.922
7			3.0	15	870.3	1.842	0.976	1.196	0.350	0.961	870.3	1.399	0.939
8				25	870.3	2.197	0.995	0.868	0.226	0.936	870.3	2.154	0.963
9	95	PS2-200	1.5	15	1120	1.841	0.993	0.770	0.304	0.950	1120	1.377	0.956
10				25	1120	2.181	0.991	0.559	0.240	0.924	1120	2.206	0.910
11			3.0	15	1120	1.264	0.990	1.196	0.298	0.961	1120	1.332	0.961
12				25	1120	2.104	0.979	0.868	0.226	0.936	1120	2.113	0.916
13		PS2-500	1.5	15	769.3	1.743	0.992	1.272	0.160	0.982	769.3	1.826	0.920
14				25	769.3	1.916	0.991	0.872	0.144	0.988	769.3	2.136	0.920
15			3.0	15	769.3	1.583	0.989	1.774	0.221	0.981	769.3	1.880	0.952
16				25	769.3	1.825	0.994	1.014	0.220	0.947	769.3	1.763	0.969
17	85	PS4-200	1.5	15	796.8	1.751	0.988	0.770	0.272	0.951	796.8	2.066	0.948
18				25	796.8	2.172	0.991	0.736	0.190	0.987	796.8	2.185	0.917
19			3.0	15	796.8	1.103	0.978	0.930	0.392	0.975	796.8	1.220	0.935
20		PS4-500	1.5	15	695.4	1.617	0.984	1.088	0.166	0.915	695.4	1.543	0.890

*porous silicas were designated as PSX-Y where X is the pH of mixture and Y is the calcination temperature.

Table3.10 The result of mass transfers resistance for various adsorption conditions

Run	Temp (°C)	Sample*	Feed flow rate (ml/min)	Bed height (cm)	Re	Sc	Sh	k_c (m/s)	$\frac{1}{kK}$	$\frac{R_p}{3k_c}$ ($\times 10^{-3}$)	$\frac{R_p^2}{15D_e}$	D_E ($\times 10^{-8}m^2/s$)
1	85	PS2-200	1.5	15	6.264	0.322	4.267	0.069	0.411	3.372	0.408	7.901
2				25	6.264	0.322	4.267	0.069	0.311	3.372	0.308	10.451
3			3	15	12.692	0.322	5.463	0.088	0.561	2.636	0.558	5.766
4				25	12.692	0.322	5.463	0.088	0.348	2.636	0.345	9.330
5		PS2-500	1.5	15	6.264	0.322	4.267	0.069	0.575	3.372	0.572	5.630
6				25	6.264	0.322	4.267	0.069	0.496	3.372	0.493	6.535
7			3	15	12.692	0.322	5.463	0.088	0.624	2.636	0.621	5.184
8				25	12.692	0.322	5.463	0.088	0.523	2.636	0.520	6.188
9	95	PS2-200	1.5	15	5.935	0.324	4.199	0.071	0.485	3.268	0.482	6.685
10				25	5.935	0.324	4.199	0.071	0.409	3.268	0.406	7.929
11			3	15	12.026	0.324	5.359	0.091	0.706	2.560	0.704	4.575
12				25	12.026	0.324	5.359	0.091	0.424	2.560	0.422	7.634
13		PS2-500	1.5	15	5.935	0.324	4.199	0.071	0.746	3.268	0.743	4.337
14				25	5.935	0.324	4.199	0.071	0.678	3.268	0.675	4.769
15			3	15	12.026	0.324	5.359	0.091	0.821	2.560	0.819	3.934
16				25	12.026	0.324	5.359	0.091	0.712	2.560	0.710	4.537
17	85	PS4-200	1.5	15	6.264	0.322	4.267	0.069	0.717	3.372	0.713	4.514
18				25	6.264	0.322	4.267	0.069	0.578	3.372	0.574	5.606
19			3	15	12.692	0.322	5.463	0.088	1.138	2.636	1.135	2.837
20		PS4-500	1.5	15	6.264	0.322	4.267	0.069	0.889	3.372	0.886	3.635

*porous silicas were designated as PSX-Y where X is the pH of mixture and Y is the calcination temperature.

3.7 Conclusion

The following conclusions can be drawn from this study:

- For the removal of water from an ethanol-water mixture in liquid phase (batch adsorption) and vapor phase (continuous adsorption) by using porous silica, it was found that the silanol group on the surface of porous silica played an important role in the adsorption water molecules via hydrogen bonding.

- The equilibrium isotherms of water adsorption in liquid phase were tested using Langmuir and Freundlich models and the results showed that the Langmuir model gave the best description of water adsorption by porous silica for all the temperature range being studied. The adsorption kinetics of water by porous silica was best described by the pseudo second-order kinetic model.

- Study on a fixed-bed adsorption using porous silica to remove water indicated that it has ability to remove water from vapor mixture of ethanol. The adsorption dynamic parameters of the fixed bed, including the breakthrough time, the adsorbed capacity at the breakthrough time and the adsorbed capacity at equilibrium, were found to increase with the increase of the bed height and the amount of silanol group, but to decrease with the increase of the adsorption temperature and the feed flow rate.

- The Levenspiel and Bischoff model which takes into account the effect of axial dispersion, for the water adsorption in fixed bed showed a poor prediction of the breakthrough results. Therefore, as a first approximation the effect of axial dispersion, for the water adsorption in fixed bed under the conditions tested in this study can be neglected.

- The testing of Thomas model with experiment breakthrough data was performed, and model parameters were determined by linear regression analysis for

water adsorption under various operation condition. The model was able to predict the breakthrough data fairly well.

- The Klinkenberg model based on the linear driving force model successfully described the experimental water breakthrough curves obtained under the tested conditions. It was also found that the Klinkenberg model parameters including mass transfer coefficient (k) and effective diffusivities (D_e) can be estimated directly from the experimental breakthrough data.



3.8 References

- Aksu Z. and Gonen F. (2004) Biosorption of phenol by immobilized activated sludge in a continuous packed bed: Prediction of breakthrough curves. **Process biochemistry**. Vol. 39, (5): 599-613.
- Brinker C.J. and Scherer G.W. (1990). Sol-gel science, the physics and chemistry of sol-gel processing. **Academic Press**. Boston.
- Banat F.A., Abu Al-Rub, and Simandl J. (2000). Separation and purification technology. Vol. 18, No. 2, 111-118.
- Carmo M. J. and Gubulin, J.C. (2002). Ethanol-water separation in the PSA process. *Adsorption*, 8: 235-248
- Chontira Boonfung and Panarat Rattanaphanee (2010). Cassava-based adsorbent for ethanol dehydration. **The Journal of KMUTNB**. Vol. 20, 2: 196-203.
- Ernest J. Henley, J.D. Seader, D. Keith Roper, (2006). Separation process principles. **John Wiley & Sons, Inc.**
- H. Zhang, W. Gu, M.J. Li, Z.Y. Li, Z.J. Hu and W.Q. Tao (2014). Experimental study on the kinetic of water vapor sorption on the inner surface of silica nano-porous materials. **Adsorption Science & Technology**. Vol. 26, 3: 209-224.
- Ho, Y.S. and McKay, G., (1998). Kinetic models for the sorption of dye from aqueous solution by wood. **Process Safety and Environmental Protection**, 76 (2): 183-191.
- International Energy Agency, **IEA** (2011)

- Inyinbor Adejumo, Adekola Folahan and Olatunji G.A. (2016). Kinetics, Isotherms and thermodynamic modeling of liquid phase adsorption of Rhodamine B dye onto *Raphia hookeri* fruit epicarp. **Water Resources and Industry**. Vol. 15, 14-27.
- Krzysztof Kupiec, Jan Rakoczy, Lukasz Zielinski and Andreas Georgiou (2008). Adsorption-desorption cycles for the separation of vapor-phase ethanol/water mixture. **Adsorption Science & Technology**. Vol. 26, 3: 209-224.
- Kuan-Shyang Wang, Chien-Chih Liao, Richard Q. Chu, and Tsair-Wang Chung. (2010). Equilibrium Isotherms of water and Ethanol Vapor on Starch Sorbent and Zeolite 3A. **Journal of Chemical & Engineering Data**. Vol. 55, 9: 3334-3337.
- Kumar P. S., Ramalingam S., Kirupha S. D., Murugesan A., Vidhyadevi T., Sivanesan S. (2011). Adsorption behavior of nickel (II) onto cashew nut shell: Equilibrium, thermodynamics, kinetics, mechanism and process design. **Chemical Engineering Journal**. Vol. 167(1):122–131.
- Ladisch, M.R. (1997). Biobased Adsorbents for Drying of Gases. **Enzyme and Micro Technology**. Vol. 20, 162-164.
- Ladisch, M.R., Marcio Voloch, Juan Hong, Paul Bienkowski and Geoyge T. Tsao (1984). Cornmeal adsorber for dehydrating ethanol vapor. **Industrial & Engineering Chemistry Process Design and Development**. Vol. 23, 437-443.
- Lagergren S. (1898). About the theory of so-called adsorption of soluble substance. **Sven. Vetenskapsakad. Handlingar**, 24: 1-39.

- Megawati, Reni Ainun Jannah and Indi Rahayuningtiyas (2016). The influence of white and blue silica gels as adsorbents in adsorptive-distillation of ethanol-water mixture. **International Conference on Engineering, Science and Nanotechnology**. Vol. 1788, 030114 (1-6).
- Pinto R. T. P., Wolf-Maciel M. R. and Lintomen, L. (2000). Saline extractive distillation process for ethanol purification. **Computers and Chemical Engineering**, 24: 1689-1694.
- Rouquerol F., Rouquerol J. and Sing K. (1999). Adsorption by powder and porous **Solid**. Academic Press, London.
- Ruthven, D. M. (1997). **Encyclopedia of Separation Technology**. New York: John Wiley.
- S Reshetnikov and I Kurzina (2019). Investigation of adsorption of water vapor on porous aluminium oxide material. **Materials Science and Engineering**. Vol. 597, 1-6.
- Weber Walter J. and Morris J. Carrell (1963). Kinetics of adsorption on carbon from solution. **Journal of the Sanitary Engineering Division**. Vol. 89(2), 31-60.
- Wilfried Cordes (2008). Vapor-liquid equilibrium of the mixture of Ethanol and Water. **Dortmund Data Bank**.
- Yakout, S.M. and Elsherif, E. (2010). Batch Kinetics, Isotherm and Thermodynamic Studies of Adsorption of Strontium from Aqueous Solutions onto Low cost Rice-Straw Based Carbons. **Carbon-Science and Technology**. Vol. 3, 144-153.

CHAPTER IV

REMOVAL OF METHYLENE BLUE DYE FROM AQUEOUS SOLUTION WITH POROUS SILICA ADSORBENT

4.1 Abstract

The adsorption of methylene blue (MB) from aqueous solution on porous silica prepared from sodium silicate by the sol-gel method was investigated. Adsorption was studied as a function of temperature (30-50 °C), adsorbent dosage (0.01-0.6 grams) and initial feed concentration of MB (50-400 mg/L). From the results obtained it was observed that the adsorption efficiency increased from 4.85 to 97.99% for PS2-200 and 6.67 to 99.77% for PS4-200 respectively, by increasing the porous silica dosage from 0.01 to 0.6 grams. The experimental kinetic data were fitted to the pseudo first-order and pseudo-second order models. The equilibrium data were analyzed by the Langmuir isotherm and Freundlich isotherm. For the MB adsorption on porous silica, it was found that the Langmuir isotherm could well describe the equilibrium adsorption and the pseudo second-order model could best predict the adsorption kinetic results.

4.2 Introduction

Methylene blue (MB) as a cationic dye is most used in color product manufactured in many industries such as textile, paper, printing, dyeing industries, and medical science. Meanwhile, huge amounts of dyes have been discharged into natural environment during the production process, which thus causes serious environmental problems (Yagub et al., 2014). However, the presence of methylene blue in industrial effluent poses serious threat to the environment because it can cause eye burns which may be responsible for permanent eye injury in human and animals. Therefore, it is quite urgent to remove the dye from water, and several methods have been devoted to resolving this issue, including photodegradation, adsorption, biodegradation, coagulation-flocculation and so forth (Cai et al., 2017). Adsorption has been considered as a viable method for removing methylene blue from aqueous solution due to its low cost, easy operation, and high efficiency process (Malamis and Katsou, 2013; Pang et al., 2013). Porous materials have attracted the attention of scientists due to commercial interest related to their applications in separations, catalysts, and purification technologies (Atyaf Khalid Hameed et al., 2016). In this work, porous silica prepared was tested as an adsorbent for the removal of methylene blue from an aqueous solution in a batch system.

The purpose of the present investigation is thus to study the removing of methylene blue from aqueous solution by sorption in a batch mode with porous silica adsorbent. This work deals primarily with studying the effect of process parameters on adsorption performance, including initial concentration of MB, amount of adsorbent, temperature adsorption, silanol contents and mean pore size of porous silica. Besides, the adsorption process was evaluated for kinetic using the pseudo-

first-order model and pseudo-second-order model as well as adsorption isotherms including Langmuir and Freundlich models.

4.3 Experimental

4.3.1 Adsorption Kinetics

Adsorption kinetic experiments were conducted for the porous silica PS2-200 and PS2-500 samples. The experiment was carried out in a 100 mL Erlenmeyer flask by mixing 50 mL of methylene blue (MB) solution of concentration 100 mg/L and 0.1 grams of porous silica and shaking the flasks at 30 °C up to 12 hours. The samples were withdrawn at several time intervals of 0, 0.25, 0.5, 1, 2, 4, 8 and 12 hours for further analysis of MB concentrations.

4.3.2 Adsorbent Dosage

The study of adsorbent dosage was conducted using porous silica PS2-200 and PS4-200 samples. 50 mL of methylene blue (MB) solution with concentration of 200 mg/L and porous silica weighing 0.01-0.6 grams were loaded into a 100 mL Erlenmeyer flask and shaking at 30 °C for 6 hours. Each solution sample for each adsorbent dosage was then withdrawn for the analysis of MB concentration.

4.3.3 Adsorption Isotherms

Batch adsorption experiments were performed by mixing 0.1 grams of porous silica samples (PS2-200 and PS2-500) with each of MB solution having initial concentration in the range 50-400 mg/L in a 50 mL Erlenmeyer flask and shaking in a temperature-controlled water bath for 24 hours. Three adsorption temperatures of 30, 40 and 50 °C were studied.

4.3.4 Calibration curve of methylene blue

MB concentration for each solution sample was determined by using an Ultraviolet Visible Spectrophotometer (UV-VIS, Varian Cary 1E) by measuring the solution absorbance at the wavelength of 628 nm. **Figure 4.1** shows the calibration curve of methylene blue, which is the plot of a absorbance of dye by UV-spectrophotometer versus MB concentration. The curve is represented by the equation $y = 4.1014x$, where y is the MB concentration (mg/L) and x is the absorbance of dye measured by the UV-spectrophotometer.

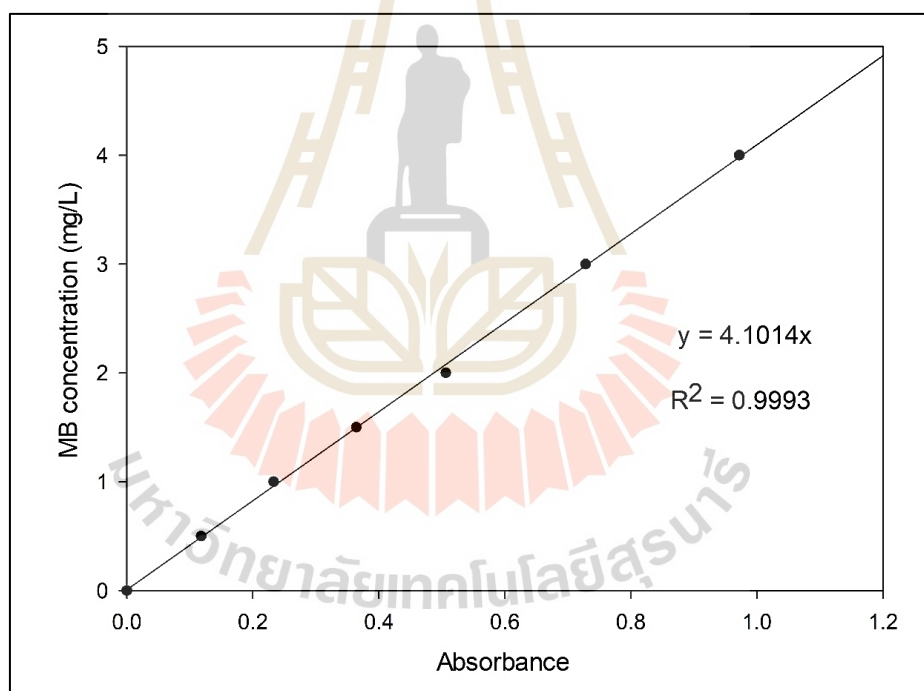


Figure 4.1 Calibration curve of methylene blue (MB) solution.

The amount of MB adsorbed onto the known weight of the porous silica in mg/g was calculated using the following equation

$$q = \frac{V(C_0 - C)}{m} \quad (4.1)$$

where, C_0 is the initial concentration of methylene blue (mg/L), C is the concentration of methylene blue at time t (mg/L), V is the solution volume (L) and m is the mass weight of porous silica (g).

4.4 Results and discussion

4.4.1 Effect of adsorbent dosage

The effect of adsorbent dosage on the methylene blue adsorption by porous silica was studied covering the dosage in the range of 0.01-0.6 g, with initial MB concentration of 200 mg/L at the adsorption temperature of 30 °C and contact time of 360 minutes and the results are shown in **Figure 4.2**. The amount of MB adsorbed (% adsorption efficiency) tended to increase approximately linearly with the increase of adsorbent dosage and become constant after a certain amount of adsorbent was reached. This critical dosage was found to be 0.3 grams and 0.4 grams for samples PS4-200 and PS2-200, respectively. The increase of adsorption efficiency with the increase of adsorbent amount is due to the corresponding increase of adsorption sites that can accommodate an increasing number of MB molecules.

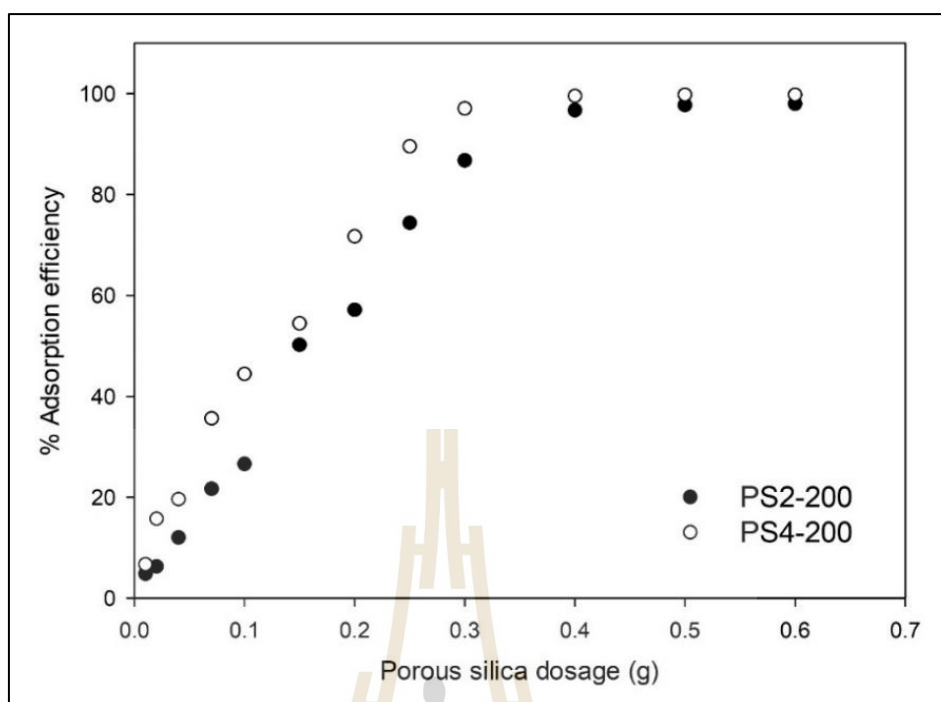


Figure 4.2 Effect of adsorbent dose on MB adsorption with initial MB concentration of 200 mg/L at the adsorption temperature of 30 °C.

4.4.2 Effect of adsorption temperature

Figure 4.3 shows the effect of temperature on the adsorption efficiency of MB by porous silica samples. Over the temperature range of 30-50 °C, there was a general tendency for the adsorption efficiency to increase with the increase of adsorption temperature, but the effect is not very pronounced. This result indicates that MB adsorption by porous silica adsorbents is an endothermic process, possibly involving some kind of chemical adsorption.

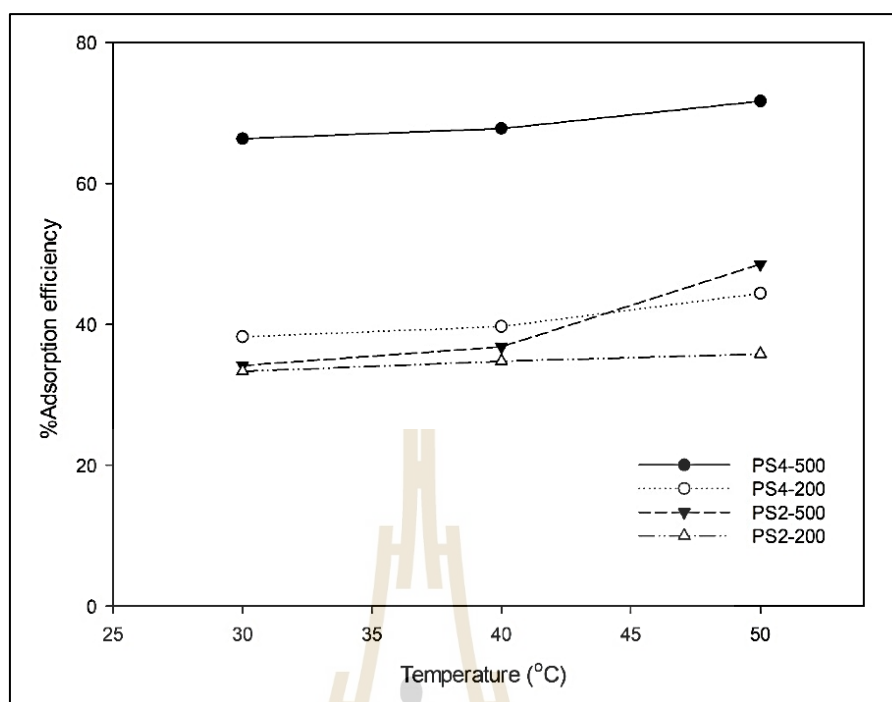


Figure 4.3 Effect of temperature on MB adsorption with initial MB concentration of 100 mg/L and 0.1 grams of porous silica

4.4.3 Effect of initial concentration

The effect of methylene blue initial concentration in the range of 50-400 mg/L on the adsorption of MB on porous silica PS4-500 (10.9 nm and silanol contents 2.77 mmol/g) and the obtained results are presented in **Figure 4.4**. It was seen that the adsorption efficiency of MB decreased with the increase of MB initial concentration. It was observed that at lower MB concentrations, an increase in the percentage MB adsorption is due to high ratio of adsorbent sites to the MB molecules, while at higher MB concentrations, the MB adsorption efficiency decreased significantly due to the saturation of the adsorbent surface between the adsorbed layers and the remaining bulk molecules (Bouaziz et al., 2015).

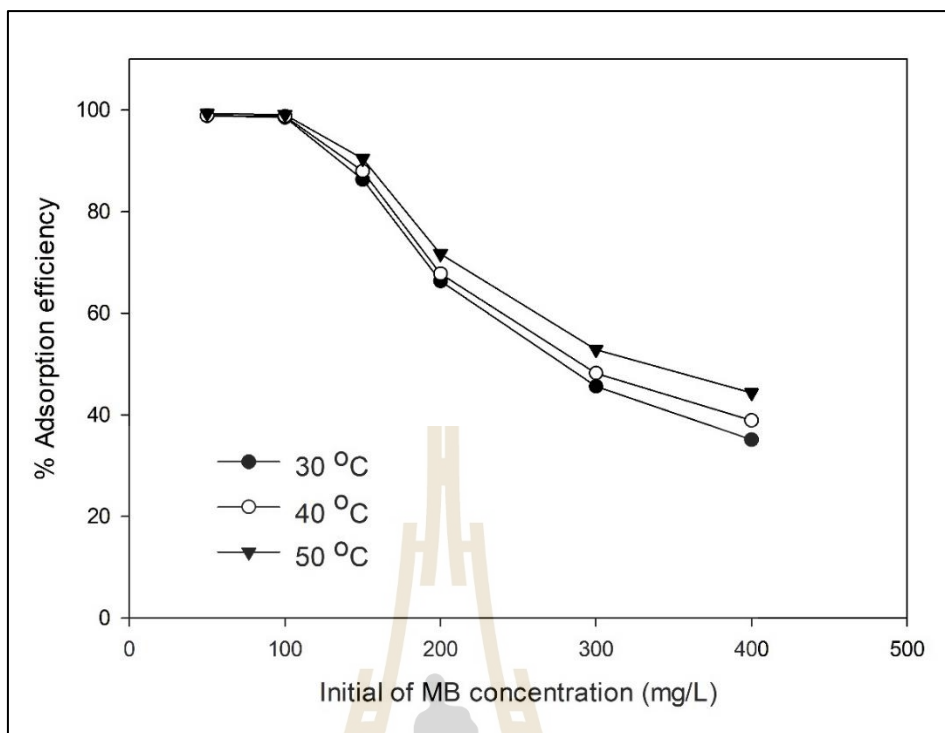


Figure 4.4 Effects of initial MB concentration on porous silica PS4-500 with different adsorption temperature

4.4.4 Adsorption kinetics

The time needed to establish an adsorption equilibrium was investigated by varying the adsorption time intervals of 15, 30, 60, 90, 120, 240, 360 and 600 minutes, using the initial MB concentration of 100 and 200 mg/L, and employing PS2-200 adsorbent at 30 °C.

Two kinetic models were used for the analysis, that is, pseudo-first-order and pseudo-second-order models. Their respective integral equations are as follows,

$$\ln(q_e - q_t) = \ln q_e - K_1 t \quad (4.2)$$

$$\frac{1}{q_t} = \frac{1}{V_0} + \frac{1}{q_e} t \quad (4.3)$$

where q_e is the amount of MB adsorbed at equilibrium (g/g)

q_t is the amount of MB adsorbed at time t (g/g)

K_1 is the pseudo-first-order rate constant for the kinetic model (min^{-1})

$V_0 = K_2 q_e^2$ is the initial adsorption rate

K_2 is the pseudo-second-order rate constant for the kinetic model ($\text{g} \cdot \text{g}^{-1} \text{min}^{-1}$)

Figure 4.4 illustrates the amount of MB adsorbed as a function of adsorption contact time. The amount of MB adsorbed was rapidly increase in the first 30 minutes. The increasing of MB adsorbed amount was slower after 30 minutes, before the MB adsorbed amount remained constant at longer equilibrium times. The kinetic curves (Figure 4.4), show that the sorption equilibrium is reached at 120 minutes after sorption starts, that is, the equilibrium time for MB adsorption from aqueous solution. Analysis of the time dependence at 30 °C using the kinetic models of pseudo-first-order and pseudo-second-order models show that MB sorption by porous silica (PS2-200) can be best described by the pseudo-second-order model (as shown by R^2 in **Table 4.1**). At equilibrium, the total MB adsorbed by PS2-200 with the MB initial concentration of 100 and 200 mg/L were 38.54 g/g and 42.17 g/g, respectively. The equilibrium concentration of MB (q_e) predicted by the pseudo-second-order model agreed very well with that derived from the experiment.

Table 4.1 List of parameters obtained from Pseudo-first-order, Pseudo-second-order model fitting for adsorption of methylene blue onto PS2-200 at 30 °C

Constants	Initial concentration of MB (mg/L)	
	100	200
q_e experimental (g/g)	38.54	42.17
Pseudo first order		
q_e calculated (g/g)	23.63	40.10
K_1 (min^{-1})	0.045	0.029
R^2	0.949	0.918
Pseudo second order		
q_e calculated (g/g)	39.06	42.74
K_2 ($\text{mg}\cdot\text{g}^{-1}\cdot\text{min}^{-1}$)	7.115	4.774
R^2	0.999	0.999

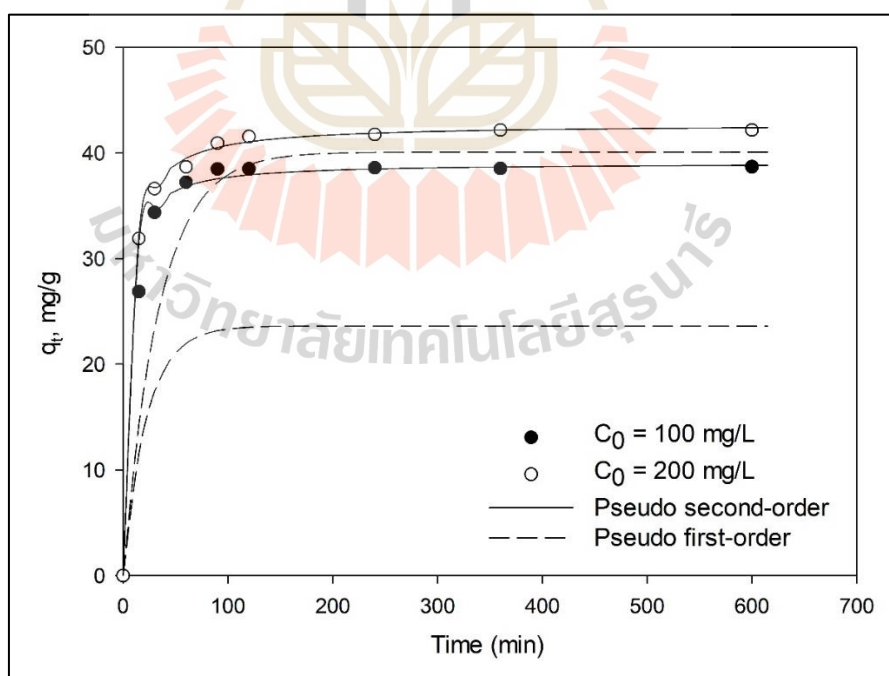


Figure 4.4 Adsorption kinetic of Methylene blue (MB) on porous silica PS2-200 at adsorption temperature 30 °C

4.4.5 Methylene blue (MB) adsorption isotherms

The Langmuir isotherm assumes that adsorption takes place on a homogenous surface, only one site can accommodate one molecule of adsorbate available and that the adsorbent is saturated after one layer of adsorbate molecules forming onto the surface (ALzaydien, A.S., 2009 and Abdel et al., 2013). **Equation 4.4** expresses the linearized form of the Langmuir adsorption isotherm. The constants (q_m and k_L) in the Langmuir isotherm equation can be determined by plotting C_e/q versus C_e according to the following linear equation of Langmuir isotherm,

$$\frac{C_e}{q} = \frac{1}{q_m k_L} + \frac{C_e}{q_m} \quad (4.4)$$

where q is the mass of adsorbate adsorbed in g/g of adsorbent, q_m is the maximum loading corresponding to complete coverage of the surface by the adsorbate in g/g of adsorbent. C_e is the equilibrium concentration of adsorbate in the fluid phase, g/mL and k_L is the Langmuir or affinity constant.

The linearized Freundlich isotherm equation that corresponds to the adsorption on a heterogeneous surface is given as **Equation 4.5**. The constants in the Freundlich isotherm (K and n) can be determined by plotting q versus C_e on a log-log scale based on the following linear equation,

$$\log q = \log K + \frac{1}{n} \log C_e \quad (4.5)$$

where q is the mass of adsorbate adsorbed in g/g adsorbent, C_e is the equilibrium concentration of adsorbate in the bulk phase g/mL, K and n are constant of the

Freundlich adsorption isotherm. The slope $1/n$ measures the surface heterogeneity. Heterogeneity becomes more prevalent as $1/n$ gets closer to zero (Peruchi et al., 2014).

Langmuir and Freundlich isotherm parameters for adsorption of MB onto porous silica are derived by fitting the experimental isotherms with those calculated by the models and are summarized in **Table 4.2**. The results indicate that the capacity of porous silica for sorption of MB increased with the increase of temperature. Besides, the equilibrium capacity (q_m) was found to increase with larger pores. It can also be seen that (PS4-200 and PS4-500) with larger mesopore volume has performed better on the adsorption of MB. The maximum adsorption capacity of MB on porous silica PS4-500 gave a maximum value of 87.72 g/g at 50 °C. The surface heterogeneity of the adsorbent became more prevalent since the value of $1/n$ was nearly zero. The adsorption isotherms of water on porous silica are shown in **Figure 4.5**, showing the relationship between the amount of MB adsorbed per unit mass of porous silica and the concentration of MB solution at equilibrium at varying temperatures. Overall, the Langmuir isotherm equation was able to describe the adsorption process better than that of Freundlich isotherm, as indicated by its higher correlation coefficient value (R^2). Hence, the adsorption of MB on porous silica can be considered as a monolayer adsorption rather than multilayer adsorption.

Table 4.2 (a) Estimated parameters of various isotherms models for adsorption of methylene blue onto PS2-200 in the liquid phase system

Adsorption temperature	Langmuir			Freundlich		
	q_m (g/g)	k_L (L/g)	R^2	K	1/n	R^2
30 °C	35.59	0.175	0.9995	24.79	0.061	0.9477
40 °C	37.31	0.163	0.9994	24.67	0.070	0.9725
50 °C	38.17	0.160	0.9994	24.14	0.079	0.9685

Table 4.2 (b) Estimated parameters of various isotherms models for adsorption of methylene blue onto PS2-500 in the liquid phase system

Adsorption temperature	Langmuir			Freundlich		
	q_m (g/g)	k_L (L/g)	R^2	K	1/n	R^2
30 °C	36.90	0.173	0.9990	25.99	0.058	0.9444
40 °C	39.53	0.157	0.9992	25.63	0.074	0.9768
50 °C	41.67	0.110	0.9975	24.80	0.086	0.9445

Table 4.2 (c) Estimated parameters of various isotherms models for adsorption of methylene blue onto PS4-200 in the liquid phase system

Adsorption temperature	Langmuir			Freundlich		
	q_m (g/g)	k_L (L/g)	R^2	K	1/n	R^2
30 °C	40.49	0.16918	0.9991	24.62	0.087	0.9189
40 °C	44.25	0.13714	0.9982	27.03	0.0833	0.9882
50 °C	50.25	0.12414	0.9979	27.67	0.1023	0.9976

Table 4.2 (d) Estimated parameters of various isotherms models for adsorption of methylene blue onto PS4-500 in the liquid phase system

Adsorption temperature	Langmuir			Freundlich		
	q_m (g/g)	k_L (L/g)	R^2	K	1/n	R^2
30 °C	70.42	0.52015	0.9997	49.61	0.0667	0.9232
40 °C	76.92	0.26804	0.9976	49.55	0.08	0.9617
50 °C	87.72	0.20141	0.9940	50.37	0.0975	0.9717

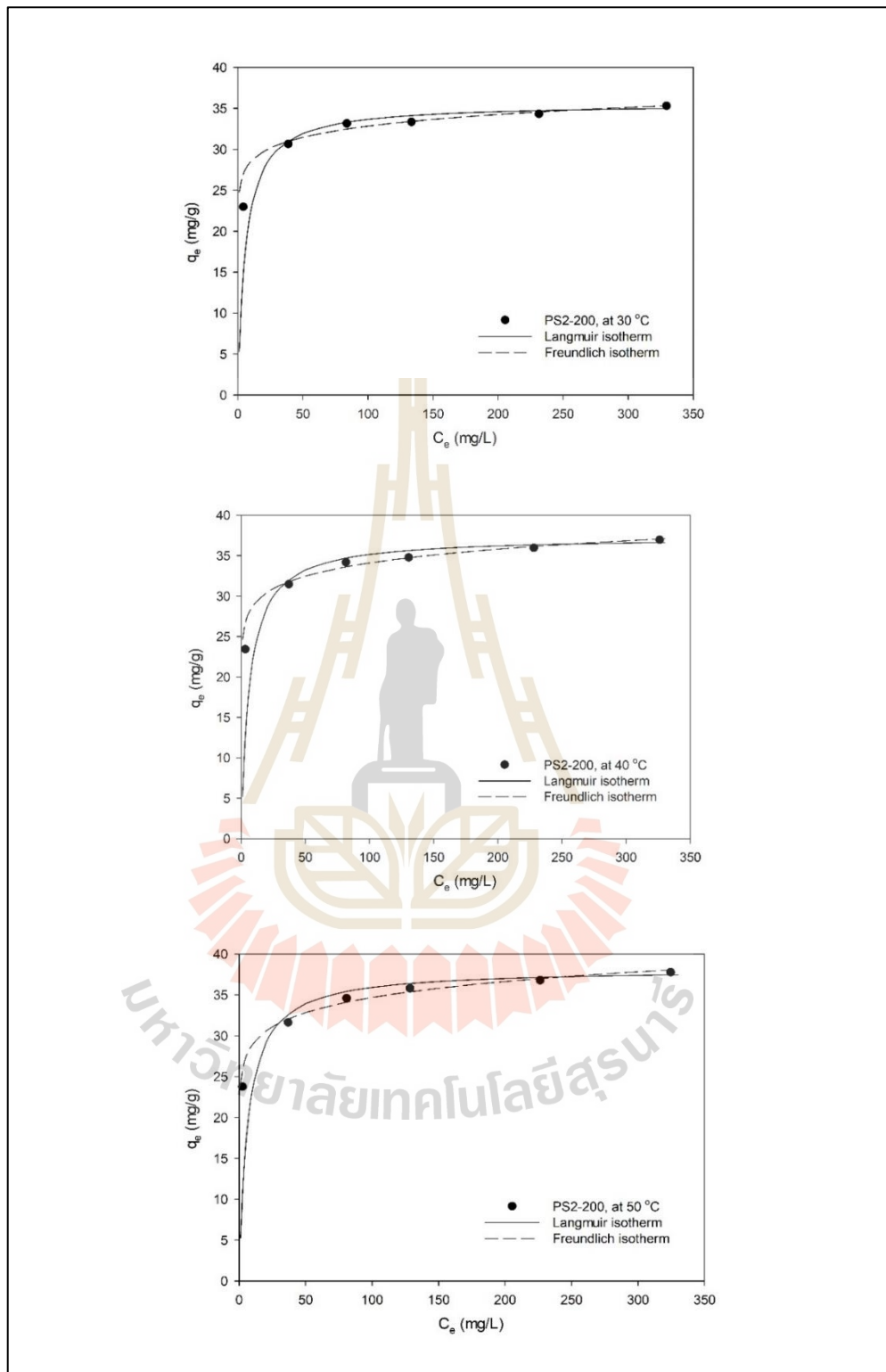


Figure 4.5 (a) Adsorption Isotherm of MB on PS2-200 with different temperature

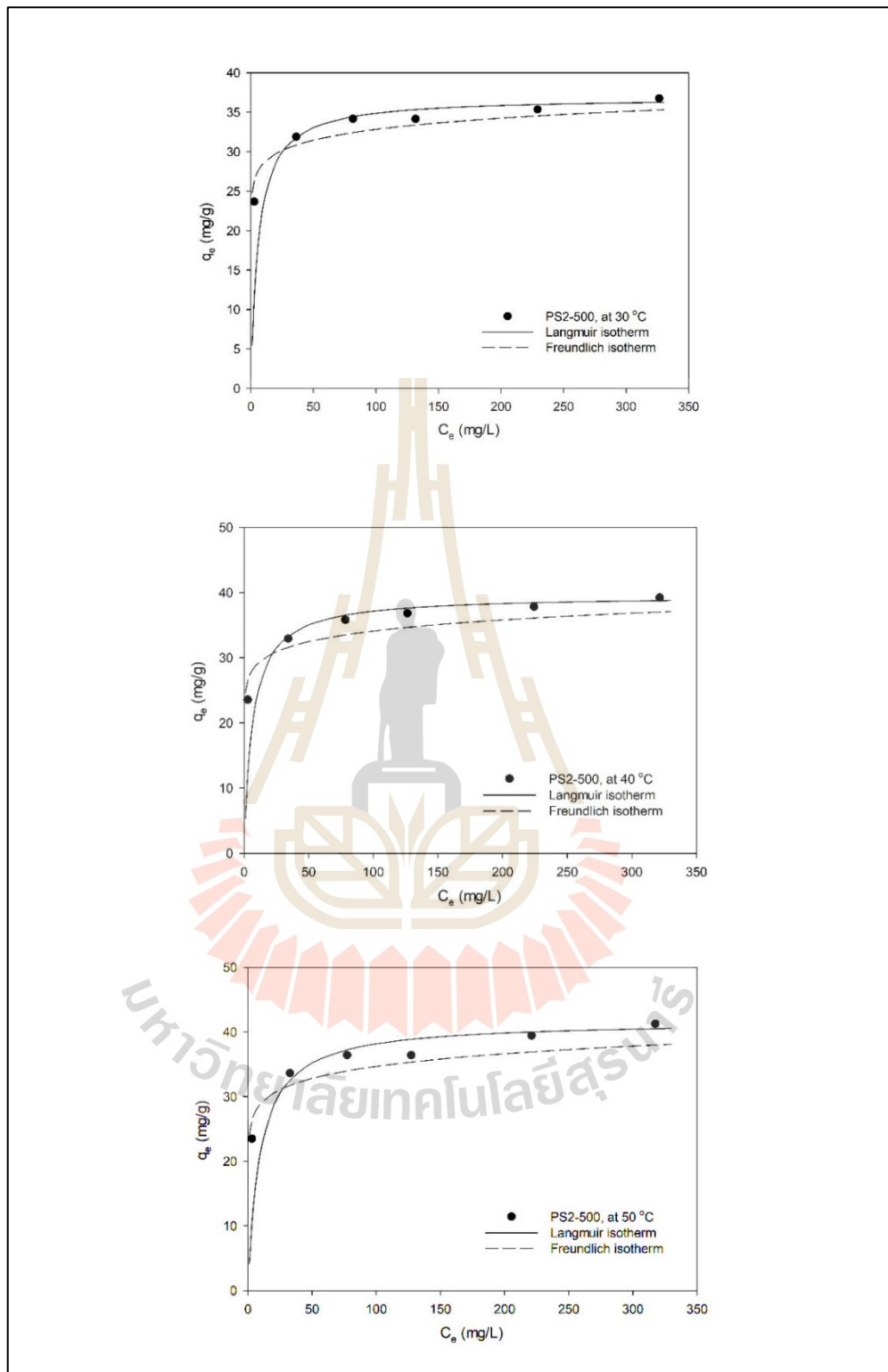


Figure 4.5 (b) Adsorption Isotherm of MB on PS2-500 with different temperature

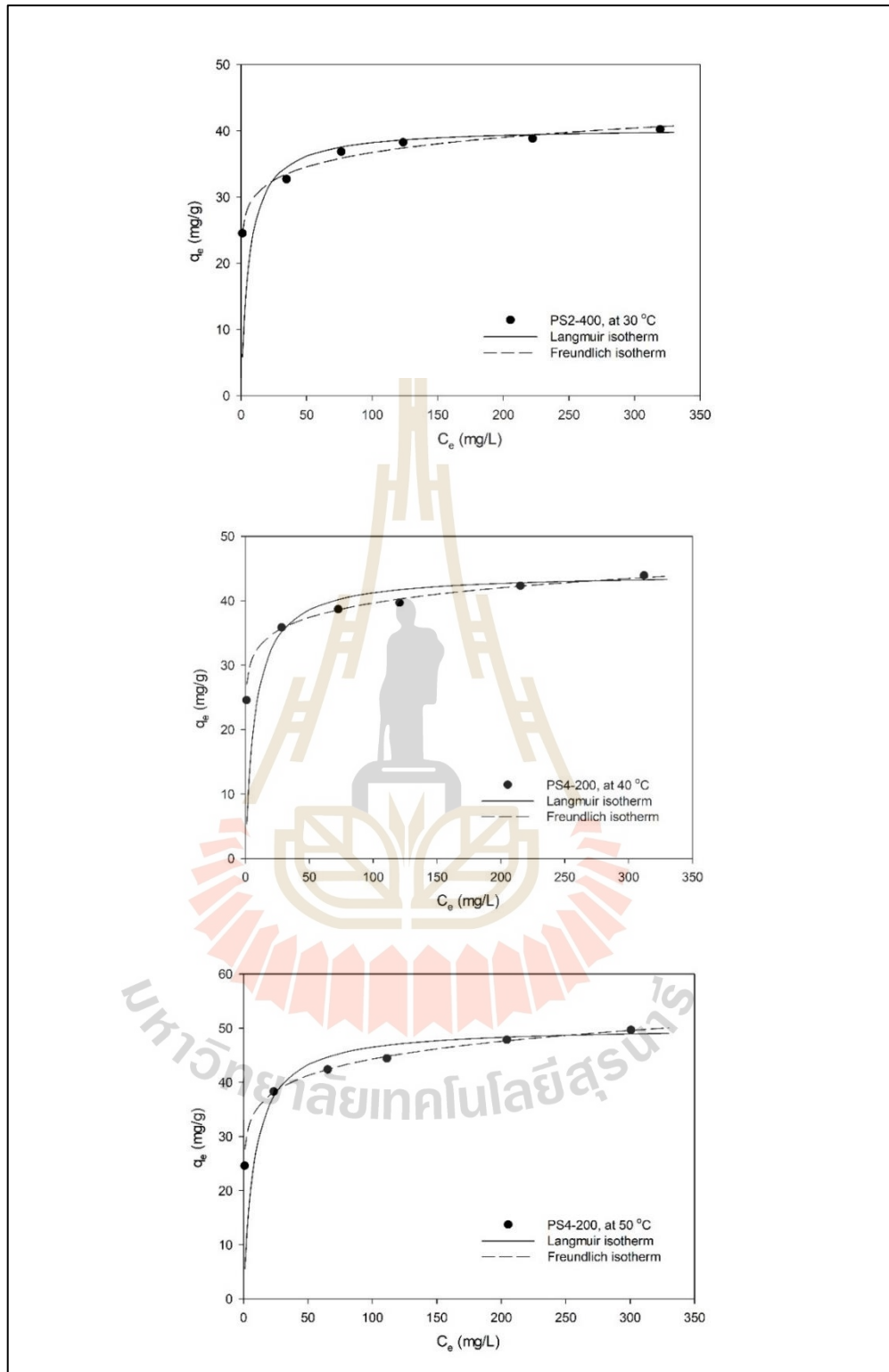


Figure 4.5 (c) Adsorption Isotherm of MB on PS4-200 with different temperature

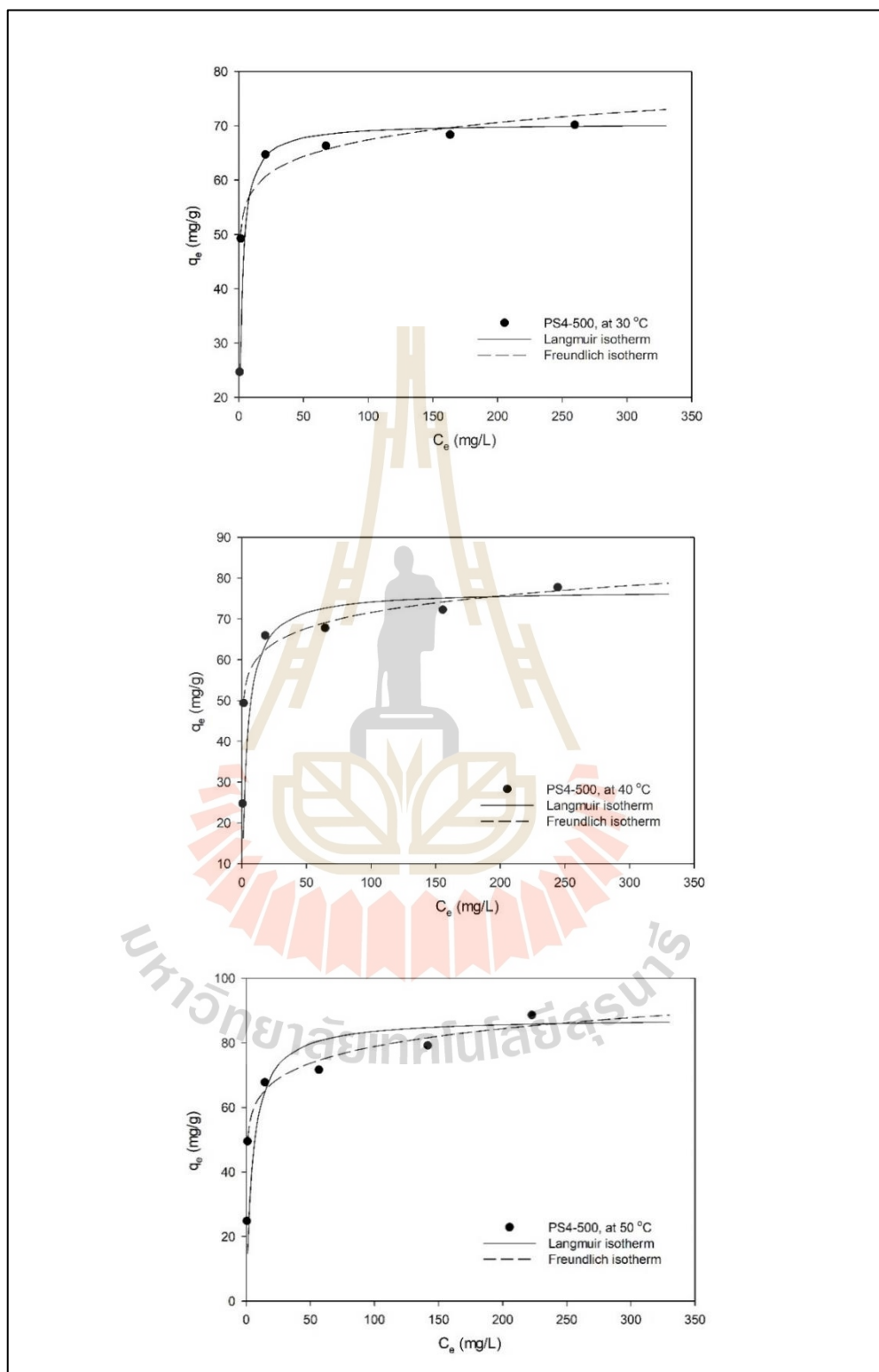


Figure 4.5 (d) Adsorption Isotherm of MB on PS4-500 with different temperature

4.5 Conclusions

The porous silica was used for the removal of methylene blue from aqueous solution employing batch adsorption experiments. The optimum amount of porous silica PS4-200 and PS2-200 are 0.3 g and 0.4 g, respectively for the initial MB concentration of 200 mg/L. The adsorption efficiency of methylene blue increased with the increase of adsorption temperature but decreased with the increase the initial concentration of methylene blue. The equilibrium data for MB adsorption by porous silica can be best described the Langmuir isotherm, with the maximum adsorption capacity of methylene blue onto porous silica (PS4-500) being 87.72 g/g at 50 °C. The methylene blue adsorption kinetic data were well fitted with the pseudo second-order model.

4.6 References

- A.A. Inyinbor, F.A. Adekola and G.A. Olatunji (2016). Kinetics, isotherms and thermodynamic modeling of liquid phase adsorption of Rhodamine B dye onto *Raphia hookerie* fruit epicarp. **Water Resources and Industry**. Vol. 15:14-27.
- A.A. Nuhu, I.C.P. Omali and O.C. Clifford (2018). Adsorption efficiency and equilibrium study of *Melaleuca leucadendron* Husk in the removal of Cu²⁺ and Cd²⁺ ions from aqueous solution. **American Journal of Engineering Research**. Vol. 7(1): 253-268.
- Abdel Ghafar H.H., Ali G.A.M., Fouad O.A. and Makhoulf S.A., (2013). Enhancement of adsorption efficiency of methylene blue on Co₃O₄/SiO₂

- nanocomposite. **Desalination and Water Treatment**. Vol. 53(11): 2980-2989.
- ALzaydien A.S., (2009). Adsorption of methylene blue from aqueous solution onto a low-cost natural Jordanian Tripoli. **American Journal of Applied Sciences**. Vol. 6(6): 1047-1058.
- Atyaf Khalid Hameed, Nugroho Dewayanto, Du Dongyum, Mohd Ridzuan Nordin and Mohd Hasbi Ab. Rahim, (2016). Kinetic and thermodynamics of Methylene Blue adsorption onto Zero Valent Iron supported on mesoporous silica. **Bulletin of Chemical Reaction Engineering & Catalysis**. Vol. 11(2): 250-261.
- Auta, M. and Hameed, B.H., (2014). Chitosan–clay composite as highly effective and low-cost adsorbent for batch and fixed-bed adsorption of methylene blue. **Chemical Engineering Journal**, 237: 352-361
- Ernest J. Henley, J.D. Seader, D. Keith Roper, (2006). Separation process principles. **John Wiley & Sons, Inc.**
- Ho, Y.S. and McKay, G., (1998). Kinetic models for the sorption of dye from aqueous solution by wood. **Process Safety and Environmental Protection**, 76 (2): 183-191.
- Lagergren S. (1898). About the theory of so-called adsorption of soluble substance. **Sven. Vetenskapsakad. Handlingar**, 24: 1-39.
- Malamis, S. and Katsou, E., (2013). A review on zinc and nickel adsorption on natural and modified zeolite, bentonite and vermiculite: Examination of process parameters, kinetics and isotherms. **Journal of Hazardous Materials**. Vol. 252–253: 428-461.

- Pang, S.C., Masjuki, H.H., Kalam, M.A. and Hazrat, M.A., (2013). Liquid absorption and solid adsorption system for household, industrial and automobile applications: A review. **Renewable and Sustainable Energy Reviews**. Vol. 28:836-847.
- Peruchi L.M., Fostier A.H. Rath S., (2014). Sorption of norfloxacin in soils: Analytical kinetics and Freundlich isotherms. **Chemosphere**. Vol. 119C, 310-317.
- Runping Han, Yu Wang, Xin Zhao, Yuanfeng Wang, Fuling Xie, Junmei Cheng and Mingsheng Tang (2009). Adsorption of methylene blue by phoenix tree leaf powder in a fixed-bed column: experiments and prediction of breakthrough curves. **Desalination**. Vol. 245: 284-297.
- Shilpi Agarwal, Inderjeet Tyagi, Vinod Kumar Gupta, Nahid Ghasemi, Mahdi Shahivand and Maryam Ghasemi (2016). Kinetics, equilibrium studies and thermodynamic of methylene blue adsorption on Ephedra strobilacea saw dust and modified using phosphoric acid zinc chloride. **Journal of Molecular Liquids**. Vol. 218: 208-218.
- Weber Walter J. and Morris J. Carrell (1963). Kinetics of adsorption on carbon from solution. **Journal of the Sanitary Engineering Division**. Vol. 89(2), 31-60.
- Yakout, S.M. and Elsherif, E. (2010). Batch Kinetics, Isotherm and Thermodynamic Studies of Adsorption of Strontium from Aqueous Solutions onto Low Cost Rice-Straw Based Carbons. **Carbon-Science and Technology**. Vol. 3, 144-153.

CHAPTER V

SIMULATION OF GAS ADSORPTION ON POROUS SILICA

5.1 Abstract

GCMC simulation was used to study the equilibrium adsorption of N_2 , CO_2 and CH_4 in porous silica. The CO_2 is modelled as a 3-center-Lennard-Jones (LJ) molecule. N_2 is modelled as linear molecule. The CH_4 is modelled as a spherical Lennard-Jones particle. The simulated adsorption isotherms of gas adsorption were used to explore and understand the adsorption behavior of gases in porous silica that may be applied to the environmental applications. The silica surfaces could contain either hydroxyl (OH) groups or defects to examine the effect of surface heterogeneity on the behavior of pure carbon dioxide (CO_2), nitrogen (N_2), and methane (CH_4) adsorption. The simulation results were compared with experimental data of CO_2 and N_2 adsorption in porous silica to arrive at the pore size distribution of the adsorbent.

5.2 Introduction

Due to the global warming crisis, the control of greenhouse gases, which consist predominantly of carbon dioxide, has received increasing attention from scientists and engineers (Lopes et al., 2009; Feng et al., 2020 and Kemper, 2015). Gas cleaning technologies have been developed to control the amount of carbon dioxide emitted to the atmosphere from the combustion of fossil fuels. In addition to mitigating CO₂ emissions from power plants burning fossil fuels, carbon dioxide removal is also an important separation process for the purification of natural gas, biogas, and landfill gas. Adsorption has become one of the attractive separation methods for CO₂ capture, due mainly to its low operating costs and low energy consumption compared with other current separation technologies such as amine absorption and membrane separation (Khandaker et al., 2020; Leung et al., 2014 and Chiang, Y.C. and Juang, R.S, 2017). Since adsorption is extensively applied to many industries for the purification and separation of gas and liquid mixtures, the development of new advanced adsorbents for the adsorption process has therefore been the focal point of many researchers. However, the porous properties of the new adsorbents should be assessed and they can be determined by characterizing the adsorbents with various kinds of adsorptive gases. Among the possible methods developed for gas cleaning, adsorption by using porous silica glass has become a promising choice because porous silica glass possesses several advantageous characteristics, such as an ability to withstand high temperatures and chemical attacks, having relatively high impact strength, showing narrow pore size distribution, easy shaping, and capability of surface grafting with various types of functional groups for specific applications (Yazawa, 1995 and Nimjaroen et al., 2009). The

investigation of CO₂ adsorption on different surface structures of porous silica glass will assist researchers to tailor a potential porous solid absorbent for CO₂ capture and obtain useful information on the adsorption equilibrium for the design of adsorption processes (Feng et al., 2020).

Methane is implicated as one of greenhouse gases that can cause global warming due to greenhouse effects, therefore the utilization and reduction of greenhouse gases are becoming more important. Adsorption technique, such as membrane technology and pressure swing adsorption together with porous adsorbents, is one of promising candidates for these separations (Policicchio et al., 2013). Therefore, study of methane adsorption helps to tailor porous solid absorbent for energy storage application, and this issue becomes an attractive area for researchers in the field of fuel cell technology (R. T. Yang, 2003). It is found in the literature that metal catalyst can enhance the adsorption of methane and this will lead to the development of methane fuel cell (R. T. Yang, 2003; Policicchio et al., 2013). In this study, porous silica glass is used as the adsorbent for investigation the adsorption behavior of methane to see whether the functional group can enhance the adsorption capacity

Monte Carlo (MC) simulation and Molecular Dynamics (MD) are the two molecular simulation tools that have been used to explore the microscopic properties of confined fluids in nanopores of different geometries (Frenkel, 2002; Allen and Tildesley, 1987). To model the structure of porous silica, a pore was assumed to be a cylinder or a slit shape pore whose walls can be structureless (amorphous) or in the form of a perfect crystal structure (Ketprasoet et al., 2015). However, in reality, porous silica glass contains functional groups, namely silanol groups (silicon atoms

attaching to OH groups), as well as defects on its surfaces. It has been reported that the adsorption behavior of fluid on porous glass can be predicted reasonably well by using a simple pore model (Xiaoning and Xiaopeng, 2007). A set of adsorption isotherms obtained by using a Monte Carlo ensemble have been compared with the adsorption isotherms derived from the experiment to evaluate the porous properties of solids. The adsorption information generated from a solid adsorbent can then be used to describe the adsorption mechanism between the adsorbent and the adsorbate molecules.

In this study, a simple model of porous silica glass was proposed as a finite-length slit pore with two parallel walls. Each wall was arranged as an assemblage of connecting SiO_4 units. The silica surfaces could contain either hydroxyl (OH) groups or defects to examine the effect of surface heterogeneity on the behavior of carbon dioxide (CO_2) capture, nitrogen (N_2), and methane (CH_4) adsorption. A highly mimetic model of porous silica was constructed to generate CO_2 adsorption isotherms for slit-shaped pores of various pore widths. In addition, the measurement of adsorption isotherms of pure CO_2 at different temperatures and that of nitrogen (N_2) isotherms at 77 K for the prepared porous silica glass were also conducted and used to determine the pore size distribution (PSD) of the porous silica. The effects of concentration and position configuration of the functional groups on the adsorption behavior of CO_2 were also investigated.

5.3 Theory and general background

In this part, the Grand Canonical Monte Carlo (GCMC) simulation method is used to investigate the adsorption behavior of single component of carbon dioxide (CO_2), nitrogen (N_2) and methane (CH_4) on porous silica model.

5.3.1 Fluid model

5.3.1.1 Carbon dioxide model

The carbon dioxide is modeled as a 3-center-Lennard-Jones (LJ) interaction site on the atom and point charge to account for quadrupole moment (Harris J. G. and Yung K. H., 1995). The carbon atom forms two double bonds. Each double bond is a group, so there are two electron groups around the central atom. The CO_2 molecule has a C=O bond length of 1.16 Å, with an O=C=O bond angle of 180.0 degrees. The potential parameters for the CO_2 force field are listed in **Table 5.1**.

5.3.1.2 Methane model and Nitrogen model

The molecular model of methane is assumed to be a spherical model of one single Lennard-Jones (LJ) fluid, N_2 is modelled as linear molecule, the assumption that methane is a non-polar molecule. The potential parameters for the CH_4 and N_2 force field are listed in **Table 5.1**.

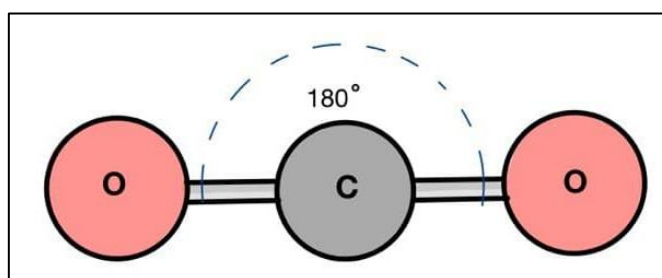


Figure 5.1 Schematic of the CO_2 molecule.

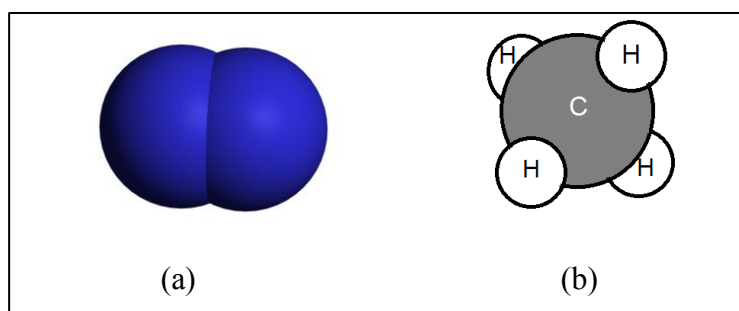


Figure 5.2 (a) schematic of the N₂ molecule and (b) schematic of the CH₄ molecule.

Table 5.1 Lennard-Jones parameters and partial charge

Site	$\frac{\epsilon_{ff}}{k_b}, [K]$	$\sigma_{ff} [\text{Å}]$	$q [e]$	Angle (degree)
C (CO ₂)	28.129	2.757	+0.6512	180
O (CO ₂)	80.507	3.033	-0.3256	
H (H ₂ O)	0.0	0.0	+0.4238	109.45
O (H ₂ O)	78.23	3.166	-0.8476	
CH ₄	148	3.73	-	
N (in N ₂)	36.0	3.310	-0.482	
COM* (in N ₂)	0.0	0.0	+0.946	
Si (silica)	0.0	0.0	+0.18	147
O (silica)	2.708	185	-0.36	
O (in OH)	78.23	3.07	-0.64	109.45
H (in OH)	0.0	0.0	+0.44	

where ε and σ are the energy well depth and the collision diameter, respectively, k_b is the Boltzman's constant and q is the point charge on each site. In this study, a cut-off radius in the calculation of interaction energy is five times the collision diameter of fluid is used. The interaction between fluids is calculated using the Lennard-Jones 12-6 equation (Do et al., 2003) following **Equation 5.1**

$$U_{ij}(r) = 4\varepsilon_{ij} \left[\left(\frac{\sigma_{ij}}{r_i - r_j} \right)^{12} - \left(\frac{\sigma_{ij}}{r_i - r_j} \right)^6 \right] \quad (5.1)$$

where r is the separation distance, ε_{ij} is the well depth of the interaction potential and σ_{ij} is the collision diameter of sites. Beside the interaction between two LJ sites, the interaction between two charges should be taken into account for polar molecules of fluid and fluid. The interaction between two charges, each of which is on different molecule, takes the form of a Coulomb law of electrostatic interaction according to **Equation 5.2**.

$$U_{ij}(r) = \frac{1}{4\pi\varepsilon_0} \cdot \frac{q_i q_j}{r^{ij}} \quad (5.2)$$

where ε_0 is the permittivity of free space, r^{ij} is the distance between two charges i and j .

5.3.2 Solid model and functional group model

The solid model used in this study is the SiO₄ crystals which formed the tetrahedral structure show in **Figure 5.3**. A silicon atom is at the center of tetrahedral and oxygen atoms are positioned at the vertices of the tetrahedron. These oxygen atoms represent the dispersive site and have negative charge -0.36e and silicon atom is the positive charge +0.18e (Burchart et al., 1992) and the angle of O-Si-O about 147.0 degrees (Calero et al., 2004). The Lennard-Jones (LJ) parameters of SiO₄ are σ_{SS} and ϵ_{SS}/k , 2.708 Å and 185.0 K, respectively. The LJ interaction energy between a fluid molecule and solid model is calculate with Lennard-Jones 12-6 equation and the cross molecular parameters are calculated from the Lorentz-Berthelot rule.

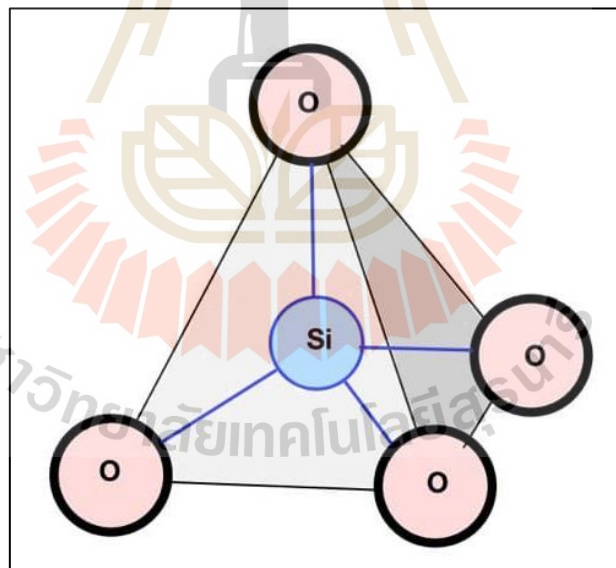


Figure 5.3 Schematic of the SiO₄ molecule.

A hydroxyl group is used to represent the functional group in the form Si-OH on the silica surface. It is modeled as a LJ dispersive site at the center of oxygen atom and single square well (SW) site at the hydrogen atom, and their molecular parameters are the same as those of the water potential model except the hydrogen bond strength. The distance of the LJ site of the OH group from the pore wall is 1.364 Å and the SW site is placed at 1.2852 Å from the LJ center with an angle of 109.0 degrees (Muller E. A. et al., 2000). The interaction energy between a fluid molecule and functional group was calculated from the Lennard-Jones 12-6 potential and electrostatic Coulomb equation.

The volume of the simulation box i.e. pore volume, the chemical potential and the temperature of the system are specified to obtain the adsorption equilibrium. One GCMC cycle consists of one thousand displacements move and attempts of either insertion or deletion with equal probability.

For an adsorption branch of the system to reach equilibrium and additional 30000 cycles are used to obtain ensemble average. The empty box as the initial configuration and the simulation box does not change. The pressure of bulk gas corresponding to a given chemical potential are calculated from the equation of state proposed by Johnson et al. (1993). Isothermic heat of adsorption and adsorption capacity were evaluated by **Equation 5.3** and **Equation 5.4**, respectively.

$$q_{st} = \frac{\langle U \rangle \cdot \langle N \rangle - \langle U \cdot N \rangle}{\langle N^2 \rangle - \langle N \rangle \cdot \langle N \rangle} + k_b \cdot T \quad (5.3)$$

$$\rho = \frac{N_{inside}}{V_{pore}} \quad (5.4)$$

where U is energy of configuration, N is number of particle and $\langle \rangle$ is defined as an average. The combinations of ε_{ij} and σ_{ij} parameters give the same pore volume. In order to resolve the pore volume while obtaining used Lorentz-Berthelot mixing rules following **Equation 5.5** and **Equation 5.6**

$$\varepsilon_{ij} = \sqrt{\varepsilon_{ii}\varepsilon_{jj}} \quad (5.5)$$

$$\sigma_{ij} = \frac{\sigma_{ii} + \sigma_{jj}}{2} \quad (5.6)$$

The fluid-fluid interaction and the functional on silica surface atoms were modeled as a combination of Lennard-Jones (LJ) and Columbic potential, where the van der Waals interactions between two Lennard-Jones (LJ) sites were calculated using the LJ 12-6 potential, with the electrostatic interactions calculated based on the Columbic potential.

5.4 Methodology and experimental

5.4.1 Experimental Isotherms for N₂ and CO₂ Adsorption

The isotherms of N₂ and CO₂ adsorption on the prepared porous silica were measured using a surface area and porosity analyzer (model ASAP 2020, Micromeritics). The measurement was performed by using about 0.2 grams of porous silica sample, which were outgassed at 150 °C for 12 h prior to the measurement. The numbers of pressure points for isotherm measurement at a given temperature were specified, and the amounts adsorbed at the equilibrium condition for each increasing pressure were recorded. The adsorption steps were performed until the maximum

pressure of one bar was reached and then the desorption steps (decreasing pressures) were carried out. The porous properties of porous silica were derived from the measured adsorption isotherms of N₂ at 77 K. The BET surface area of the porous silica was computed using the BET equation (Do, 1998). The mesopore volume and mesopore surface area were estimated by the BJH theory (Do, 1998). The total pore volume was calculated from the amount of N₂ adsorbed at the relative pressure (p/p^0) of 0.98, and this value was converted to the volume of N₂ in liquid state. The micropore volume was determined by subtracting the total pore volume from the mesopore volume. The average pore size was calculated from $4V/A$, where V and A are the total pore volume, and the BET surface area, respectively. The adsorption behavior of CO₂ by porous silica was evaluated from the measured isotherms of CO₂ at 273, 283, and 293 K.

5.4.2 Computational methodology

5.4.2.1 Fluid model of CO₂

The fluid model of CO₂ used for the GCMC simulation is the 3-Center-Lennard-Jones (LJ) molecule proposed by Harris and Yung (Harris and Yung, 1995). The model consists of interaction sites situated at the center of mass containing three-point charges, that is, one positive charge for the carbon atom and two negative charges for the oxygen atoms. The distance between the C-O bond of the CO₂ molecule is 1.16 Å, while the bond angle of O-C-O is fixed at 180°. **Table 5.1** shows the molecular parameters and partial point charges of CO₂ and SiO₄ used for the simulation, where ϵ is the energy well depth of the atoms., k_b is the Boltzman's constant, and the point charge on each site is designated as q .

5.4.2.2 Fluid model of N₂ and CH₄

The N₂ force field consists of three sites. Each nitrogen atom is modeled as Lennard-Jones site separated by the bond length of 1.10 Å. The gas-phase quadrupole moment of N₂ (Jeffrey and Siepmann, 2001) was produced by point charges of -0.482 e on each Lennard-Jones site. To maintain charge neutrality, a point charge of +0.946 e was placed at the center of mass (COM) of N₂ molecule. And the fluid model of CH₄ is a spherical Lennard-Jones particle and a non-polar molecule. The Lennard-Jones parameters of N₂ and CH₄ are listed in **Table 5.1**.

5.4.2.3 Porous silica model

The porous silica model used in this study is taken as a slit-shape pore whose length is finite with equal dimensions in the X and Y axes of 60 Å. The slit pore consists of two opposite walls in parallel and the separating distance between the two walls is represented as the pore width (H), as shown in **Figure 5.4**. Each wall is composed of SiO₄ unit linkage, which forms a tetrahedral configuration. The center of each unit is a silicon atom and the four tetrahedron vertices are the position of the oxygen atoms. The dispersive sites having a negative charge of $-0.36e$ are located at the oxygen atoms, while the silicon atom has a positive charge of $+0.18e$ (Burchart et al., 1992). The molecular parameters of SiO₄ used in this study are shown in **Table 5.1** with ϵ_{ss}/k_b of 185.0 K, σ_{ss} of 2.708 Å (He and Seaton, 2003), and the angle of O-Si-O is about 147° (Calero, 2004). The solid configuration model is depicted in **Figure 5.4**, each wall consists of an assemblage of SiO₄ crystals. In the figure, yellow spheres and grey spheres represent silicon and oxygen atoms, respectively.

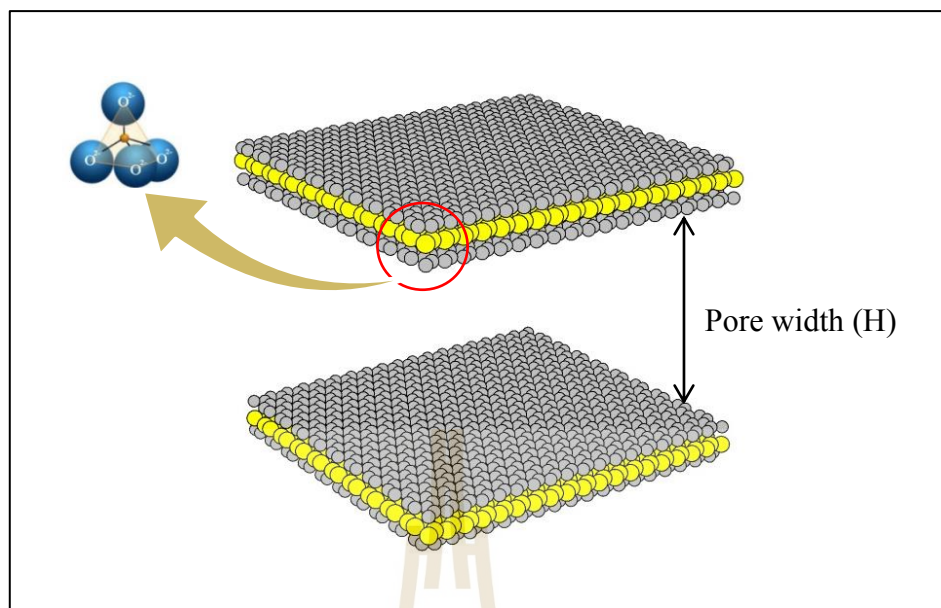


Figure 5.4 The solid model of porous silica used in this study

5.4.2.4 Model of surface functional groups

The model for a silanol functional group (Si-OH) existing on the silica surface is essentially represented by the presence of hydroxyl (OH) group. The dispersive sites of the OH group are located at the oxygen atom having a charge of $-0.64e$ and at the hydrogen atom having a positive charge of $+0.45e$. The molecular parameters of OH are also presented in **Table 5.1** with ϵ_{ss}/k_b of 78.23 K, and σ_{ss} of 3.07 Å (Jorge, 2002). The center of the oxygen atoms of the OH group is 1.364 Å from the pore wall and perpendicular to the wall. The separating distance between the hydrogen and oxygen atom is 0.96 Å, and the angle between the oxygen and hydrogen atom of the O-H group is about 109° (Burchart et al., 1992).

In this work, two models for the functional group allocation or the placement configuration of the functional group were investigated to examine how the functional group positions could affect the CO₂ capture in porous silica. For

the first model, OH groups are randomly placed on the inner surface of each wall, as delineated in **Figure 5.5 (a)**. As to the second model, OH groups are fixed and located along the pore edges, as shown in **Figure 5.5 (b)**. The reason for choosing this type of functional group model is because there is a possibility that the surface functional groups could situate around the edges of the adsorbent sheet, as reported, for example, for the case of activated carbon, which contains various types of surface functionalities at the edge sites of the graphene planes (Bansal and Goyal, 2005). From here on, the first model and the second model are referred to as the *random* topology model and the *fixed* topology model, respectively. In the **Figures 5.5**, the yellow spheres represent the silicon atoms and the grey spheres represent the oxygen atoms of SiO_4 . The red spheres and small white spheres represent the oxygen and hydrogen atoms of the OH functional group.

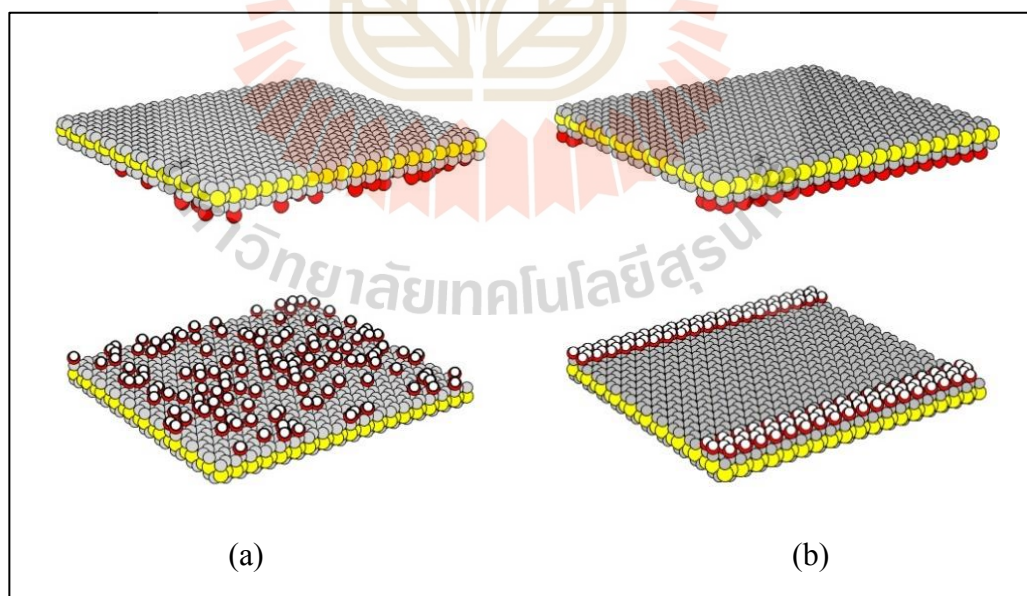


Figure 5.5 Two proposed models for OH groups presenting on the inner walls of porous silica surfaces (a) the random and (b) the fixed topologies.

5.4.2.5 Defective surfaces

In reality, the surface of porous silica is not homogeneous, and its surface structure is not perfect crystals. To account for this surface heterogeneity, the solid model whose surfaces contain some forms of defects is introduced to explore whether the defects can affect the adsorption behaviour of CO₂ in porous silica. The defects are firstly created by randomly removing some silicon atoms from the inner wall of SiO₄ structure, thus forming initially a small hole on the solid surface. Next, either silicon or oxygen atoms, located at the boundary of a hypothetical sphere forming the initial hole having an effective radius R_c , are then randomly removed as shown in **Figure 5.6**. The different pit sizes of the surface defects are noticeable because of the possible overlapping of the adjacent pits upon increasing the numbers of atom removal. Both the magnitude of the effective radius and the percentage area of defects are specified for modeling the effect of a defective surface on CO₂ adsorption, as described in the literature (Do D.D. and Do H.D, 2006).

5.4.2.6 Grand Canonical Monte Carlo ensemble

The Grand Canonical Monte Carlo (GCMC) simulation was chosen to investigate the adsorption mechanism of carbon dioxide in porous silica. The simulation box volume (V_{pore}) is determined from the pore length in X and Y axes denoted as LX and LY, respectively, and pore width (H) to give $V_{\text{pore}} = LX \times LY \times H$. In this ensemble, the chemical potential, the simulation box volume, and the system temperature are specified to establish the equilibrium state. A total of 1000 transposition moves, insertions, and deletions with equal probability are specified in one cycle of GCMC calculation was showed in **Figure 5.7**. In this study, 20,000 GCMC cycles are used for the equilibrium state evaluation, and a further 20,000

cycles are applied in the sampling step to evaluate the average properties. The initial configuration of an empty box is used to carry out a simulation until it reaches an equilibrium at which the number of particles in the statistical sense does not change, and then the number of particles is averaged (N_{inside}). The correlation between bulk pressure and chemical potential is evaluated by using the equation of state proposed by Johnson et al. (Johnson et al., 1993). The adsorption capacity or pore density is then evaluated according to **Equation 5.4**.

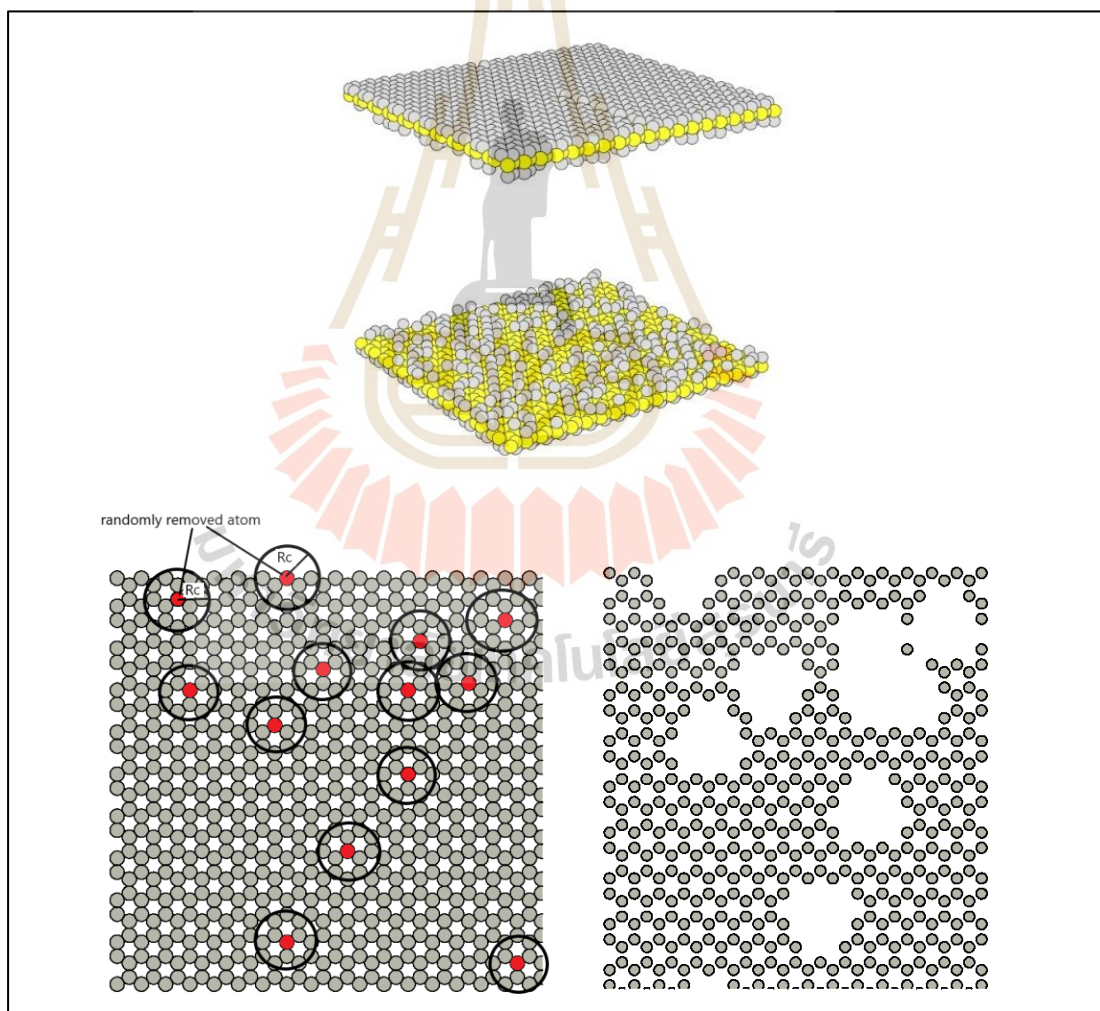


Figure 5.6 A characteristic of defective surfaces of the porous silica model.

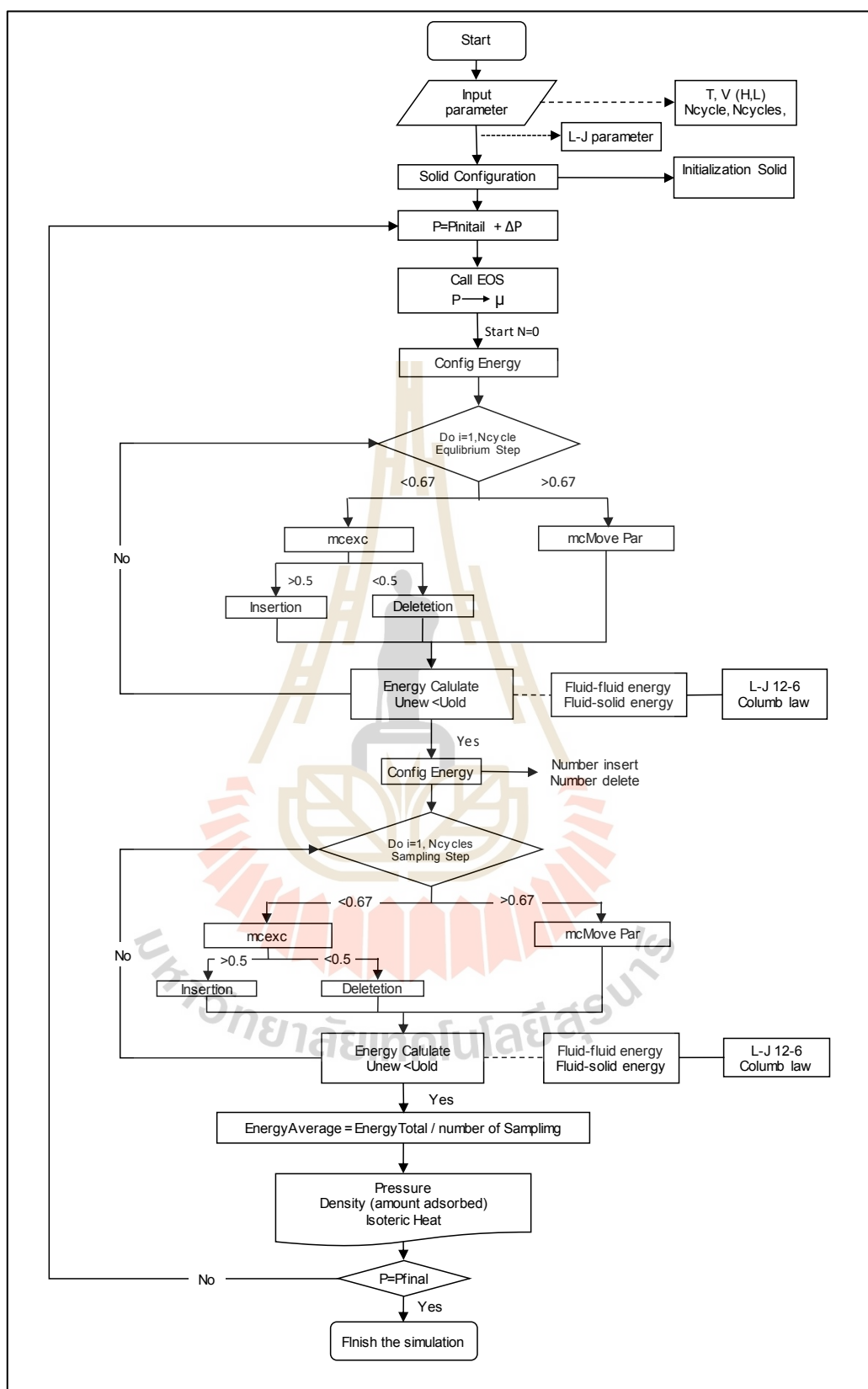


Figure 5.7 Flow chart of computer simulation

5.5 Results and discussion

Firstly, the experimental data of nitrogen adsorption at 77 K and the porous properties of porous silica glass obtained from nitrogen adsorption isotherms will be discussed. Secondly, the adsorption isotherms for carbon dioxide at various temperatures obtained from the ASAP2020 will be presented. Then, the adsorption isotherms of CO₂ at 283 K in finite-length pore model of silica glass with different pore widths will be given to illustrate the different adsorption behavior of CO₂ inside the pores. Later, the effects of the functional group and its concentration on carbon dioxide adsorption will be revealed, as well as the effect of the functional group allocation. Gas adsorption behavior on the defective surface will be compared with that of the perfect surface. Finally, the simulation results and the experimental adsorption data of CO₂ on porous silica glass will be compared to see which types of porous silica glass are most favorable for the effective capture of CO₂.

5.5.1 Experimental results

5.5.1.1 Porous properties and silanol group contents of porous silica

Figure 5.8 shows isotherms of N₂ adsorption at 77 K by the tested porous silica. The adsorption isotherms for PS2-200 and PS2-500, having small pore sizes, showed a continuous increase in the amount of N₂ adsorbed with an increase of relative pressure up to the value of 0.17, before it approached a constant value at higher relative pressures. These isotherms did not show hysteresis loops and their shapes resembled the initial part of the Type II isotherm, according to the IUPAC classification (Sing et al., 1985). The porous silica synthesized at pH 3 (PS3-200), having an intermediate pore size, showed an adsorption isotherm with a hysteresis loop. According to the IUPAC classification of isotherms with hysteresis

loops (Sing et al., 1985), this porous silica exhibited Type H2 isotherm. It showed a broad, almost flat plateau, and the steep characteristic of a desorption branch. This type of isotherm indicates that the pore structure of an adsorbent consists of interconnected networks of pores having different shapes and sizes (Rouquerol et al., 1999). The isotherms of porous silica having large pore sizes (PS4-200 and PS4-500) also showed isotherms with hysteresis loops, which can be classified as Type H1 isotherm (Sing et al., 1985). The isotherms showed a relatively narrow loop, with very steep and almost parallel adsorption and desorption branches, indicating that the adsorbent has a narrow distribution of uniform pores (Rouquerol et al., 1999).

The derived N₂ adsorption isotherms of the prepared porous glass were used to determine the porous properties of the adsorbents and the results are presented in **Table 5.2**. Based on the percentage of mesopore volume, it can be seen that all the porous glass samples exhibited mesoporous types of adsorbent materials, with the mesopore volume varying from 62.4% to 98.5%. The average pore size increased from the value of 2.4 to 10.3 nm as the pH changed from the value of 2 to 4 (compare samples PS2-200, PS3-200, and PS4-200). The increase in pore size of the porous glass with increased pH was also observed in the previous studies (Witton and Chareonpanich, 2012; Muñoz-Aguado and Gregorkiewitz, 1996). This was hypothesized to result from the increasing formation of highly branched silica oligomers due to the increased condensation rate of silanol species that can prevent gel shrinkage as the pH of solution was increased. Increasing the pH also enhanced the development of mesopores of the prepared porous silica. The mesopore volume and the total pore volume increased almost threefold as the pH increased from the value of 2 to 4. On the other hand, the total BET surface area was found to decrease

with the increase of pH, with the value decreasing almost twofold from 798 to 413 m^2/g . The porous properties of the porous silica were also affected to a certain extent by the change in the calcination temperature. However, the average pore size remained almost unchanged by the increase in the calcination temperature from 200 to 500 $^{\circ}\text{C}$. However, an increase in the calcination temperature from 200 to 500 $^{\circ}\text{C}$ decreased the BET surface area by 21% and 2.2% for the PS2 and PS4 samples, respectively.

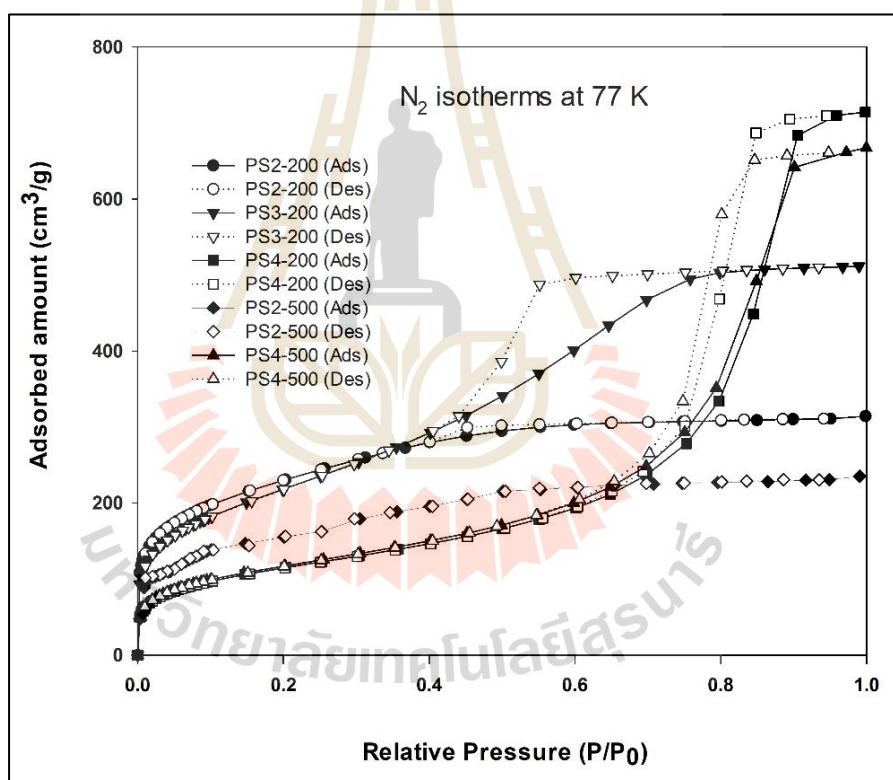


Figure 5.8 Isotherms of N₂ adsorption at 77 K on the prepared porous silica samples

Table 5.2 Porous properties of porous silica synthesized in this study.

Samples *	Average Pore Size (nm)	BET Surface Area (m ² /g)	Micropore Volume (cm ³ /g)	Mesopore Surface Area (m ² /g)	Total Pore Volume (cm ³ /g)	Mesopore Volume (cm ³ /g)
PS2-200	2.4	798	0.183 (37.6%)	719	0.487	0.304 (62.4%)
PS2-500	2.2	630	0.062 (15.9%)	596	0.391	0.329 (84.1%)
PS3-200	5.0	778	0.062 (7.8%)	739	0.791	0.729 (92.2%)
PS4-200	10.3	413	0.017 (1.5%)	399	1.105	1.088 (98.5%)
PS4-500	10.9	404	0.016 (1.6%)	390	1.032	1.016 (98.4%)

5.5.1.2 GCMC Simulation Results for Nitrogen adsorption

The simulation isotherm versus pressure for N₂ at 77K in porous silica of various pore width from 7-15 Å, and pore width from 20-40 Å up to saturation pressure obtained by GCMC method, are shown in **Figures 5.9** and **Figures 5.10**, respectively. The simulation isotherms of N₂ in the porous silica model show the single layer of particles in the pore width less than 20Å was showed in Figure 5.8. The isotherm drops with increasing of pore widths. For pore large than 20Å, N₂ molecules can form a monolayer along the pore wall and then the additional layers next to the monolayer. It is noted that the behavior of N₂ adsorption isotherms obtained using the GCMC is quite similar to that obtained by the experiment as one can see in **Figure 5.8**, that is, the adsorption capacity decreases with an increase in the pore width. The N₂ adsorption isotherms of porous silica simulation in the pore width less than 20Å and larger than 20 Å same as the N₂ adsorption isotherms of porous silica (PS2 series) and (PS4 series), respectively.

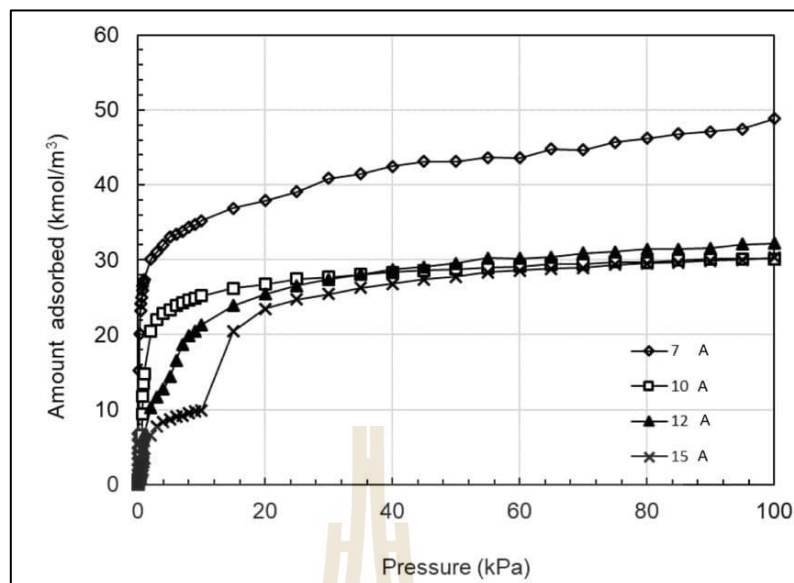


Figure 5.9 Simulation results of N_2 in porous silica at 77 K for various pore width from 7-15 Å

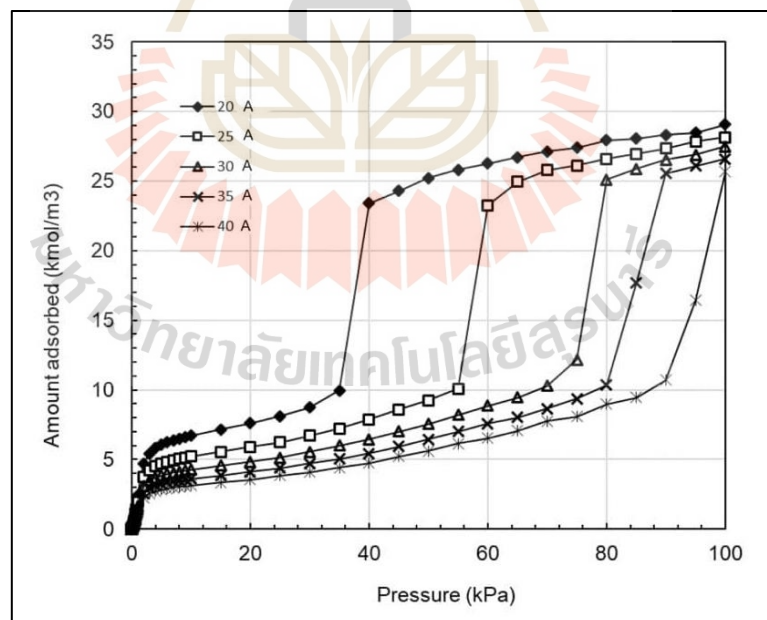


Figure 5.10 Simulation results of N_2 in porous silica at 77 K for various pore width from 20-40 Å

5.5.1.3 Experimental isotherms for CO₂ adsorption

The adsorption isotherms of CO₂ at 283 K obtained for porous silica glasses, PS2-200, PS3-200, and PS4-200, having average pore widths of 2.4, 5.0, and 10.3 nm, respectively, are shown in **Figure 5.11 (a)** and **(b)**. In **Figure 5.10 (a)**, the adsorbed amount of CO₂ in mmol/g of adsorbent is plotted against the pressure in kPa. For comparison with the simulation result, the adsorbed amount of CO₂ is converted from mmol/g to kmol/m³ by dividing the number of mmol/g with the total pore volume (cm³/g) shown in **Table 5.2** and plotted against pressure as shown in **Figure 5.11 (b)**. The amounts of CO₂ adsorbed increased with an increase in pressure and adsorption in smaller pores (2.4 and 5.0 nm for PS2-200 and PS3-200, respectively) were greater than that in the larger pores of 10.3 nm (PS4-200), due largely to the stronger interaction between carbon dioxide and silica glass surfaces in the smaller pores. It is interesting to observe from **Figure 5.11 (a)** that for pressures less than, say, about 24 kPa, the amount of CO₂ adsorbed by PS3-200 having a pore width of 5.0 nm and the silanol content of 6.05 mmol/g was slightly greater than that by PS2-200 with 2.4 nm pore width and 7.94 mmol/g of the silanol content. However, at higher pressures, the adsorption capacity for the pore width of 5.0 nm was significantly greater than that for the pore width of 2.4 nm, with the discrepancy becoming larger as the pressure was progressively increased. It could be possible that the porous silica with larger pore size (PS3-200) could allow the diffusion of CO₂ molecules into the pores at a much faster rate to the adsorption sites, and hence giving the increase in the adsorbed amounts of CO₂ (Witoon and Chareonpanich, 2012).

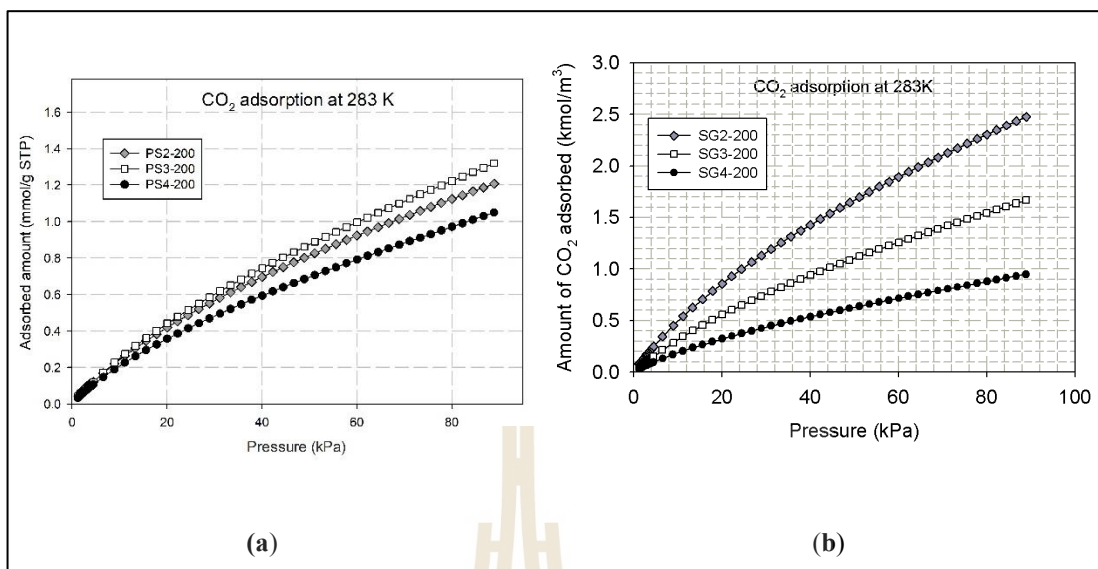


Figure 5.11 CO₂ adsorption isotherms at 283 K for porous silica prepared at different pH

(a) adsorbed amount plotted in mmol/g

(b) adsorbed amount plotted in kmol/m³

Porous silica adsorbents with two different silanol contents were prepared using calcination temperatures of 200 and 500 °C, and their effects on the adsorption isotherms of CO₂ at 273 K are displayed in **Figures 5.12** and **5.13** for porous silica prepared at pH 2 and pH 4, respectively. The absolute pressure versus amount of CO₂ adsorbed in mmol/g (a) and kmol/m³ (b) are presented in these figures. It is observed from **Figure 5.13** that, in the case of larger pore silica (PS4 series), the amount of CO₂ adsorbed for porous silica with a higher content of the silanol group (PS4-200) was notably greater than that for the silica glass with a lower content of functional group (PS4-500). This clearly indicates that the adsorption of CO₂ could be promoted by the presence of surface functional groups. However, for silica glass with a smaller pore size (PS2 series), there is little significant effect of the

functional group content on the adsorption isotherm of CO₂, as shown in **Figure 5.12 (a)**. If the adsorption isotherms are plotted in mole per unit volume (kmol/m³) as shown in **Figure 5.12 (b)**, we observe that the adsorption isotherm obtained for a lower content of functional group (PS2-500) was greater than that for a greater amount of the silanol group (PS2-200). In **Table 5.2**, we observe that the mesopore volume of PS2-500 is greater than that of PS2-200, although the total pore volume of PS2-500 and functional group concentration are less than those of PS2-200. Therefore, when the adsorption isotherm is plotted in per unit volume, the adsorption isotherm of PS2 series shows a significant difference between mmol/g and kmol/m³. The number of moles of CO₂ adsorbed per gram of PS2 series is not much different, and, when we divide this amount of total pore volume, it leads to the greater adsorption isotherm in kmol/m³ of PS2-500. The initial adsorption occurs at the functional group as the stronger interaction between solid and fluid and leads to the fluid cluster formation. The cluster may cause the difficulty for further fluid molecules to move inside the smaller pores; therefore, at higher pressures, the adsorption is affected by not only the functional group content but also the diffusion effect as well.

Next, the temperature effect on the adsorption isotherms of CO₂ was investigated. In **Figure 5.14**, the CO₂ adsorption on porous silica prepared at pH 2 and at calcination temperatures of 200 °C for different adsorption temperatures are presented. The shape of the isotherms is similar to that of the initial part of the Type II isotherm, according to IUPAC classification (Sing et al., 1985). There is a general tendency for the adsorption capacity to decrease with an increase in the adsorption

temperature, which implies that the adsorption of CO_2 on porous silica is an exothermic process, that is, it is a physical adsorption phenomenon.

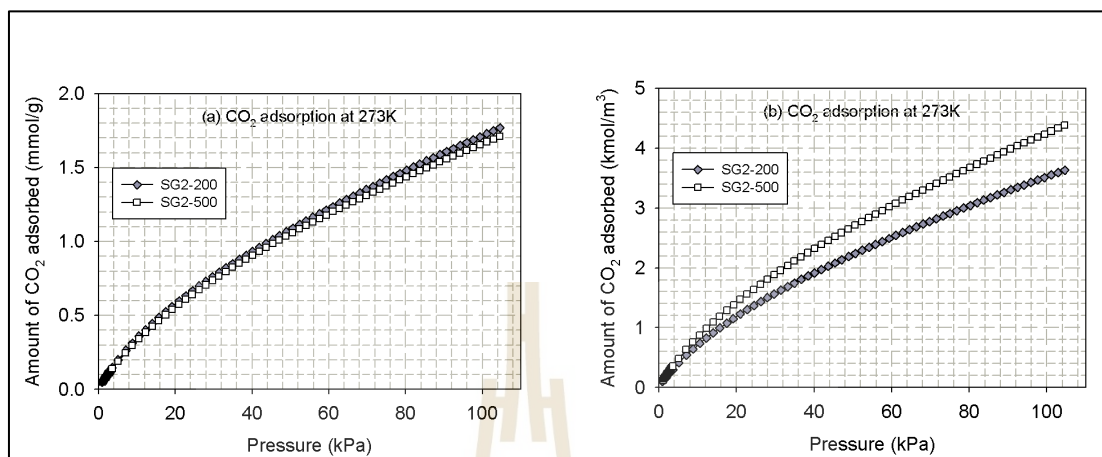


Figure 5.12 CO_2 isotherms at 273 K for porous silica prepared at pH 2

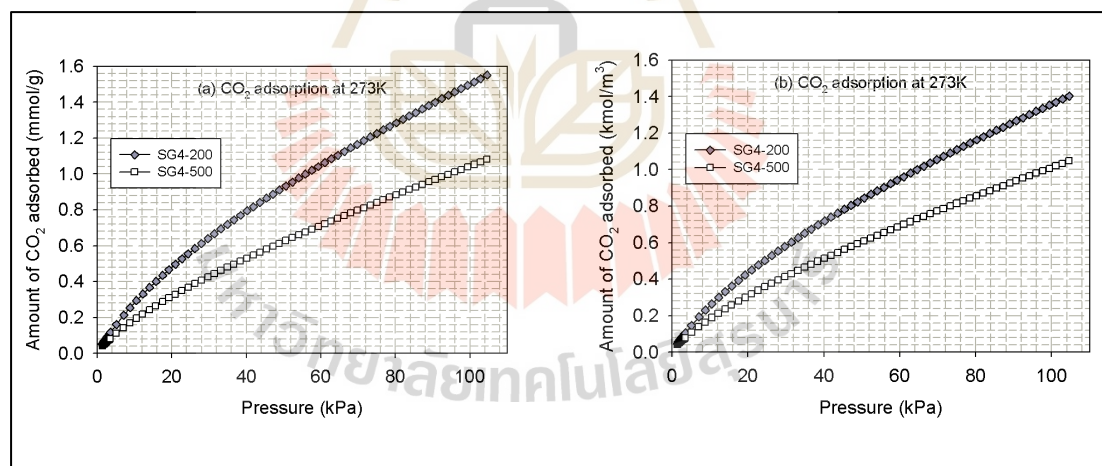


Figure 5.13 CO_2 isotherms at 273 K for porous silica prepared at pH 4

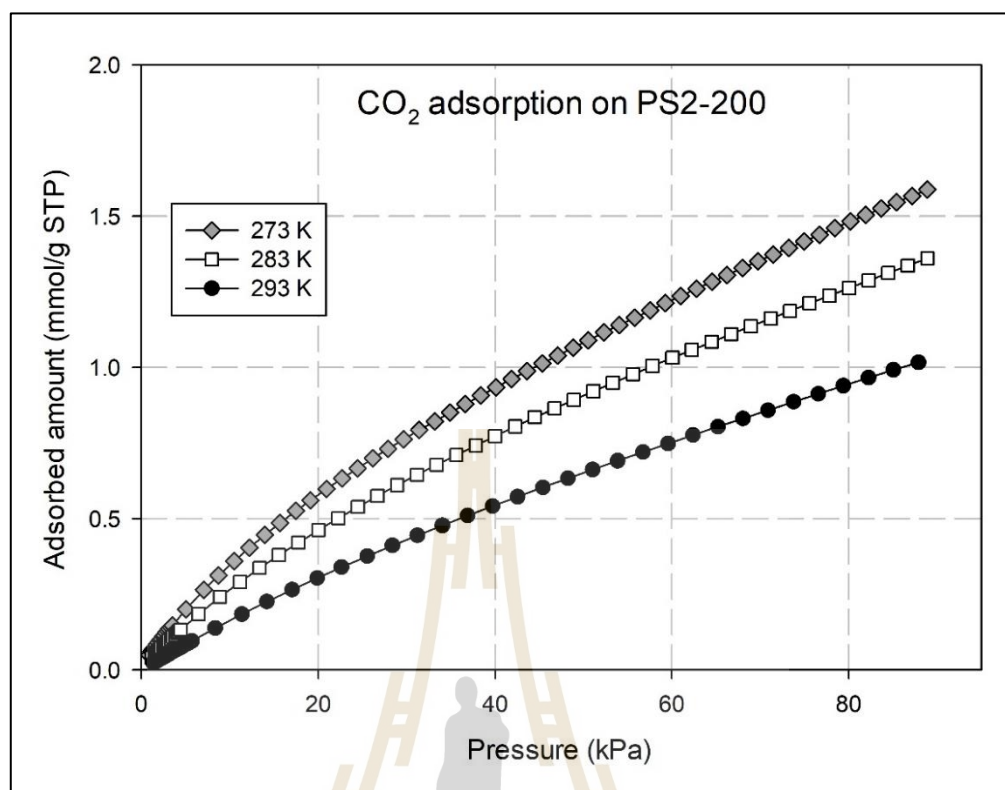


Figure 5.14 Experimental CO₂ adsorption isotherms at 273, 283 and 293 K for the prepared porous silica.

5.5.2 GCMC simulation results carbon dioxide adsorption

5.5.2.1 Adsorption isotherms for various pore widths

The isotherms for CO₂ adsorption at 283 K on homogeneous surfaces of porous silica with various pore widths and pressures up to 4500 kPa obtained by the GCMC simulation are presented in **Figure 5.15**. From the shape of the isotherm curve, the adsorption of CO₂ in the finite-length slit pore model of silica for 1 nm pore width shows the continuous formation of a monolayer. For pore widths larger than 1 nm, a monolayer along the pore wall can be firstly observed and an additional adsorbed layer follows. For the finite-length pore model of porous silica, the phase transition can be observed, and the adsorption isotherm has a smooth

phase transition that is similar to that observed for activated carbon (Wongkoblap et al., 2005). The adsorption in the finite-length pore model is narrower and the two contact layers can be seen where the pore density of about 10 kmol/m^3 occurs at different pressures for each pore width. The contact layer occurs at a higher pressure when the pore becomes larger, and beyond this pressure the pores are then filled. The inner core is gradually filled due to the lower interaction between fluid and solid at the pore mouth region and a meniscus is observed (Wongkoblap and Do, 2006). When the pressure is further increased, the phase transition from a gas-like phase to a liquid-like phase takes place, and the pore density becomes close to 19.6 kmol/m^3 , which is the saturated condition of liquid carbon dioxide at 283 K. This transition occurs at pressures of about 1500, 2500, 3000, 4000, and 4500 kPa for the pore widths of 2, 3, 4, 5, and 6 nm, respectively. The maximum capacity for the saturation condition decreases with an increase in pore widths, and this may be due to the packing effect where different numbers of CO_2 molecules are closely packed in the pore. The compression of the adsorbed phase from the liquid-like phase to a highly liquid-like phase or solid-like phase is also observed for pore widths smaller than 6 nm. This is because of the stronger interaction between fluids and solids for the smaller pores. It is noted that the behavior of adsorption isotherms obtained using the GCMC is quite similar to that obtained by the experiment as one can see in **Figure 5.11 (b)**, that is, the adsorption capacity decreases with an increase in the pore width.

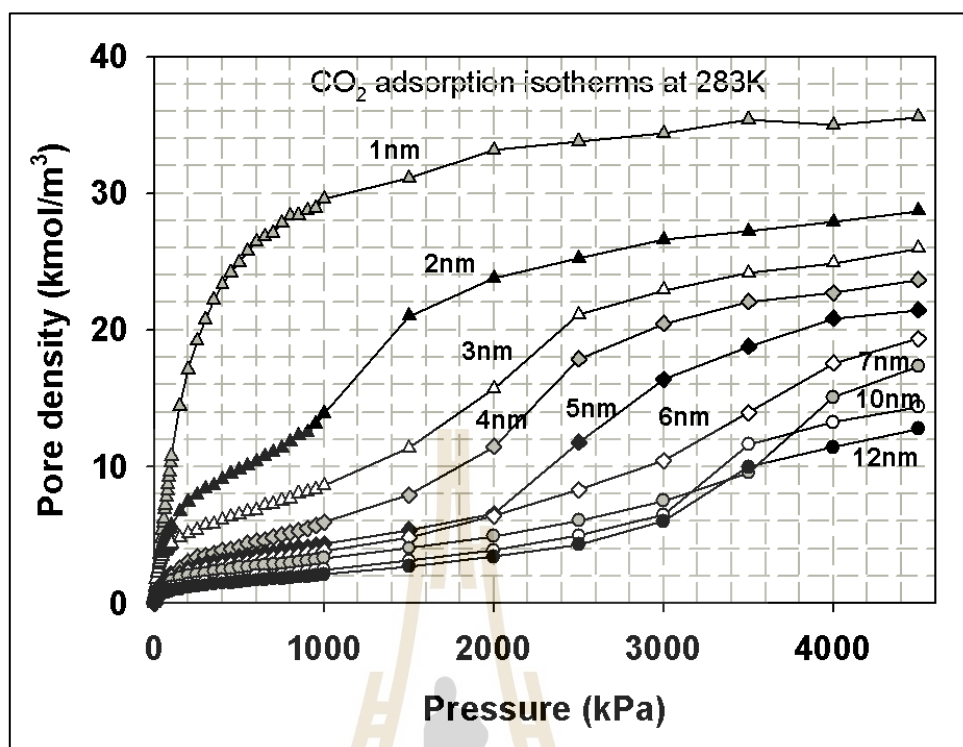


Figure 5.15 Adsorption isotherms of CO₂ on finite-length slit pore model of porous silica at 283 K.

5.5.2.2 Effects of functional group concentration on CO₂ adsorption isotherms

The effect of pore width on the adsorption isotherms of CO₂ was presented in the previous section. Next, the study of the effect of functional group concentration on CO₂ adsorption at 283 K for pore width of 2 nm, which is close to the average pore width of PS2 porous silica, will be presented. The random topology mentioned in **Section 5.4.2.3** is first considered, and for this model the surfaces are covered with the OH groups of 5%–20%. The adsorption of CO₂ in homogeneous finite-length pores (diamond-shape symbols), and three isotherms obtained for heterogeneous finite-length pores with different OH concentrations; 5% of OH

(square symbols), 10% of OH (upward triangle symbols), and 20% of OH (circle symbols), respectively, are shown in **Figure 5.16**. As shown in **Figure 5.16 (a)**, the adsorption isotherms obtained for heterogeneous pores are greater than those for the homogeneous pores (without OH groups) at pressures lower than 200 kPa. This behaviour should be attributed to the stronger interaction between CO₂ and the silanol groups on the pore walls. However, at pressures greater than 200 kPa, the opposite behaviour is observed, as shown in **Figure 5.16 (a)** and **(b)**. This behaviour is probably caused by the reduction of pore volume as the number of functional groups is increased. An early onset in the adsorption isotherms is observed in the heterogeneous pores, and the adsorption isotherms increase with an increase in the contents of the functional groups at low pressures, as seen in **Figure 5.16 (a)**. This is due to the stronger potential energy of interactions between CO₂ molecules and the number of OH groups on the solid surfaces. When the first layer is completely formed as shown in **Figure 5.17 (d)**, the further adsorption is dominated by the interaction between fluids. Therefore, the number of CO₂ molecules increases with pressure. However, in this study, the simulation box volume (V_{pore}) is fixed as described in section of computation methodology; therefore, the number of functional groups on the solid surfaces will reduce the pore space for CO₂ to occupy. This will lead to the adsorption isotherm of the homogeneous pore being greater than those of the heterogeneous pore. The contribution of the functional groups can enhance the adsorption of fluid at the first layer and becomes less significant for additional adsorption especially for the small pores.

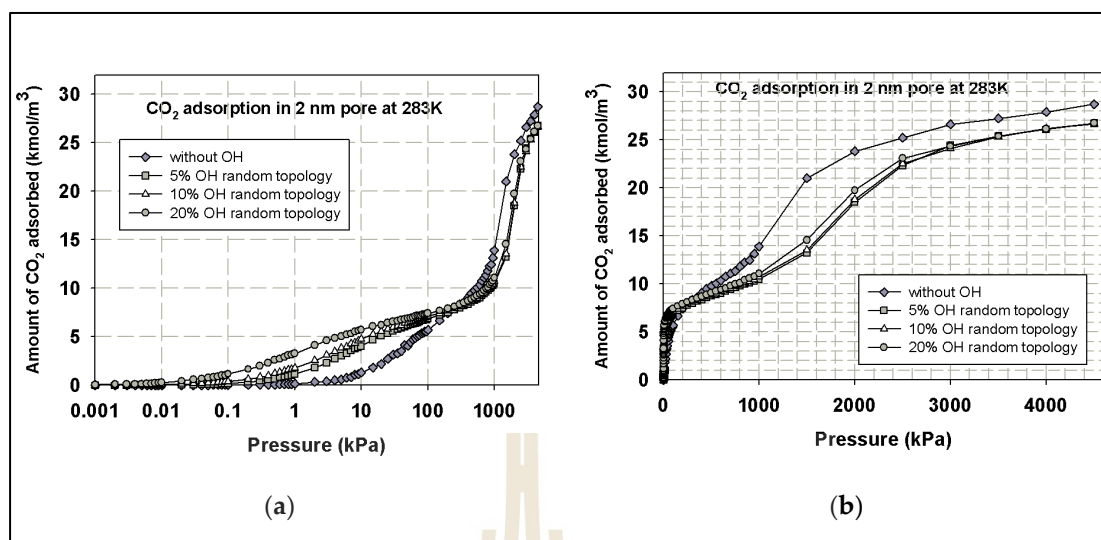


Figure 5.16 CO₂ adsorption isotherms at 283 K in a slit pore model of porous silica with 2 nm. width and different concentrations of OH (a) plotted in semi-log scale and (b) plotted in linear scale.

Figure 5.17 presents the microscopic configurations of CO₂ in a finite-length slit pore model without functional group and **Figure 5.18** presents the microscopic configurations of CO₂ in a finite-length slit pore model where 20% of the OH groups are placed randomly on the surfaces at different pressures. The initial adsorption occurs at the functional group sites, and then an adsorbed phase is formed at the contact layer next to the pore walls at low pressures, as shown in **Figure 5.18 (b)**. When the pressure is further increased, the second layer is formed and followed by the pores filling in the inner cores, as can be seen in **Figure 5.18 (e)** and **(f)**. Then, when the contact layers are completed, the heterogeneous surface effects on the second and higher layers become negligible (Borowko, 2002). In these figures, the large and small grey spheres represent the solid model of SiO₄ crystals, the large green spheres and

small green spheres represent the oxygen atoms and the hydrogen atoms of OH group, respectively, and the large black spheres and small red spheres represent the carbon atoms and oxygen atoms of the CO₂ molecules, respectively.

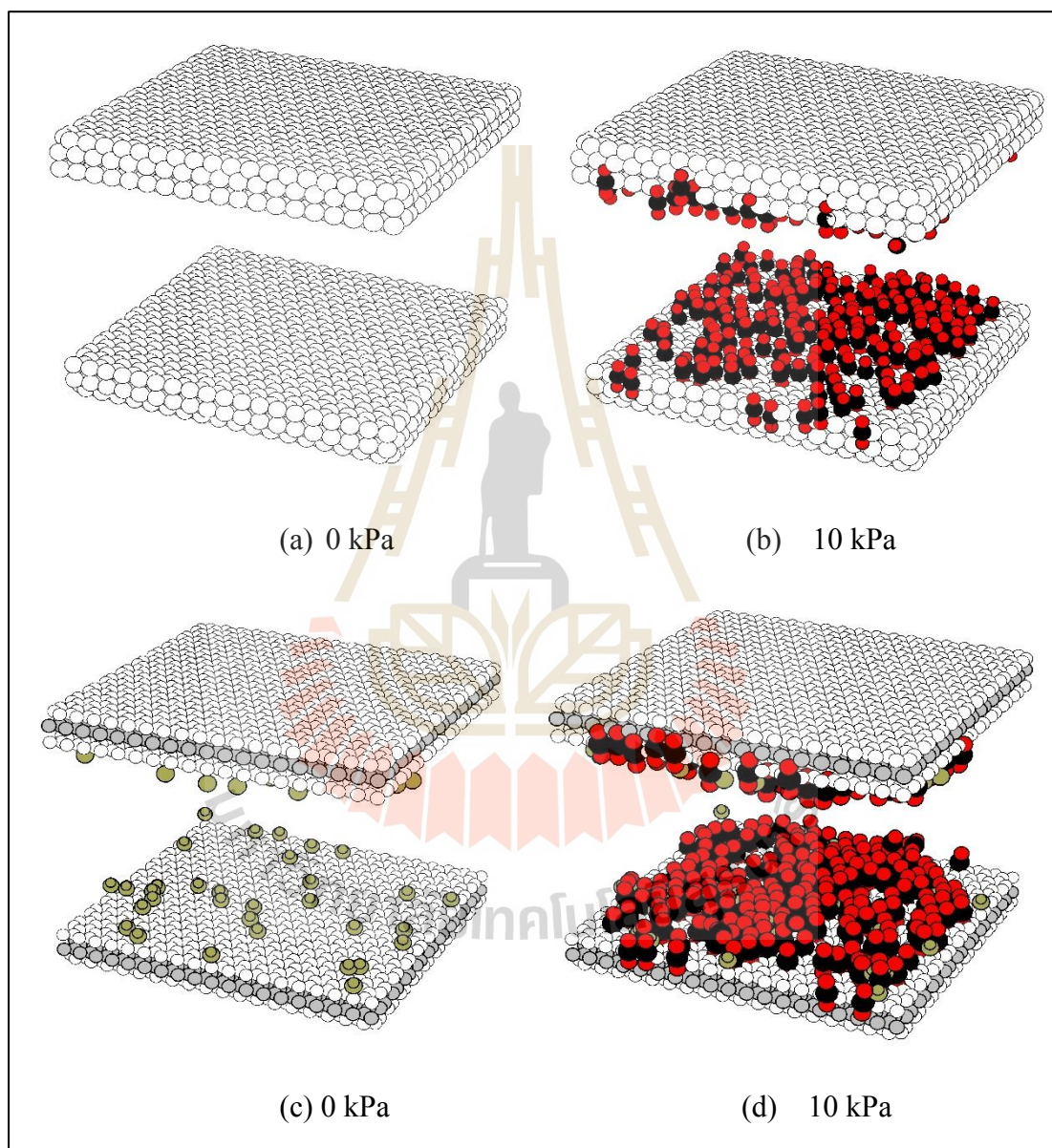


Figure 5.17 Snapshots of CO₂ molecules in heterogeneous porous silica of 2 nm. in widths at 283 K

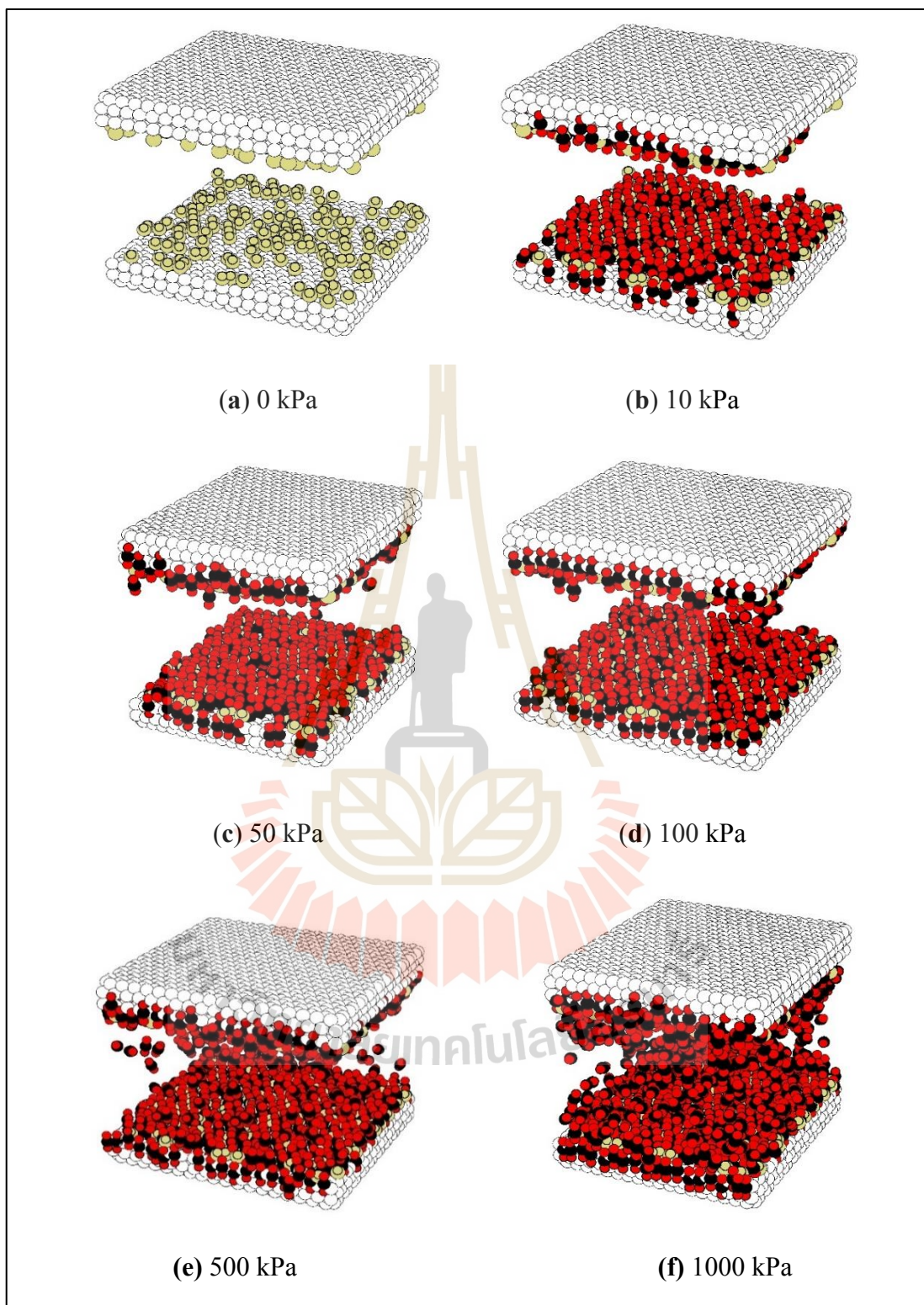


Figure 5.18 Snapshots of CO₂ molecules in heterogeneous porous silica of 2 nm. in widths at 283 K and 20% of the functional groups.

5.5.2.3 Effects of the functional group allocation on the adsorption of CO₂

The effect of functional group allocation (placement scheme) on the adsorption behavior of CO₂ in finite-length pores of porous silica was also investigated. As seen previously in **Section 5.5.2.2** for pore widths of 2 nm, it was found that the isotherms obtained for the random topology model were greater than those obtained for the pores without the silanol group at pressures lower than 200 kPa, and that the opposite behaviour was observed at higher pressures. Typical simulated adsorption isotherms obtained for the 4 nm. Pore width at 283 K and with 20% of the functional groups being placed as random topology and fixed topology are presented in **Figure 5.21**. For comparison, the isotherm obtained for 4 nm pore width without the functional groups are also presented in the same figure. The adsorption isotherms obtained for both models are greater than those obtained for homogeneous pores at pressures lower than 1500 kPa. At higher pressures, the adsorption isotherms obtained from pores without functional groups become greater than those obtained from the heterogeneous pore models. It is further noted that adsorption of CO₂ for the fixed topology model is greater than that for the random topology model at pressures lower than 0.1 kPa, snapshot of CO₂ molecules in porous silica of 4 nm at 0.1 kPa in **Figure 5.19 (a) and (b)**. This is because the number of functional groups at the pore entrance in the case of the fixed topology model are greater than those in the case of the random topology model. The initial formation of the adsorbed layer at the pore entrance, where the interaction between the OH group and fluid is very strong, could lead to greater adsorption isotherms as observed in the case of the fixed topology model. For pressure ranging from 0.1 to 10 kPa, it is observed that the adsorption isotherms obtained from the random topology model become greater than that

obtained from the fixed topology model as can be seen in **Figure 5.19 (c) and (d)**. This may be due to the fact that the adsorption occurs not only at the pore entrance but it could also occur inside the pores as well. As mentioned above, the adsorption isotherms from the random topology is greater than those from the fixed topology where the functional groups are allocated at the pore entrance and this may lead to the difficulty for CO₂ to diffuse into the inner pore, as observed for the case of the experimental isotherms in **Section 5.5.1.3** for the smaller pore widths of sample PS2-200. Over a pressure range higher than 20 kPa, showing Snapshots of CO₂ molecules in **Figure 5.20**, the isotherms obtained from the fixed topology become greater than those from the random topology and then they tend to merge together at very high pressures. This may imply that the functional groups could be formed at the pore edges in the case of smaller pores, while the functional groups may be distributed along the solid surfaces if the pores are large enough. If the mesoporous porous silica containing suitable amounts and distribution of OH groups could be synthesized, this material could be employed to adsorb carbon dioxide at an ambient temperature.

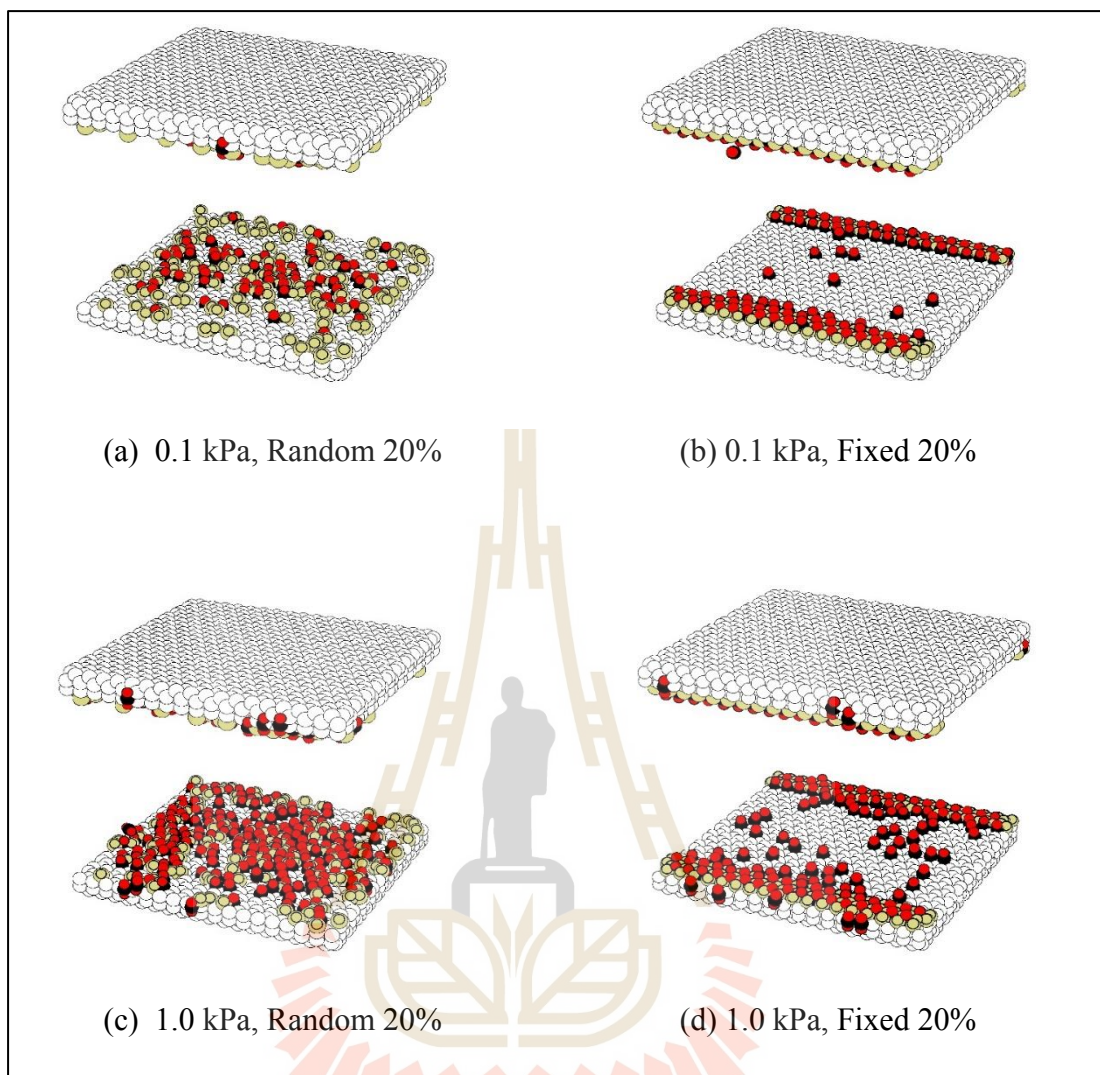


Figure 5.19 Snapshots of CO₂ molecules in heterogeneous porous silica of 4 nm. in widths at 283 K and 20% of the functional groups.

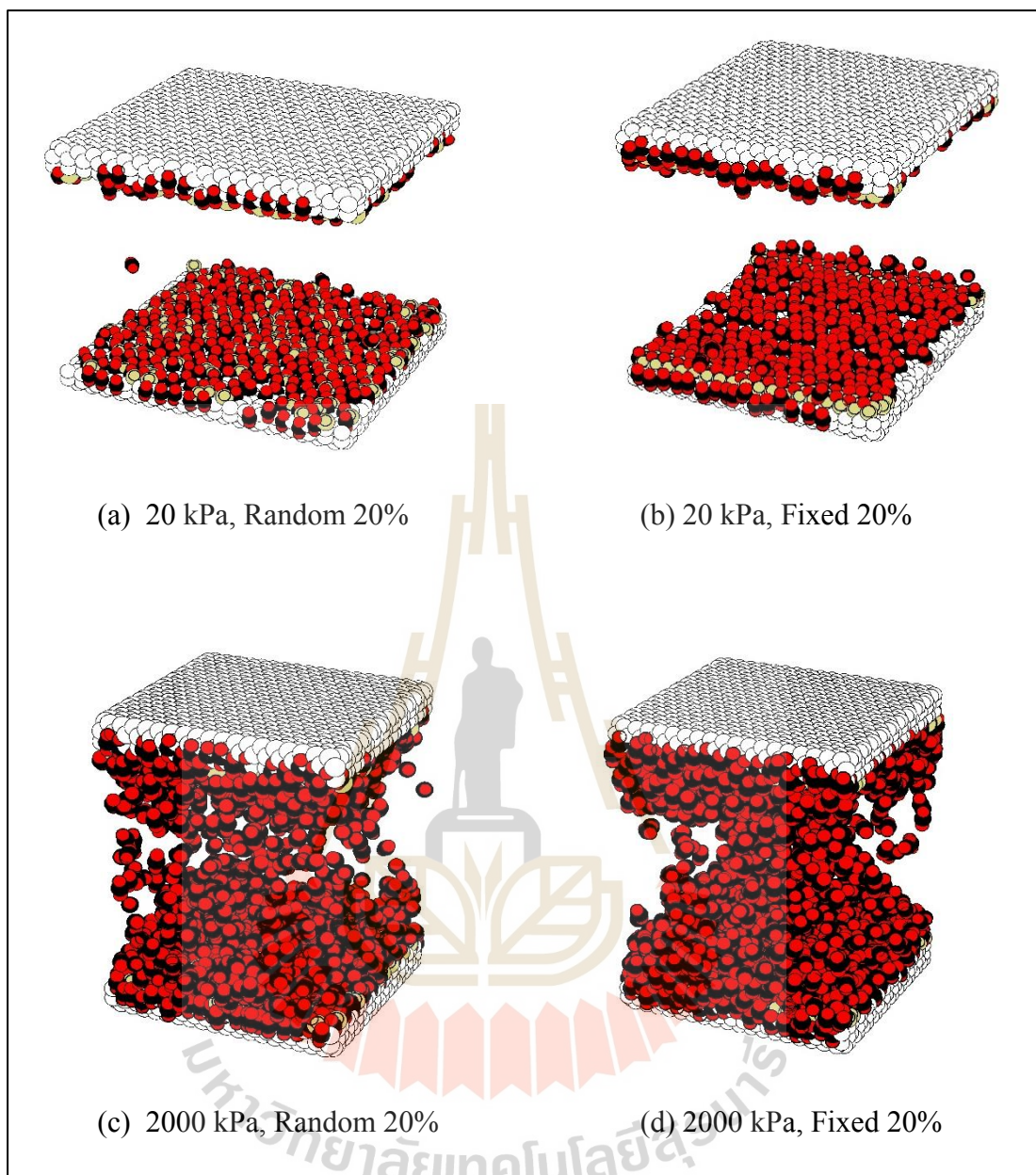


Figure 5.20 Snapshots of CO₂ molecules in heterogeneous porous silica of 4 nm. in widths at 283 K and 20% of the functional groups at pressure more than 20 kPa.

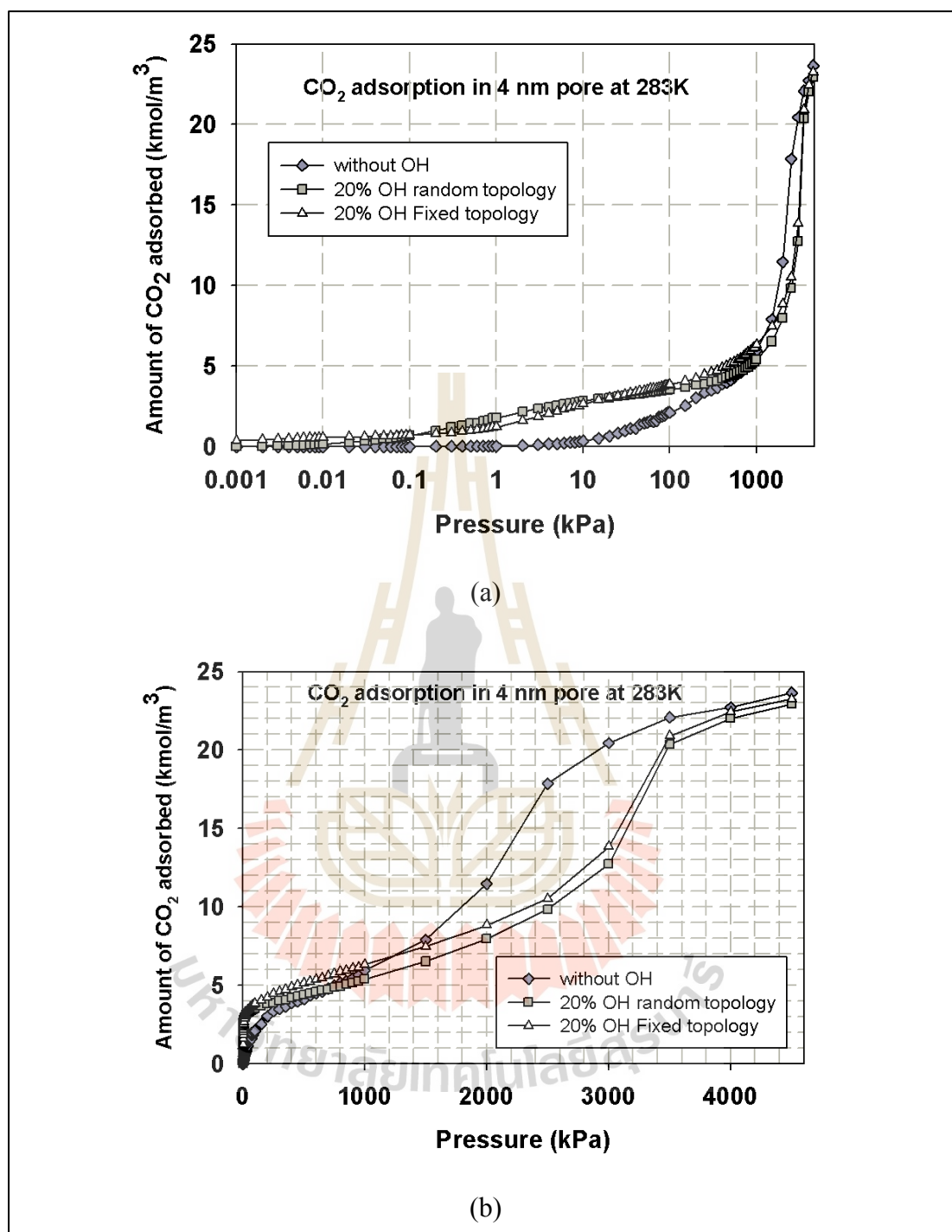


Figure 5.21 Effects of functional group allocation on CO₂ adsorption isotherms at 283 K for the porous silica model of 4 nm widths at (a) plotted in semi-log scale and (b) plotted in linear scale.

5.5.2.4 Adsorption of CO₂ on a defective surface

Figure 5.22 depicts the simulated isotherms of CO₂ adsorption at 283 K derived from a perfect homogeneous surface model, and the defective heterogeneous surface model. The adsorption isotherms for a defective surface show an early onset of adsorption and are greater than those in the case of the homogeneous pores. This may be due to the presence of surface defect pits where CO₂ molecules are strongly adsorbed because of the greater interaction between CO₂ and surface atoms around the defective hole. When the formation of two contact layers along the pore wall is accomplished, the defective surface shows a slight effect on the adsorption of a further layer. However, the adsorption capacity at the saturation condition for the case of the defective surface pore model is still greater than that of the perfect surface pore model. This may be due to the packing efficiency effect, that is, the amount of CO₂ molecules can accommodate not only in the inner core volume but also inside the defective spaces as well.

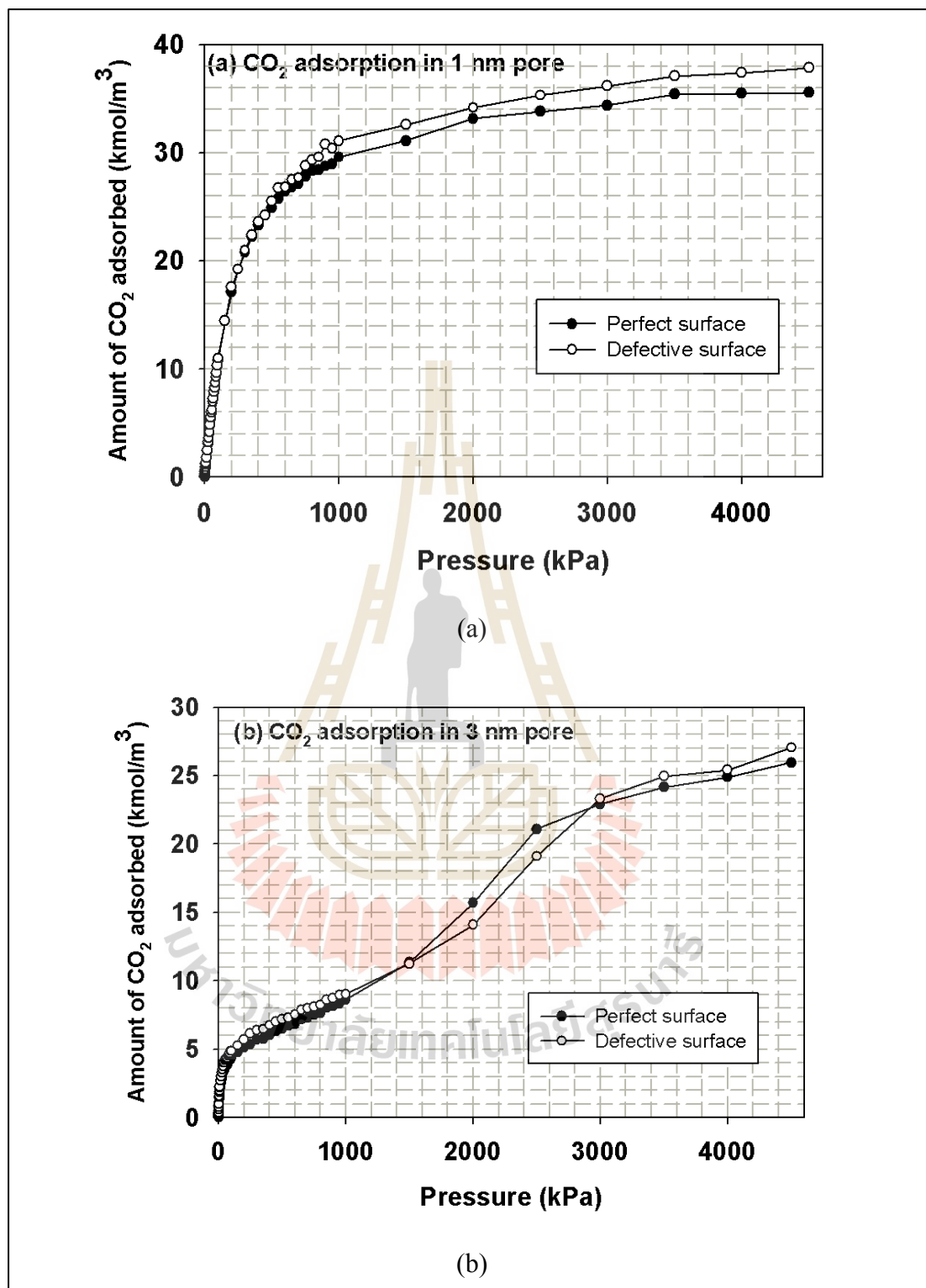


Figure 5.22 CO₂ adsorption on perfect and defective surfaces of pore walls of

(a) 1 nm and (b) 3 nm pore widths.

5.5.2.5 Comparison between the experiment and GCMC simulation method

Pore size distribution (PSD) of the prepared porous silica can be determined based on the method proposed by Samios et al., (1997) by comparing the experimental CO₂ isotherms and the isotherms calculated using the GCMC ensemble. A set of 12 CO₂ adsorption isotherms obtained from the GCMC simulation was calculated for finite-length pores of 1 to 12 nm in width, up to the saturation vapour pressure of CO₂ at 283 K (4500 kPa) for which the results were previously shown in **Figure 5.15**. Then, these adsorption isotherms are compared with the experimental adsorption isotherms for PS2-200 using an optimization solver of EXCEL program. The simulated isotherms from the optimization method (line) are compared with the experimental data, as shown in **Figure 5.23**. It is clear that both isotherms agree very well. The total pore volume obtained from CO₂ adsorption isotherms at 283 K is 0.2019 cm³/g, which is lower than that obtained from N₂ adsorption isotherms at 77 K (**Table 5.2**) of 0.487 cm³/g. This discrepancy arises from the fact that the experimental adsorption of CO₂ was not performed up to the saturation pressure condition at 283 K. The PSD of the prepared porous silica obtained by using CO₂ adsorption isotherms is displayed in **Figure 5.24**. It shows a bimodal characteristic consisting of the first larger area covering pore sizes from 0–5 nm and a second smaller area in the range of 7–9 nm pore sizes. The average pore size is estimated to be around 2 nm, which is close to that derived from the adsorption data of N₂ at 77 K (2.4 nm), as presented in **Section 5.5.1.1**. A good agreement of the adsorption results between the experiments and the simulation has proved that the simple finite-length

slit pore model based on the assemblage of SiO_4 units is adequate for describing the adsorption phenomena in a porous silica adsorbent.

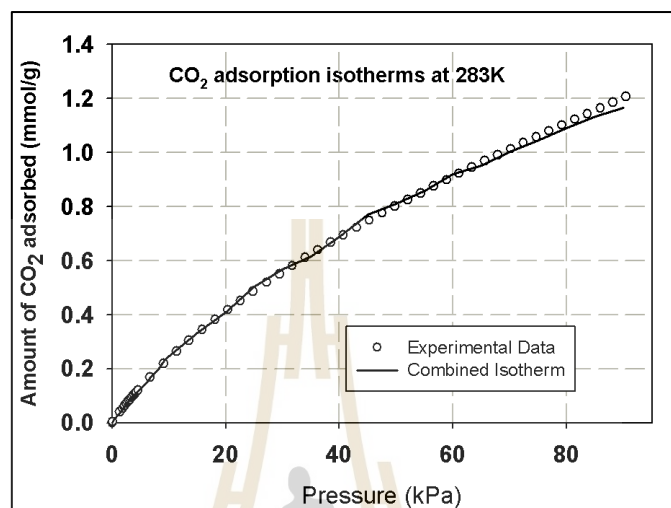


Figure 5.23 Comparison of experimental and simulated isotherms for CO₂ adsorption by porous silica glass (sample PS2-200) at 283 K.

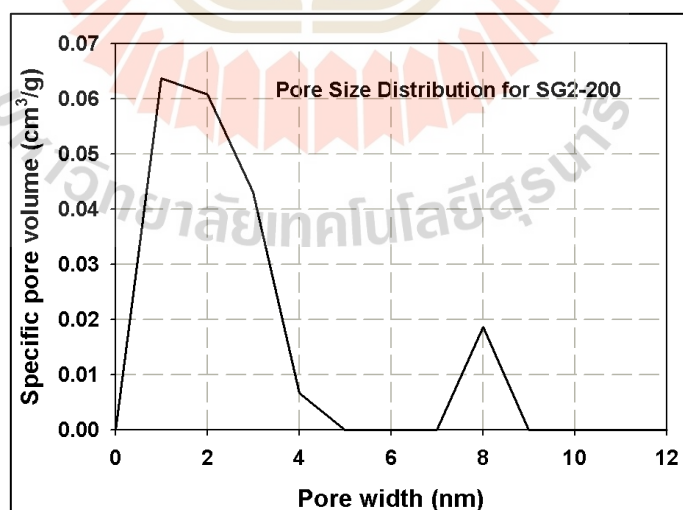


Figure 5.24 Calculated PSD obtained from CO₂ adsorption isotherms using GCMC simulation.

5.5.3 GCMC Simulation results for methane adsorption

5.5.3.1 Methane adsorption isotherm

The adsorption isotherms of CH₄ versus pressures for various pore widths (from 7 to 40Å) at 298 K are shown in **Figure 5.25**. The solid model of random topology and 5% of functional group are used to obtain the adsorption isotherm. The adsorption of methane increases with pressures and the continuous pore filling of monolayer can be observed. The capillary condensation cannot be observed, this is due to that CH₄ behaves as supercritical fluid at 298 K. When pore width increases, the adsorption isotherm decreases, due to the less interaction between solid and methane in the case of larger width (Wongkoblap et al., 2010; D. D. Do and H. D. Do, 2003; Chiang et al., 2016). It is noted that the number of adsorbed molecules in the larger pore increases with pore width, although the pore density is decreased. The maximum adsorption isotherm can be obtained in the case of pore having width of 7Å, this is due to that methane having the collision diameter (σ_{ff}) of 3.73Å can be packed tightly inside the pore. Therefore, the maximum gas uptake can be obtained if the pore width is fitted tightly with the single layer of fluid at specific surface area and temperature (D. D. Do and H. D. Do, 2003).

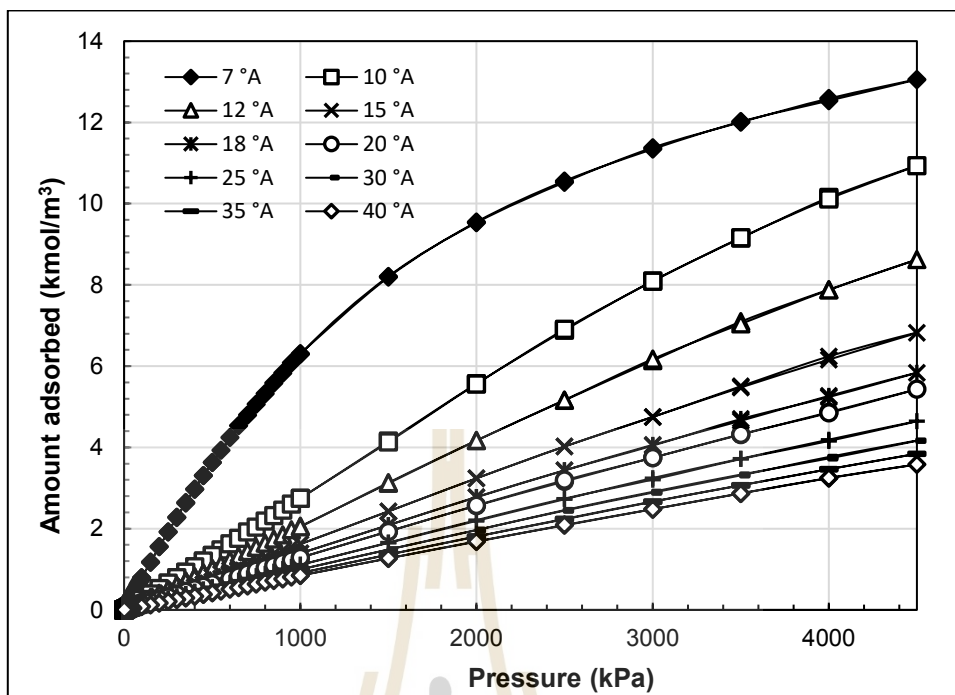


Figure 5.25 Methane adsorption isotherms for various pore widths with the random topology contained 5% of functional group at 298 K.



5.5.3.2 Effects of temperature on methane adsorption

The adsorption is carried out for the random pore topology and the concentration of functional group 5% at different temperatures. The adsorption isotherms of CH₄ in pore having width of 10Å at 283 K and 298 K obtained by using the GCMC method are shown in **Figure 5.26**. The isotherm obtained for methane adsorption at 283K is similar to that obtained at 298 K, a single layer of pore layering phenomenon is observed. However the adsorption isotherm at 283 K is greater than that at 298K, this suggests that adsorption of methane in porous glass is physical adsorption. The adsorbed molecules attain the greater energy to evaporate due to the exothermic process (Wongkoblap and Do, 2006).

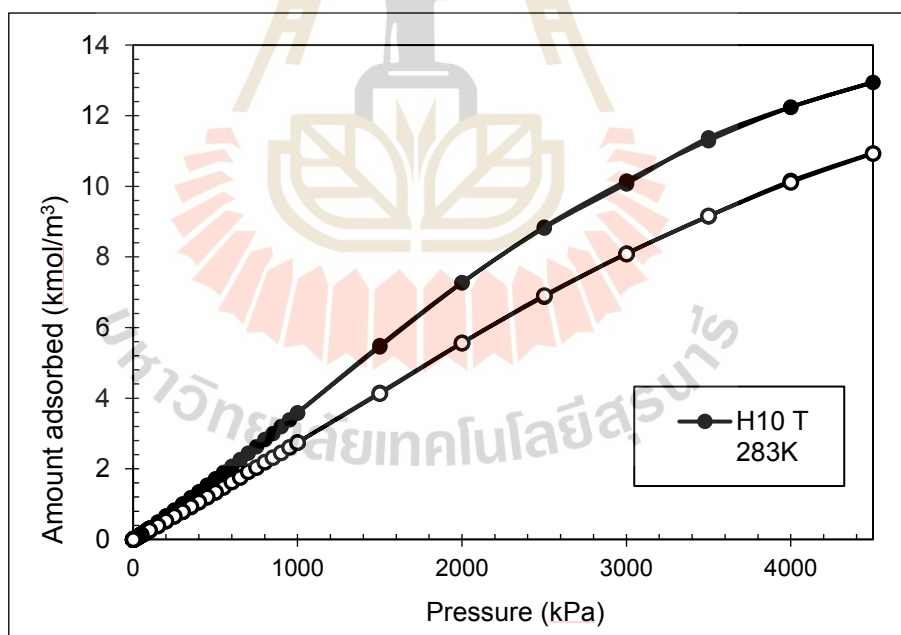


Figure 5.26 Isotherms obtained for CH₄ adsorption in the random pore topology having width of 10Å and 5% of functional groups at 283 and 298 K

5.5.3.3 Effects of silanol groups concentration on methane adsorption

In the previous section, we have shown how pore width and temperature affected on the adsorption behavior, now turn to the effects of functional group concentration on adsorption of methane in porous silica glass at 298 K. The isotherms obtained for CH₄ in the random pore topology contained either 5% or 10% of OH group and 10Å width are shown in **Figure 5.27**. At low pressures, the functional group shows insignificant effect on adsorbed isotherm, the concentration of functional group becomes significant when pressures increase. The isotherm obtained in the case of 10% of OH group is less than that in the case of 5% of functional group, because the larger number of functional groups of 10% reduces the pore volume for methane adsorption. However an insignificant effect at lower pressures can imply that the pore blocking effect is not occurred in the case of methane adsorption.

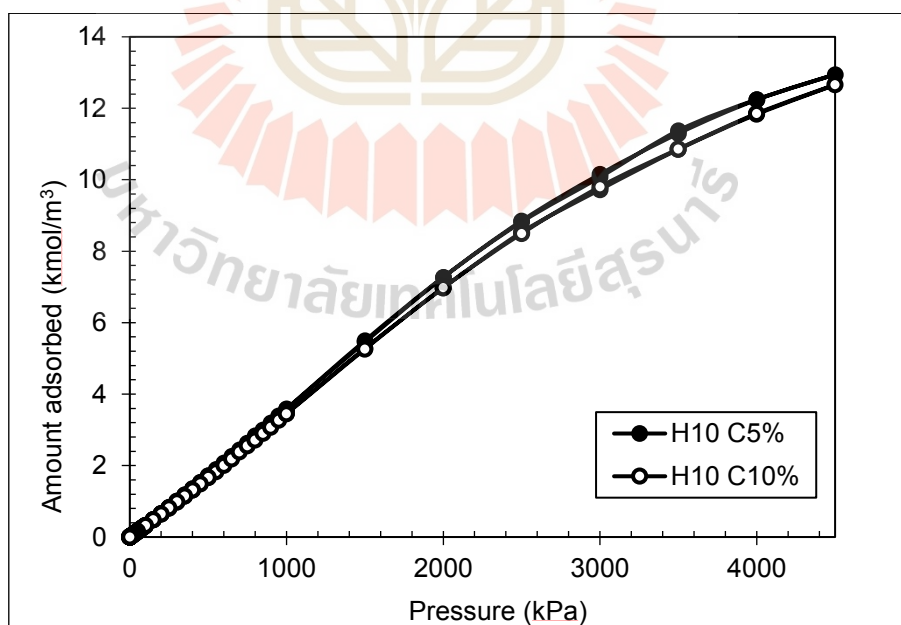


Figure 5.27 Adsorption isotherms of CH₄ in pore having width of 10Å with different concentration of functional group at 298 K.

5.5.3.4 Effects of silanol group topology on methane adsorption

Having seen the functional group concentration effect, now the discussion for the effect of functional group topology on methane adsorption will be presented. Adsorption isotherms obtained for 10Å width with 10% of hydroxyl group at 298K for different functional group topologies are shown in **Figure 5.28**. The isotherm obtained for the fix topology is greater than that for the random topology. The reason is that methane molecules interact with the functional group at the pore mouth and create the nucleation such that molecules can enter the pore and formed the monolayer, as shown in snapshots of **Figure 5.29**. The adsorption isotherms obtained for both topologies are similar to that observed in the experiment. Snapshots of methane adsorption for the random and fix topologies are also shown in **Figure 5.30**, the formation of two contact layers adjacent to the two walls at low pressures is observed which is similar to the adsorption of fluid in activated carbon (Wongkoblap and Do, 2006).

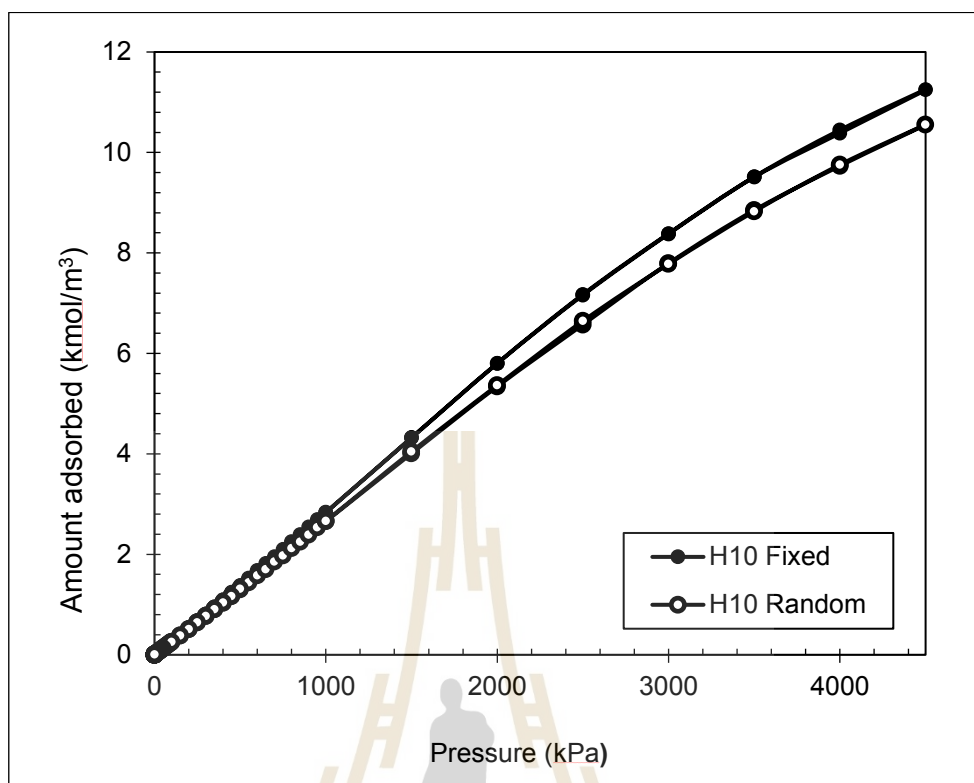


Figure 5.28 Adsorption isotherms of methane at 298K in pore having width of 10Å with different functional group topologies.

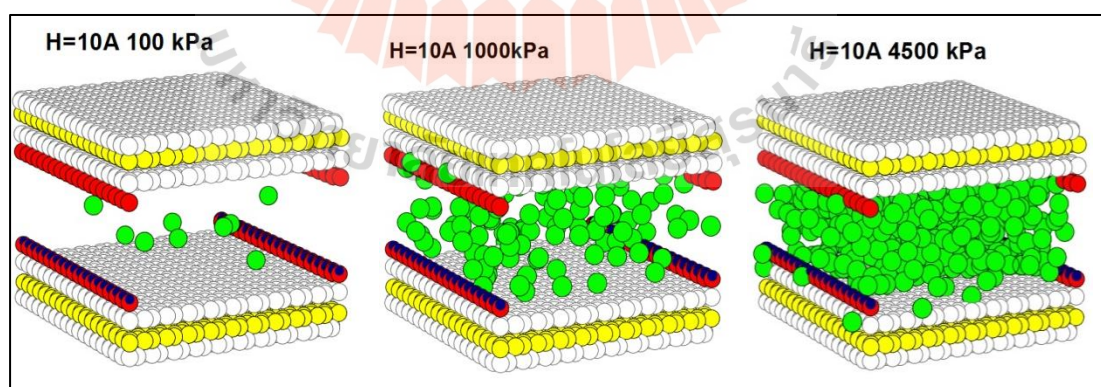


Figure 5.29 Snapshots of methane particles in heterogeneous porous silica of 10Å width contained 10% of functional group for the fix topology.

In these figures, white spheres represent oxygen atoms of SiO_4 , yellow spheres represent silicon atoms, red spheres represent oxygen atom of functional group, small blue spheres represent hydrogen atoms of functional group and green spheres represent methane particles.

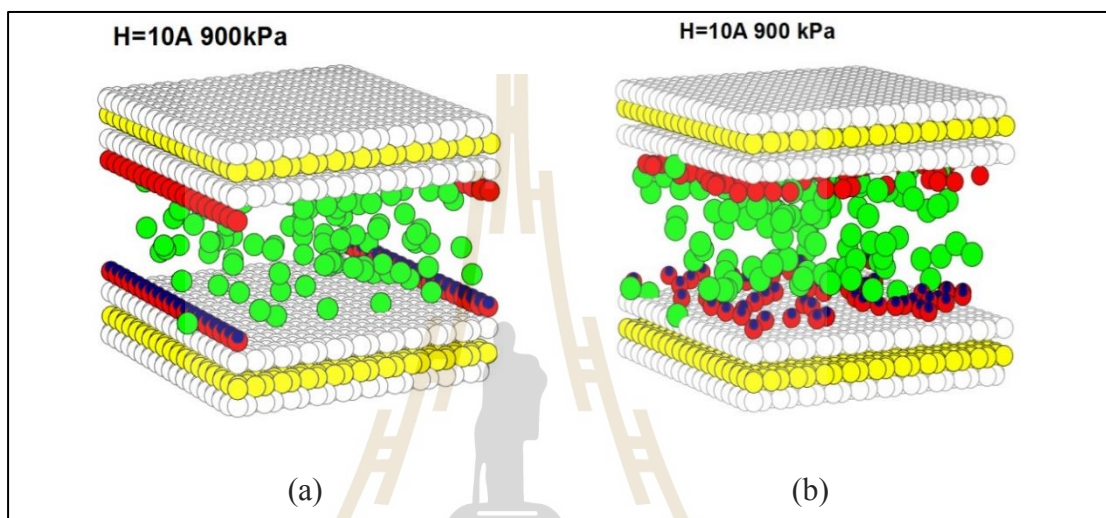


Figure 5.30 Snapshots of methane particles in heterogeneous porous silica of 10\AA width contained 10% of functional group for the random topology (a) and the fix topology (b).

5.6 Conclusions

In this study, simple porous silica models for homogeneous and heterogeneous surfaces were proposed and CO₂ is used as a probe molecule for the adsorption study. The adsorption behavior of CO₂ on porous silica model depends on the pore width, surface heterogeneity and adsorption temperature. The defective surface and surface containing silanol functional groups were used to represent the surface heterogeneity effect. The amount of CO₂ adsorption decreased with the increase in pore width. The adsorption decreased with an increase in the adsorption temperature, thus indicating the physical adsorption of CO₂ in porous silica. CO₂ adsorption on a defective surface was higher than that on a homogeneous perfect surface, with the rapid rising of the amount adsorbed being noticed at relatively low pressures, due principally to the initial forming of two contact adsorbed layers along the pore wall. The adsorption of CO₂ increased with an increase of functional group contents due to the stronger interaction between the fluid and the silanol group. The placement scheme of the functional group also affects the adsorption isotherms; the adsorption for the fixed topology model was greater than that for the random topology model at a low-pressure range but became less than that of the random topology at higher pressures, possibly caused by the diffusion effect (mass transfer resistance) of CO₂ to the inner pore. The simulated isotherms for different single pore widths together with the experimental isotherm data can be used to compute the pore size distribution. It was demonstrated that the finite-length slit pore model, whose walls consist of an assemblage of connected SiO₄, can be used to represent the structure of porous silica for a successful simulation study of CO₂ adsorption.

The adsorptions of CH₄ in finite-length slit pores of porous silica in the presence and absence of functional group are presented. The adsorption of methane in heterogeneous finite-length pore is quite similar to that in homogeneous finite-length pore. The continuous adsorption isotherm of the formation of monolayer at room temperature can be observed, and the adsorption isotherm decreases if the pore width increases due to the weak interaction between fluid and solid. The adsorption decreases by increasing temperature resulting the exothermic process of methane adsorption in porous silica. The adsorption decreases with an increase of functional group due to the decreasing of pore volume at high pressures. The topology of functional group also affects the adsorption of methane in porous glass, the adsorption for fix allocation of functional groups at the pore mouth is greater than that allocated randomly. This is due to the greater interaction between fluid and functional group at pore mouth which becomes the nucleation for further adsorption inside the pore.

5.7 References

- Allen, M.P.; Tildesley, D.J. *Computer Simulation of Liquids*; **Clarendon Press**: Oxford, UK, 1987.
- Birkett GR., and Do D.D. (2008). Characteristic heats of adsorption for slit pore and defected pore models. **Langmuir**, 24: 4853-4856.
- Brinker C.J. and Scherer G.W. (1990). *Sol-gel science, the physics and chemistry of sol-gel processing*. **Academic Press**. Boston.
- Burchart, E.D.; Vandegraaf, B.; Vogt, E.T.C. A consistent molecular mechanics force field for aluminophosphates. **J. Chem. Soc. Faraday Trans.** 1992, 88, 2761–2769

- Calero S., Dubbeldam D., Krishna R., Smit B., Vlugt T.J.H., Denayer J.F.M., Martens J.A. and Maesen T.L.M. (2004). Understanding the Role of Sodium during Adsorption: A Force Field for Alkanes in Sodium-Exchanged Faujasites. **Journal of the American Chemical Society**. 126(36): 11377-11386
- Chaturaporn Nimjaroen, Shigeki Morimoto and Chaiyot Tangsathitkulchai (2009). Preparation and properties of porous glass using fly ash as raw material. **Journal of Non-Crystalline Solids**, Vol. 355:1737-1741
- Chiang, Y.C.; Juang, R.S. (2017). Surface modification of carbonaceous materials for carbon dioxide adsorption: A review. **J. Taiwan Inst. Chem. Eng.** Vol. 71, 214–234.
- Do, D.D. (1998). Adsorption Analysis: Equilibria and Kinetics; **Imperial College Press**.
- Do D.D. and Do, H.D. (2003). Pore Characterization of Carbonaceous Materials by DFT and GCMC Simulations: A Review. **Adsorption Science and Technology**, 21(5): 389-423
- Do D. D. and Do H. D. (2003). Refined method of potential enhancement in the equilibria characterization of activated carbon. Comparison with GCMC and DFT. **Langmuir**. vol. 19:8302
- Ek, S.; Root, A.; Peussa, M.; Niinisto, L. Determination of the hydroxyl group content in silica by thermogravimetry and a comparison with H MAS NMR results. **Thermochim. Acta** 2001, 379, 201–212.
- Feng, L.; Shen, Y.; Wu, T.; Liu, B.; Zhang, D. and Tang Z. (2020). Adsorption equilibrium isotherms and thermodynamic analysis of CH₄, CO₂, CO, N₂, and H₂ on NaY Zeolite. **Adsorption**. doi:10.1007/s10450-020-00205-8

- Frenkel, D.; Smit, B. Understanding Molecular Simulation; **Academic Press**: New York, NY, USA, 2002
- He, Y.; Seaton, N.A. Experimental and computer simulation studies of the adsorption of ethane, carbon dioxide, and their binary mixtures in MCM-41. **Langmuir** 2003, 19, 10132–10138
- Harris, J.G.; Yung, K.H. Carbon dioxide's liquid-vapor coexistence curve and critical properties as predicted by a simple molecular model. **J. Phys. Chem.** 1995, 99, 12021–12024.
- Johnson J.K., Zollweg J.A. and Gunnins K.E. (1993). The Lennard-Jones equation of state revisited, **Molecular Physics**, 78(3): 591-618
- Kemper J. (2015). Biomass and carbon dioxide capture and storage: A review. **Int. J. Greenh. Gas Control**. Vol. 40, 401–430.
- Ketprasoet, N.; Nimjaroen, C.; Tangsathitkulchai, C.; Wongkoblaph, A. Adsorption and isosteric heat studies for adsorption of fluid on porous silica glass using GCMC simulation. In **The 9th South East Asian Technical University Consortium (SEATUC) Symposium Proceedings**; 2015; Suranaree University of Technology: Nakhon Ratchasima, Thailand, 2015.
- Khandaker, T.; Hossain, M.S.; Dhar, P.K.; Rahman, Md.S.; Hossain, Md.A.; Ahmed, M.B. Efficacies of carbon-based adsorbents for carbon dioxide capture. **Processes** 2020, 8, 654.
- Kim, J.M.; Chang, S.M.; Kong, S.M.; Kim, K.S.; Kim, J.; Kim, W.S. (2005). Control of hydroxyl group in silica particle synthesized by the sol-precipitation process. **Ceram. Int.** Vol. 35, 1015–1019.

- Leung, D.Y.C.; Caramanna, G.; Maroto-Valer, M.M. (2014). An overview of current status of carbon dioxide capture and storage technologies. **Renew. Sustain. Energy Rev.** Vol. 39, 426–443
- Lopes F.V.S., Grande,C.A.; Ribeiro A.M. Loureiro,J.M. Evaggelos O. Nikolakis V. and Rodrigues A.E. (2009). Adsorption of H₂, CO₂, CH₄, CO, N₂ and H₂O in activated carbon and zeolite for hydrogen production. **Sep. Sci. Technol.**Vol, 44, 1045–1073
- Nawrocki J. and Buszewski B. (1988). Influence of silica surface chemistry and structure on the properties, structure and coverage of alkyl-bonded phases for high-performance liquid chromatography. **Journal of Chromatography.** 449: 1–24
- Thongthai Witoon and Metta Chareonpanich (2012). Effect of pore size and surface chemistry of porous silica on CO₂ adsorption. **Songklanakarin Journal of science and Technology.** Vol. 34: 403-407.
- Wongkoblapp A. and Do D. D. (2006). The effects of energy sites on adsorption of Lennard-Jones fluid and phase transition in carbon slit pore of finite length: A computer simulation study. **Journal of Colloid and Interface Science.** vol. 297: 1-9
- Wongkoblapp A., Intomya W., Somrup W., Charoensuk S., Junpirom S. and Tangsathitkulchai C. (2010). Pore size distribution of carbon with different probe molecules. **Engineering Journal.** vol. 14(3):45-56.
- Xiaoning, Y.; Xiaopeng, Y. (2007). Adsorption and structure of Lennard-Jones model fluid in slit like amorphous silica nanopores. **Colloids Surfaces A Physicochem. Eng. Asp.** Vol. 301, 166–173.

Yazawa, T. Present Status and Future Potential of Preparation of Porous Glass and Its Application in Porous Ceramic Materials; Liu, D.-M., Ed.; **Trans. Tech. Publications**: Switzerland, 1995; pp. 125–146



CHAPTER VI

CONCLUSION AND RECOMMENDATIONS

6.1 Conclusions

The purposes of this thesis research are to prepare porous silica from sodium silicate by the sol-gel method and to study its adsorption behavior. The prepared porous silica was characterized for their physicochemical and porous properties. In addition, the porous silica was employed as an adsorbent for ethanol dehydration in both the batch liquid system and the vapor-phase fixed-bed system, and for the removal of methylene blue from aqueous solution in batch adsorption. GCMC simulation was also investigated for pure CO₂, N₂ and CH₄ adsorption behavior by the porous silica. The following conclusions can be drawn.

Porous glass preparation

- The pore size and silanol content of porous silica products could be controlled, respectively, by varying the pH of the solution and the calcination temperature, giving the pore size and silanol content in the range of 2.2-10.9 nm and 2.77-7.94 mmol/g, respectively.
- The porous silica obtained was amorphous and the BET results showed that the specific surface of the porous silica was in the range from 404 to 798 m²/g.
- Sol-gel process is an effective means for controlling the pore structure and the amount of silanol group of porous silica. The use of low pH value and a low calcination temperature during the preparation step gave the largest specific surface

area and the amount of silanol content. It was also found that other porous properties such as mesoporous area and total pore volume showed the same trend as to the effect of pH and calcination temperature.

Water adsorption on porous silica

Liquid phase system

- The water adsorption from ethanol solution by the prepared porous silica in batch operation was studied to arrive at the kinetics and isotherm data of water adsorption. The kinetic of water adsorption by porous silica was studied by following the amount adsorbed as a function of time over the temperature range from 20-40 °C. Overall, the pseudo second-order kinetic model can best predict the water adsorption kinetics.

- From the batch adsorption study, it was found that the adsorption isotherm of water can be well described by the Langmuir isotherm equation followed by the Freundlich isotherm equation.

- It was found that the silanol group (Si-OH) on the surface of porous silica played an important role for the increase of water adsorption via the hydrogen bonding.

Fixed-bed adsorption

- Water removing from ethanol-water vapor mixture by using the prepared porous silica was also conducted in a continuous fixed-bed operation to arrive at the breakthrough data as a function of adsorbent bed height, feed flow rate, adsorption temperature and amount of silanol content.

- The Klinkenberg model based on the linear driving force model successfully described the experimental water breakthrough curves obtained under the

tested conditions. It was also found that the Klinkenberg model parameters including the particle mass transfer coefficient (k) and the effective diffusivities (D_e) can be estimated independently from experimental data.

Methylene blue adsorption on porous silica

From the batch adsorption study, it was found that the adsorption isotherms of methylene blue can be reasonably well described by the Langmuir isotherm and the adsorption results indicated that MB adsorption by porous silica is an endothermic process. Porous silica with a larger mean pore size gave a larger adsorbed capacity. The pseudo second-order kinetic model can best predict the methylene blue adsorption kinetics on the prepared porous silica.

Computer simulation

The adsorption behavior of CO₂ on porous silica model depends on the pore width, surface heterogeneity and adsorption temperature. The defective surface and surface containing silanol functional groups were used to represent the surface heterogeneity effect. The amount of CO₂ adsorption decreased with the increase in pore width. The adsorption decreased with an increase in the adsorption temperature, thus indicating the physical adsorption of CO₂ in porous silica glass. CO₂ adsorption on a defective surface was higher than that on a homogeneous perfect surface, with the rapid rising of the amount adsorbed being noticed at relatively low pressures, due principally to the initial forming of two contact adsorbed layers along the pore wall. The adsorption of CO₂ increased with an increase of silanol group contents due to the stronger interaction between the fluid and the silanol groups. The placement scheme of the functional group also affects the adsorption isotherms; the adsorption for the

fixed topology model was greater than that for the random topology model at a low-pressure range but became less than that of the random topology at higher pressures, possibly caused by the diffusion effect (mass transfer resistance) of CO₂ to the inner pore. The simulated isotherms for different single pore widths together with the experimental isotherm data can be used to compute the pore size distribution. It was demonstrated that the finite-length slit pore model, whose walls consist of an assemblage of connected SiO₄, can be used to represent the structure of porous silica glass for a successful simulation of CO₂ adsorption.

The adsorption of CH₄ in heterogeneous finite-length pore is quite similar to that in homogeneous finite-length pore. The continuous adsorption isotherm of the formation of monolayer at room temperature can be observed, and the adsorption isotherm decreases if the pore width increases due to the weak interaction between fluid and solid. The adsorption decreases by increasing temperature resulting from the exothermic process of CH₄ adsorption in porous silica. The adsorption decreases with an increase of functional group due to the decreasing of pore volume at high pressures.

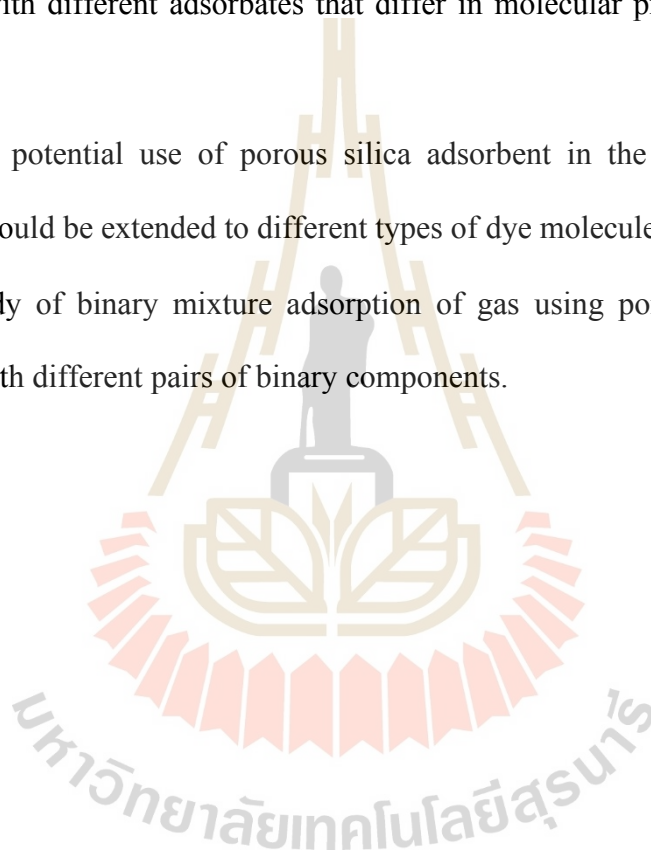
6.2 Recommendations for further works

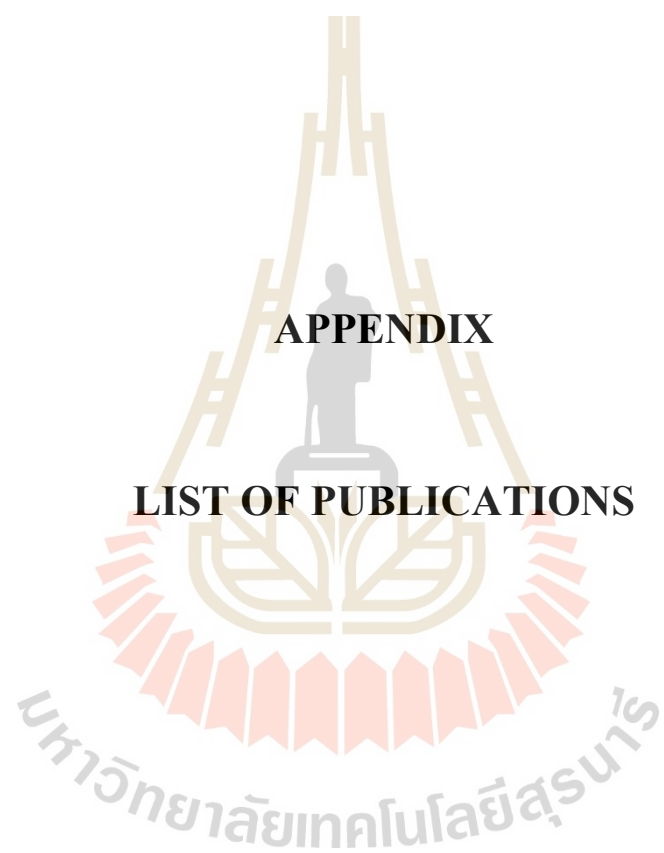
- The scanning electron micrographs of porous silica prepared at different pH of solution and calcination temperatures should be obtained to clearly show the porous structure of porous silica.

- The fixed-bed adsorption for liquid systems by porous silica should be carried out with different adsorbates that differ in molecular properties such as size and polarity.

- The potential use of porous silica adsorbent in the area of liquid-phase adsorption should be extended to different types of dye molecules.

- Study of binary mixture adsorption of gas using porous silica should be performed with different pairs of binary components.





APPENDIX

LIST OF PUBLICATIONS

LIST OF PUBLICATIONS

Chontira Boonfung, Niphat Ketprasoet, Chaiyot Tangsathitkulchai, and Atichat Wongkoblap (2018). Effects of functional group and surface roughness on adsorption of carbon dioxide in porous glass by Grand Canonical Monte Carlo Sim. **The Journal of KMUTNB**. Vol. 28, 1: 113-122.

Pongpon Teerachawanwong, Bharanabha Makkaron, Chontira Boonfung, Chaiyot Tangsathitkulchai, and Atichat Wongkoblap (2019). Computer simulation study for functional group effect on methane adsorption in porous silica glass. **Engineering Journal**. Vol. 23, 197-122.

Chontira Boonfung, Chaiyot Tangsathitkulchai and Atichat Wongkoblap (2020). Carbon dioxide capture in homogeneous and heterogeneous surfaces of porous silica glass. **Processes**.8:1260.

BIOGRAPHY

Miss Chontira Boonfung was born on April 3, 1984. She graduated in primary school from Charoen Witthaya School and secondary school from Amnatcharoen School, Amnatcharoen Province. In 2006, she graduated a bachelor's degree in chemical engineering from Suranaree University of Technology (SUT). In 2010, she graduated a master's degree in chemical engineering from Suranaree University of Technology (SUT). In 2014, she continued her doctoral degree study in Chemical Engineering at SUT under the supervision of Prof. Dr. Chaiyot Tangsathitkulchai. She received a support in form of scholarship from The Royal Golden Jubilee (RGJ) Ph.D. Program under The Thailand Research Fund (TRF).

